

ALMA MATER STUDIORUM - UNIVERSITÀ DI BOLOGNA

SCUOLA DI INGEGNERIA E ARCHITETTURA

DIPARTIMENTO DI INGEGNERIA INDUSTRIALE

CORSO DI LAUREA MAGISTRALE IN INGEGNERIA MECCANICA

TESI DI LAUREA

in

PROPULSORI TERMICI E IBRIDI PER AUTOVEICOLI M.C.I.

**Development, Testing and Potential Benefits of a Closed-Loop Combustion
Controller on a Turbocharged GDI Engine**

CANDIDATO
Nicola Silvestri

RELATORE
Prof. Nicolò Cavina

CORRELATORI
Prof. Davide Moro
Prof. Enrico Corti
Ing. Andrea Businaro
Ing. Lucio Calogero
Ing. Ruggero Cevolani
Ing. Marco Cappa

Anno Accademico 2015/2016

Sessione III

Abstract

La riduzione dei consumi e delle emissioni inquinanti, accompagnata dalla domanda di veicoli sempre più performanti, costituisce una delle principali sfide nello sviluppo di nuovi sistemi di propulsione per l'industria automobilistica. La soddisfazione di questi requisiti, imposti dalle sempre più stringenti normative e da scelte di marketing, comporta una costante ricerca di soluzioni volte a migliorare l'efficienza dei motori a combustione interna.

Nei motori ad accensione comandata, la fase della combustione rappresenta uno dei principali parametri che influenzano l'efficienza di conversione dell'energia chimica del combustibile in lavoro meccanico.

La scarica elettrica generata dalla candela costituisce l'attuazione principale per il controllo dell'inizio del processo di combustione. Accensioni troppo ritardate non consentono di sfruttare l'intera corsa di espansione del pistone, mentre accensioni troppo anticipate comportano un aumento di pressione quando il pistone si trova ancora in fase di compressione, causando quindi una perdita di lavoro utile.

L'istante in cui viene dato il comando di accensione, detto 'anticipo', viene attualmente controllato in catena aperta per mezzo di mappe salvate nella centralina elettronica di controllo motore. E' richiesta quindi una complessa procedura di calibrazione a banco per definire l'anticipo di accensione ottimo per ogni condizione di funzionamento del motore. La velocità di rotazione, il carico, il rapporto aria/combustibile, la temperatura dell'aria e dell'acqua, la fasatura delle valvole di scarico e aspirazione e l'invecchiamento del motore sono solo alcune delle variabili che influenzano il processo di combustione e che devono quindi essere considerate in fase di calibrazione delle mappe di anticipo.

Un'alternativa è costituita da un sistema di controllo dell'anticipo di accensione in catena chiusa su di una misura reale del processo di combustione, in modo da regolare l'anticipo per produrre sempre una corretta fasatura della combustione. Tuttavia, l'implementazione di un sistema basato su di una misura di pressione all'interno del cilindro, a causa di costi elevati e problemi di affidabilità dei sensori, non è per il momento perseguibile nell'ambito di applicazioni industriali. Un'alternativa al segnale di pressione è costituita dalla misura della corrente di ionizzazione all'interno del cilindro, effettuata usando la candela stessa come sensore: tutti i più recenti motori prodotti da Ferrari adottano infatti un'apposita centralina e bobine di accensione per la misura della corrente di ionizzazione, attualmente impiegata per diagnosticare la presenza di combustioni detonanti.

Nell'ambito di questo lavoro di tesi è stata condotta una campagna di misure sperimentali per quantificare il livello di correlazione tra alcune caratteristiche del segnale di corrente di ionizzazione e gli indici impiegati per descrivere la fase di combustione derivati dal segnale di pressione.

La fase di implementazione ha portato allo sviluppo e alla sperimentazione di un innovativo controllo in catena chiusa dell'anticipo di accensione. Il sistema è stato testato tramite un ambiente di simulazione appositamente sviluppato e successivamente implementato e collaudato su di un motore Ferrari sovralimentato, al banco prova ed in vettura. Il risultato principale è quindi un innovativo sistema di controllo dell'anticipo, cilindro per cilindro, che è in grado di adattare continuamente l'attuazione sia alla variazione dei parametri interni di funzionamento del motore, sia a quelli esterni.

Index

1	Introduction.....	9
2	Internal Combustion Engines for Automotive Applications.....	10
2.1	Powertrain Development Trends.....	10
2.1.1	Carbon Dioxide Regulation	10
2.1.2	Pollutant Emissions Standards	14
2.1.3	Gasoline Direct Injection	17
2.1.4	Turbocharging and Downsizing.....	19
2.1.5	48 Volts Hybrid Systems and E-Boosting	20
2.2	Ferrari S.p.A.....	22
2.2.1	Cars Produced	22
2.2.2	Engines Produced.....	24
2.3	Combustion in Spark-Ignition Engines	26
2.3.1	Physics of the Combustion Process	26
2.3.2	Pressure Signal	29
2.3.3	Heat Release.....	33
2.3.4	Combustion Phase Indicators.....	36
2.4	Engine Control Unit	38
2.4.1	Vehicle Torque Structure	38
2.4.2	Sensor and Actuators of a Modern Engine Management System.....	39
2.4.3	Ignition Angle Control Loop.....	41
2.5	Ionization Current for Ignition Control	43
2.5.1	Ion Generating Process and Measurement.....	43
2.5.2	Ionization Current Feature	44
2.5.3	Ionization Current Applications for Ferrari	45
3	Correlation Analysis	49
3.1	Offline Processing of Raw Signals.....	49
3.1.1	Offline Algorithm	49

3.1.2	Experimental Activity	50
3.1.3	Raw Signal Correlation Results	51
3.2	Real Time Processing of Ion Signal	56
3.2.1	Experimental Activity Requirements	56
3.2.2	Dynamic Spark Sweep	58
3.2.3	Conversion from Sample Based to Angle Based	60
3.2.4	Real Time Algorithm Performance	62
3.3	Other Combustion Features from Steady State Tests	63
4	Open Loop Combustion Phase Evaluation	69
4.1	Combustion Analysis	70
4.2	Evaluation of Possible Improvements in Fuel Economy	73
5	Closed Loop Combustion Control	77
5.1	Controller Structure and Feedback Selection	77
5.2	Offline Controller Performance Evaluation	80
5.2.1	Engine Simulation Environment	80
5.2.2	Offline Simulation Results	82
5.3	Real Time Combustion Controller with Pressure Signal Feedback	84
5.3.1	Controller Layout	84
5.3.2	Controller Algorithm	85
5.3.3	First Set: Step Response	86
5.3.4	Second Set: Steady State Tests	88
5.3.5	Third Set: Transient Tests	95
5.3.6	Fourth Set: Vehicle Implementation	97
5.4	Real Time Combustion Controller with Ion Signal Feedback	100
6	Conclusions	103
7	Bibliography	105

1 Introduction

Performance improvement, CO₂ reduction and pollutant emission minimization are some of the key challenges facing the development of new powertrains in the automotive industry. The need to meet these requirements drives the development of engines' efficiency.

In a Spark Ignition Internal Combustion Engine, one of the most effective factors influencing performance and efficiency is the combustion phasing. The electrical discharge in the spark plug is main actuation to control the beginning of the combustion process. Late ignition timing does not make use of the full stroke of the piston, and less work is produced. Early ignition timing produces a high pressure too early, when the piston is moving up, and work is lost.

This fundamental engine parameter is currently controlled in an open-loop by means of maps stored in the Engine Control Unit memory. A complex calibration procedure on the engine test bench is therefore required to define the optimal spark advance angle for every engine operating condition. Engine speed, load, air to fuel ratio, air/water temperature, valve timing and engine ageing are just some of the variables that influence the combustion process and must be considered when "mapping" the ignition timing.

A better choice, thanks to the development of electronics, would be a spark advance controller based on a real time measurement of the combustion process, so that the ignition timing could be set to produce always the combustion phasing corresponding to the maximum efficiency. Nevertheless, the implementation of an in-cylinder pressure based controller is connected with high cost and poor pressure sensor reliability for industrial application. An alternative for the pressure signal is the measurement of the ionization current inside the cylinder, using the spark plug itself as sensor: all latest Ferrari production engines are equipped with the necessary hardware, since ionization current is already used to detect knock and misfire. An experimental campaign is performed to define the correlation level between features of the ionization current signal and the pressure based combustion phase indicators.

The implementation phase led to the development and testing of a closed-loop spark advance controller, through a simulation environment and at the test bench on a Ferrari turbocharged engine. The main result is therefore an individual cylinder spark advance controller that is continuously able to adapt its actuation both to engine internal parameters' variations as well as to varying external conditions.

2 Internal Combustion Engines for Automotive Applications

Since their introduction, internal combustion engines have continued to improve as the knowledge of engine processes has increased, as new technologies became available, as demand for new types of engine arose, and as environmental constraints on engine use changed. Internal combustion engines, and the manufacturer that develop and produce them, play a dominant role in the fields of automotive industry. Aim of this Chapter is to provide an overview of the actual trends in powertrain development, starting from the market requirements to latest technical innovations. Particular attention is given to the combustion phenomena in Spark Ignition engines, since the efficiency of the fuel's energy conversion process depends strongly on how combustion takes place and to the latest application of electronics in the engine management. Among the innovations, the ion current system for combustion control is presented, together with its applications on Ferrari's engines.

2.1 Powertrain Development Trends

Up to now, the technological development of the powertrain has taken place between two divergent demands. On the one hand, legislators have called for reduced emissions and, on the other, customers for higher performance, comfort and safety.

In this section a summary of European Union regulations on emissions from light-duty vehicles is presented, focusing on the target for CO₂ and pollutant emissions reduction and the need of improving testing procedures: the Worldwide Harmonized Light-duty Vehicles Testing Procedure (WLTP) for measuring CO₂ and Real Driving Emissions (RDE) for measuring regulated pollutants under real-life conditions.

The last paragraphs provide a summary of the actual trend in powertrain development. Particular attention is given to the analysis of turbocharged and downsized gasoline engine, together with low-voltage hybrid systems. These measures help improving efficiency and performance of the powertrain, while satisfying legal requirements for CO₂ and pollutant emission standards.

2.1.1 Carbon Dioxide Regulation

Carbon dioxide is one of the main products of hydrocarbon combustion, together with water. It is measured in emission tests and it is strictly correlated with fuel consumption. Carbon dioxide cannot be defined as a pollutant as it is an inert gas and not directly harmful to humans or animals. However, it is the main anthropologic cause of the greenhouse effect that is leading to an increase in average Earth's atmospheric temperature and to dramatic climatic changes.

Light-duty vehicles are responsible for around 12% of total EU emissions of carbon dioxide: that's why EU legislation sets mandatory CO₂ emission reduction targets for new cars.

The European legislation defines an individual annual target for each manufacturer, based on the average mass of all its new cars registered in the EU in a given year. From 2015, manufacturers must ensure that 100% of the new cars registered in the EU each year have average emissions that are below their respective targets. Only the fleet average is regulated, so manufacturers are still able to make vehicles with emissions above their indicative targets if these are offset by other vehicles which are below their indicative targets. In case manufacturer's average emission level is above the target set by the limit value curve, it will have to pay an excess emissions premium. The more a manufacturer goes above the target, the higher the premium.

Significant technical advancements have been made in recent years. The figures for Europe clearly illustrate this. Since 2007, CO₂ emissions from cars in Europe have sunk by 18% [1], even though performance and vehicle weight have increased over the same period. As shown in Figure 2.1, emission standards are set to become stricter in all the world's major automotive markets. Europe leads the way here: Regulation (EC) N°443/2009 sets in 95 grams of CO₂ per kilometer the fleet average to be achieved by all new cars in 2020, while the average emissions level of a new car sold in 2015 was already 119.6 grams of CO₂ per kilometer, significantly below the 2015 target of 130 grams of CO₂ per kilometer.

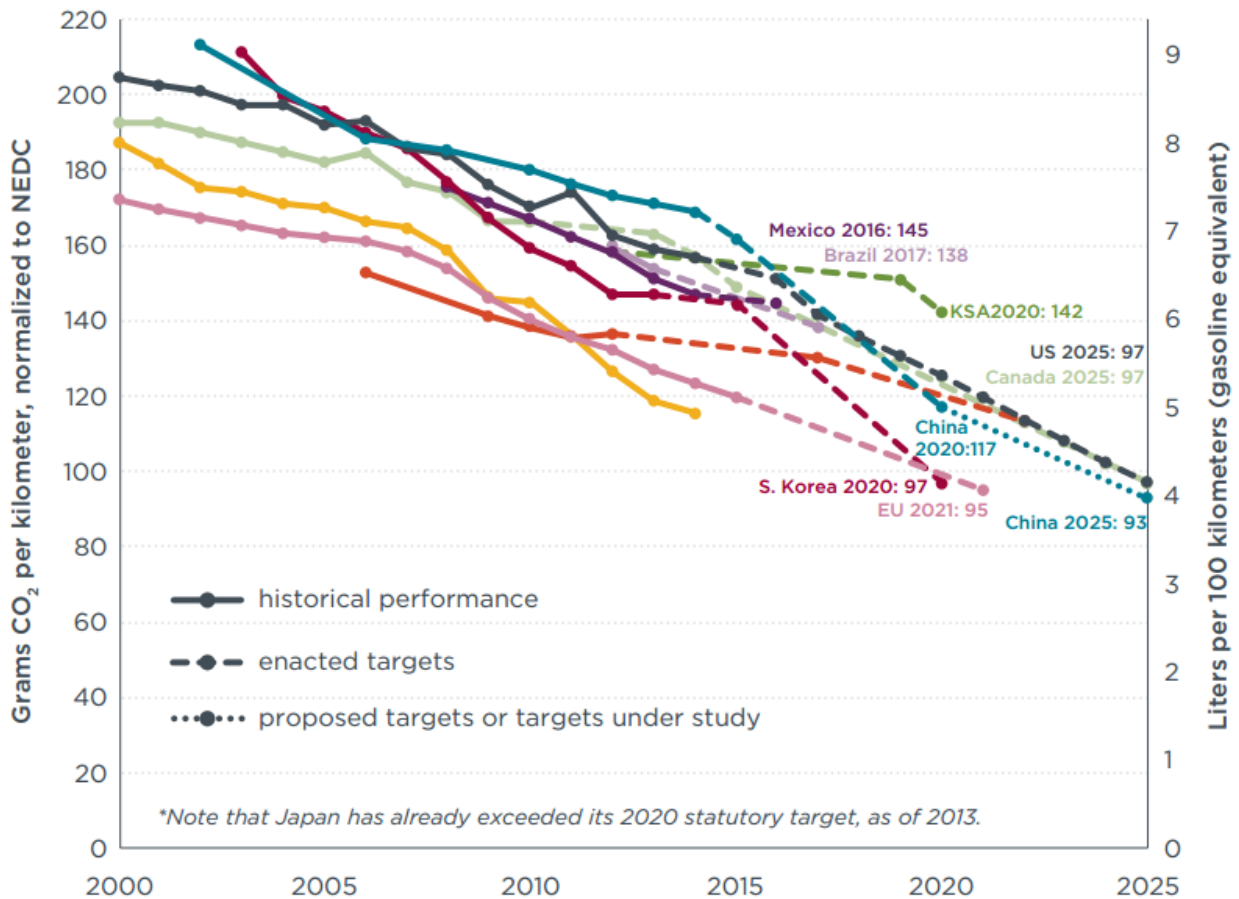


Figure 2.1 - Comparison of global CO₂ regulations for new passenger cars, normalized to NEDC [2].

Must be noticed that all CO₂ limits reported above refer to emissions measured on the New European Driving Cycle (NEDC), in accordance with Regulation (EC) No 715/2007.

With regards to how these emission are measured, in 2014 the European Commission highlighted the need to amend the NEDC driving cycle to ensure its representativeness over real driving conditions and to avoid the underestimation of real CO₂ emissions and fuel consumption. Working in this direction, the European Commission proceeded through the development of a Worldwide harmonized Light-vehicles Test Procedure (WLTP) [1].

In March 2016, WLTP was approved and will be implemented in September 2017, coinciding with the adoption of the updated EURO6d (European Emission Standards) regulation. Additionally, as part of the WLTP implementation in the EU, the CO₂ targets defined for 2020 based on NEDC testing will need to be translated to WLTP equivalent values.

Table 1 quantifies the main descriptive parameters of the new WLTC (Worldwide Harmonized Light Vehicles Test Cycle) driving cycle compared to the NEDC cycle. The acronym WLTC is

used to specifically identify the test cycle only, while WLTP indicates the complete framework of the test procedure.

Table 1 - Descriptive parameters of the driving cycles NEDC (currently used for CO₂ emissions measurement) and WLTC [3]

	Units	NEDC	WLTC
Start condition		cold	cold
Duration	s	1180	1800
Distance	km	11.03	23.27
Mean velocity	km/h	33.6	46.5
Max. velocity	km/h	120.0	131.3
Stop phases		14	9
Durations:			
• Stop	s	280	226
• Constant driving	s	475	66
• Acceleration	s	247	789
• Deceleration	s	178	719
Shares:			
• Stop		23.7%	12.6%
• Constant driving		40.3%	3.7%
• Acceleration		20.9%	43.8%
• Deceleration		15.1%	39.9%
Mean positive acceleration	m/s ²	0.59	0.41
Max. positive acceleration	m/s ²	1.04	1.67
Mean positive 'vel * acc' (acceleration phases)	m ² /s ³	4.97	4.54
Mean positive 'vel * acc' (whole cycle)	m ² /s ³	1.04	1.99
Max. positive 'vel * acc'	m ² /s ³	9.22	21.01
Mean deceleration	m/s ²	-0.82	-0.45
Min. deceleration	m/s ²	-1.39	-1.50

The key elements that should be considered when evaluating CO₂ emissions on WLTC instead of NEDC are a longer and more dynamic driving cycle, including a more flexible gear shift strategy for manual transmissions, a higher vehicle test mass and a lower engine temperature at test start.

Regarding the journey to fully implement WLTP, the phased approach adopted by the European Union can be summarized as follows:

Up to August 2017:

- NEDC testing will remain in place;
- Vehicle manufacturers will prepare for WLTP and in some cases already begin to publish WLTP figures.

September 2017 to December 2019:

- WLTP type approval testing will be introduced for new vehicles;

- New vehicles will be tested both using both NEDC and WLTP type approval procedures;
- The legally binding values for the CO₂ monitoring will remain the NEDC based results;
- WLTP based results can be used for customer information (sales brochures and CO₂ labeling);
- As further focus is placed on WLTP results by various stakeholders, it is expected that national tax regulations will adapt to utilizing WLTP based CO₂ values. Correspondingly vehicle manufacturers will optimize vehicle development for this test rather than NEDC.

From 2020 onwards:

- New vehicles will be tested using WLTP type approval procedure only;
- CO₂ emission targets will have to be met in the WLTP;
- For this, it is necessary to translate the existing 95 g/km NEDC based target into an equivalent WLTP based target (expected to be about 100 g/km).

The Commission is currently preparing a proposal for future CO₂ emission targets that will contribute to meeting the European Union's 2030 climate targets. The future CO₂ emission standards will be defined on the basis of the emissions measured on the WLTP, with the expectation that the new test procedure will offer a more robust basis for defining the reductions expected and for ensuring that they will actually be delivered.

2.1.2 Pollutant Emissions Standards

Besides CO₂ emission, European Union sets objectives for air pollutant emissions, in order to reduce harmful effects on human health. The main air quality pollutant emissions from internal combustion engines are:

- carbon monoxide (CO);
- oxides of nitrogen (NO and NO₂);
- un-burnt hydrocarbons (HC);
- particulate matter (PM).

Emissions of these pollutants are regulated since 1991 by the "European Emission Standards". In Table 2, the light-duty vehicles Euro 6 emission standards, introduced in September 2014, are compared with the previous Euro 5 standards. Considering first the standards for diesel vehicles (see Table 2), Euro 6 is a significant advancement over Euro 5 with regard to NO_x limits (56% reduction). On the other hand, the recent diffusion of gasoline direct injection (GDI) technology led

to the introduction of limits on particle number emissions also for gasoline vehicles (numerically the same as those for diesel cars).

Table 2 - The light-duty Euro 5 and Euro 6 vehicle emission standards on the New European Driving Cycle (NEDC). Pollutant emission are measured in g/km. [4]

Pollutant	Euro 5 Light-Duty		Euro 6 Light-Duty	
	Gasoline	Diesel	Gasoline	Diesel
CO	1.0	0.5	1.0	0.5
HC	0.1 ^a		0.1 ^e	
HC+NO _x		0.23		0.17
NO _x	0.06	0.18	0.06	0.08
PM	0.005 ^c	0.005	0.005 ^c	0.005
PN (#/km)		6.0 x 10 ¹¹	6.0 x 10 ¹¹ ^d	6.0 x 10 ¹¹

The pre-defined light-duty vehicles measurement cycle for all the past Euro emissions standards and for Euro 6 as well, is the already mentioned New European Driving Cycle (NEDC).

Since the agreement of Regulation 715/2007, when Euro 6 limits were first announced, research has shown the NEDC to be a poor representation of real-world driving, with serious implications for emissions, particularly those of NO_x from diesel cars.

Different studies ([5],[6]), through the use of a Portable Emissions Measurement Systems (PEMS), revealed how the large majority of passenger cars certified to the Euro 6 standard (in laboratory condition), have NO_x emission levels several times above the regulated limit when driven under normal, 'real world', condition. This problem was highlighted in the recent Volkswagen case. Thanks to the use of PEMS, on September 2015 the US EPA served a notice of violation on Volkswagen Group, alleging that many VW and Audi automobiles sold in the U.S had a "defeat device" in diesel engines that could detect when they were being tested, changing the performance accordingly to improve results. Nevertheless, systematic vehicle testing, for example by the German government (reported in Figure 2.2), confirms that high real-world NO_x emissions are an industry-wide problem, not restricted to the confirmed illegal defeat devices present on some Volkswagen models.

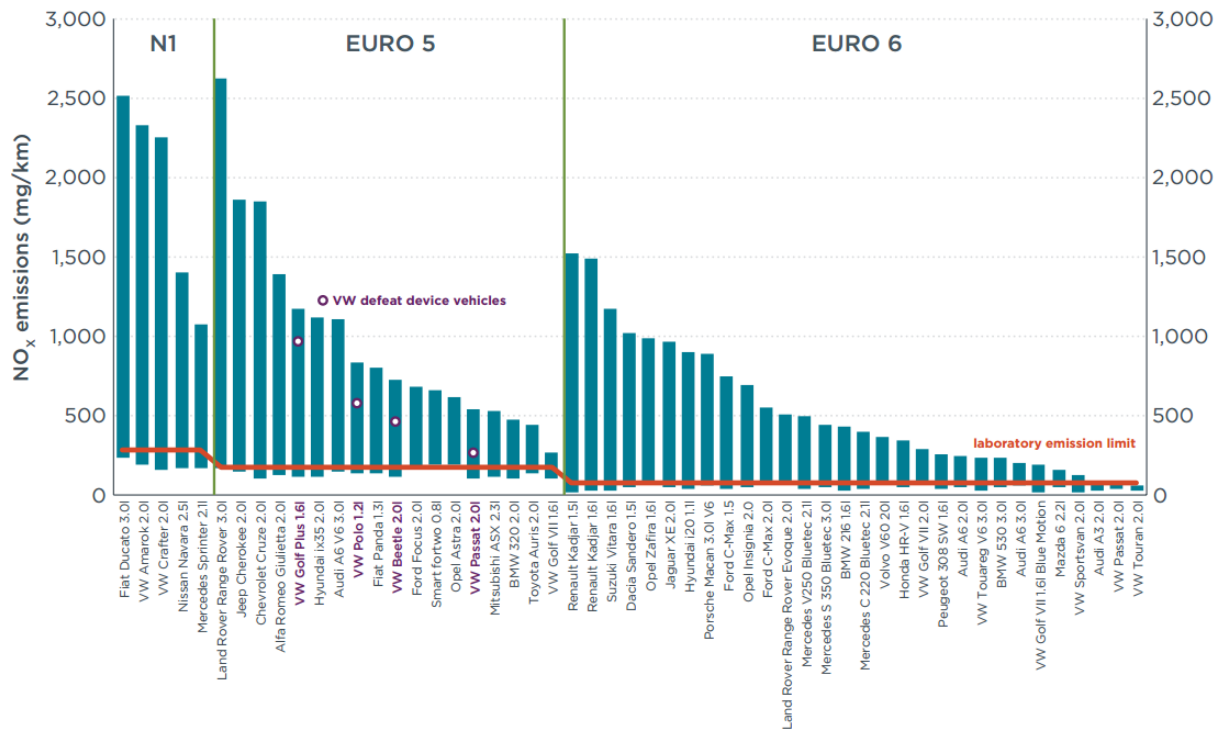


Figure 2.2 - Overview of laboratory and on-road vehicle emissions test results by the German Ministry for Transport, April 2016 (lower emission level corresponds to NEDC laboratory test, upper level to max. on-road test result) [7].

To reduce this gap, member states meeting in the Technical Committee of Motor Vehicles (TCMV) in October 2015, have approved the use of Real Driving Emissions (RDE) tests to determine whether a new car model is allowed to be put on the market.

It's important to highlight that the RDE procedure complements the current laboratory based procedure, and will be used to check if the vehicle emission levels of nitrogen oxides (NO_x), and at a later stage also particle numbers (PN), measured during the laboratory test, are confirmed in real driving conditions.

Under Real Driving Emission, a car will be driven on public roads and over a wide range of different conditions. PEMS installed on the vehicle (Figure 2.3) will collect data to verify NO_x emissions are 'not to exceed' euro emission standards by a certain Conformity Factor.

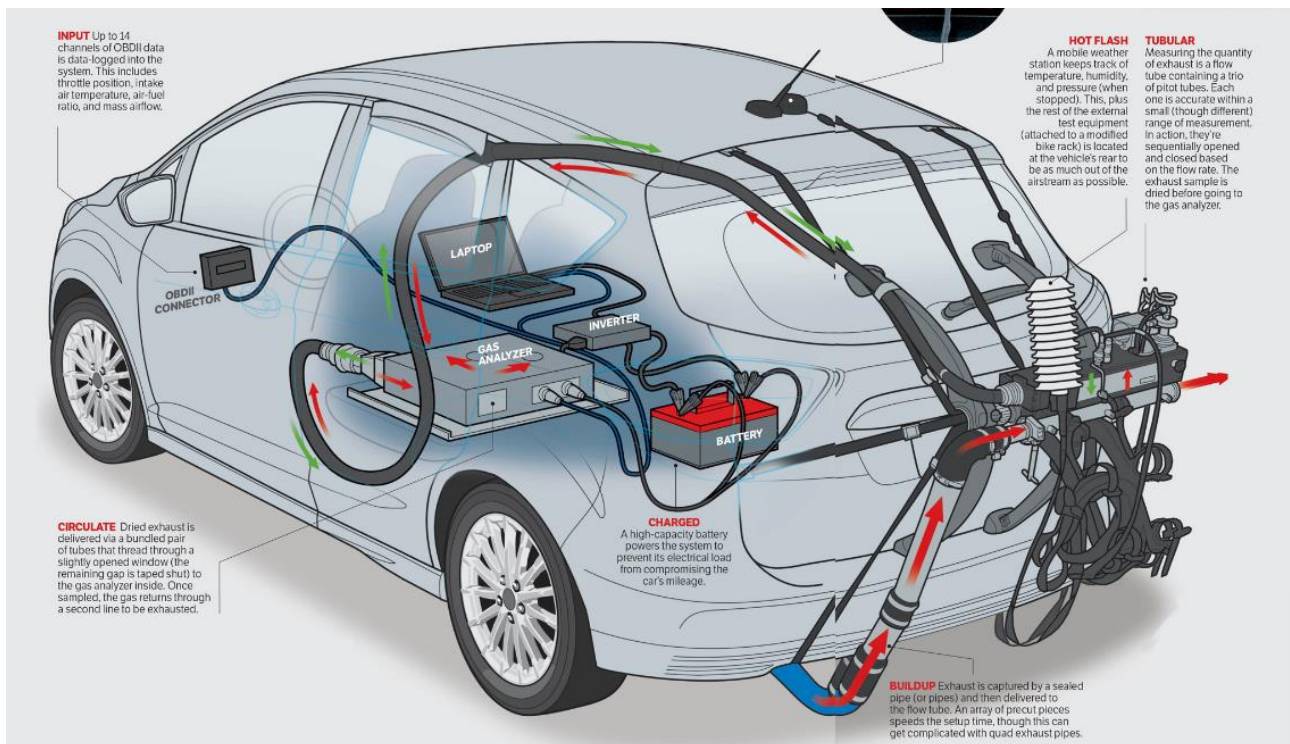


Figure 2.3 – Portable Emission Measurement System (PEMS)

According to the agreed Real Driving Emission test procedure, car manufacturers must reduce the divergence in two steps:

- Car manufacturers will have to bring down the discrepancy to a Conformity Factor of maximum 2.1 (110%) for new models by September 2017 (for all new vehicles by September 2019);
- This discrepancy will be brought further down to a Factor of 1.5 (50%), taking account of technical margins of error, by January 2020 for all new models (by January 2021 for all new vehicles). As the technology improves, the conformity factor will be reduced further.

A third Real Driving Emission step is currently being prepared by the European Commission.

2.1.3 Gasoline Direct Injection

Among the measure for improving efficiency and performance of a spark ignition engine, Gasoline Direct Injection (GDI) has seen a rapid diffusion over the past years, often accompanied by other engine technologies such as turbocharging, supercharging and variable valve timing (VVT).

Previous fueling systems, from carburetors to throttle body fuel injection to Port Fuel Injection (PFI), all mixed the air and fuel before the mixture entered the cylinder. As shown in Figure 2.4, with Gasoline Direct Injection, fuel is injected directly into the cylinder during the intake phase, so that only air flows through the intake valves.

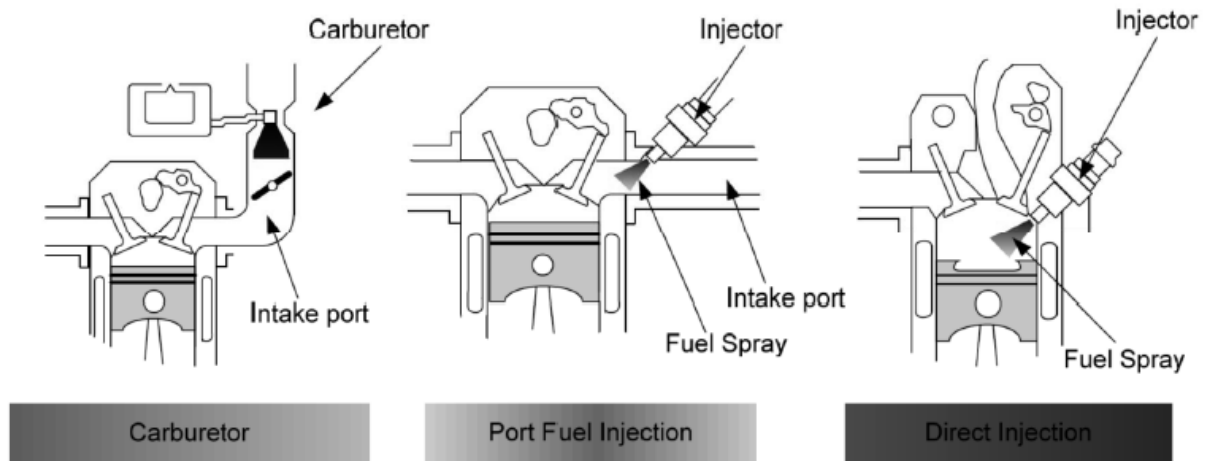


Figure 2.4 - Fuel injection system evolution [8]

Injected fuel evaporation creates a cooling effect, improving volumetric efficiency and reducing compression temperatures and, hence, knock (see Section 2.3). It also allows valve timings that promote scavenging of the cylinder during high-load operation, further reducing charge temperatures while increasing trapped air mass. With Gasoline Direct Injection, the compression ratio in a turbocharged engine can be higher than with Port Fuel Injection and engine efficiency is improved.

Gasoline Direct Injection also enables stratified charge mode at partial loads: the idea is to deliver a mixture that is sufficiently rich for combustion near the spark plug and a very lean mixture and residual gases in the remainder of the cylinder. This can be made through multiple fuel injections, even during the compression phase. While running on stratified charge mode, the delivered power is no longer controlled by the quantity of admitted air, but by the quantity of gasoline injected, as in a Diesel engine. The engine could be operated un-throttled like the Diesel engine, reducing pumping work and increasing efficiency. The main drawback of lean-burning is that a complex catalytic converter system is required to reduce NO_x emissions. Lean-burn engines do not work well with the 3-way catalytic converter, which requires stoichiometric mixtures to promote oxidation and reduction reactions.

Port Fuel Injection engines do have some limited advantages over GDI engines due to the fact that the intake system acts as a pre-vaporizing chamber. When fuel is injected directly into the engine cylinder, the time available for mixture preparation is reduced significantly. As a result, the atomization of the fuel spray must be fine enough to permit fuel evaporation in the limited time available between injection and ignition. Fuel droplets that are not evaporated are very likely to participate in diffusion burning, or to exit the engine as particulate emissions (PN).

To summarize, Gasoline Direct Injection improved performance depends on [9]:

- higher compression ratio (charge cooling with injection during induction);
- higher knock limit (charge cooling with injection during induction);
- increased volumetric efficiency (charge cooling with injection during induction);
- Improved transient response (fuel is injected later)
- less pumping loss (un-throttled, stratified mode);
- less heat losses (un-throttled, stratified mode);

while, the critical points of a GDI engine are:

- complexity of the control and injection technologies required (i.e. cost);
- difficulty in controlling the stratified charge combustion over the required operating range;
- increased particulate emissions;
- high local NO_x production under part-load, stratified charge operation;
- three-way catalysis cannot be efficiently utilized during stratified charge operation.

2.1.4 Turbocharging and Downsizing

Turbochargers increase engine power by increasing intake charge air density, thus increasing the air mass flow to the engine. This extra air allows introducing additional fuel (to maintain stoichiometric conditions desirable for modern exhaust after treatment technology). Consequently, the direct impact of turbocharging is to increase engine power and fuel flow for a given engine displacement volume.

Higher output results in higher combustion pressures which increase the temperature of the unburned gases being compressed ahead of the flame front, and this leads to increased knock (see Paragraph 2.3). Historically, manufacturers reduced compression ratios in turbocharged engines to control knock and detonation, leading to efficiency reductions. Thus, until recently, turbochargers were used primarily to increase performance in sport vehicles.

Today, turbochargers are used to reduce fuel consumption indirectly, by enabling engine downsizing. The increased specific power provided by a turbocharger allows the entire engine to be downsized while maintaining the same level of performance. At a constant vehicle demand for performance, a smaller displacement engine operates at higher loads, resulting in lower throttling losses under normal driving conditions. Smaller engines typically also have lower friction losses due to smaller bearings and cylinders.

2.1.5 48 Volts Hybrid Systems and E-Boosting

Perhaps one of the most significant advancement in downsized turbocharged engines comes from the recent trend of powertrain electrification. As shown in Figure 2.5, powertrain electrification comprises a wide spectrum of applications, ranging from micro-hybrids over mild and full hybrids up to pure electric vehicle.

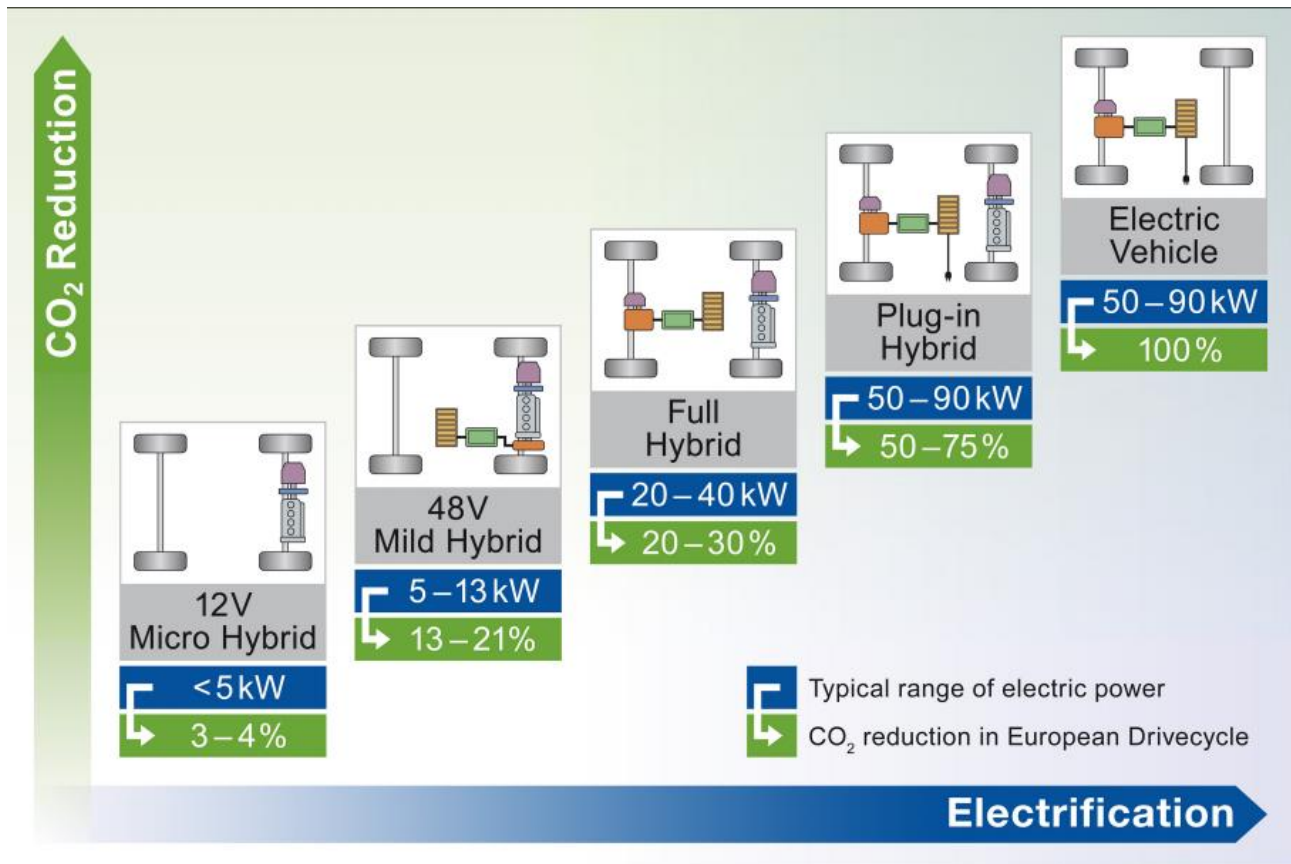


Figure 2.5 – Different electrification levels for light-duty vehicle’s powertrain.

Manufacturers and suppliers are searching for the right level of hybridization with the best payback for the consumer. In the last years, there has been an important trend in developing of 48 Volts Mild Hybrid system: compared to a full-hybrid, they're significantly cheaper thanks to the lack of a large electric motor and battery, and most importantly, they can be added to traditional powertrains relatively easily by manufacturers. They might also be used by some manufacturers as stepping stones to higher-voltage systems, while the costs of all hybrid systems come down.

With a nominal 12V on board grid, the peak power from a motor-generator is limited at about 3kW, due to high current losses, which constrains the maximum torque available and, of equal importance, any kinetic and thermal energy recovery. With a nominal 48 Volts on-board grid, the industry has access to approximately 12.5 kW electrical power, which makes all the difference to

powertrain efficiency and performance, while the DC voltage remains well below the safety critical 60 Volt level.

Unlike more expensive full hybrids, 48 Volts systems are not designed to propel the vehicle, but higher voltage and greater energy storage capacity, compared to 12 Volts systems, allows regenerative braking energy and permits accessory operation with the engine off. Mild hybrids also enable more robust start-stop systems, in particular start-stop coasting (or sailing): here the engine is shut off at high speed, and the 48 Volts system maintains power to all electronics and electrical devices [10]. Some of the possible advantages in an urban driving cycle through the employment of a mild-hybrid system are summarized in Figure 2.6.

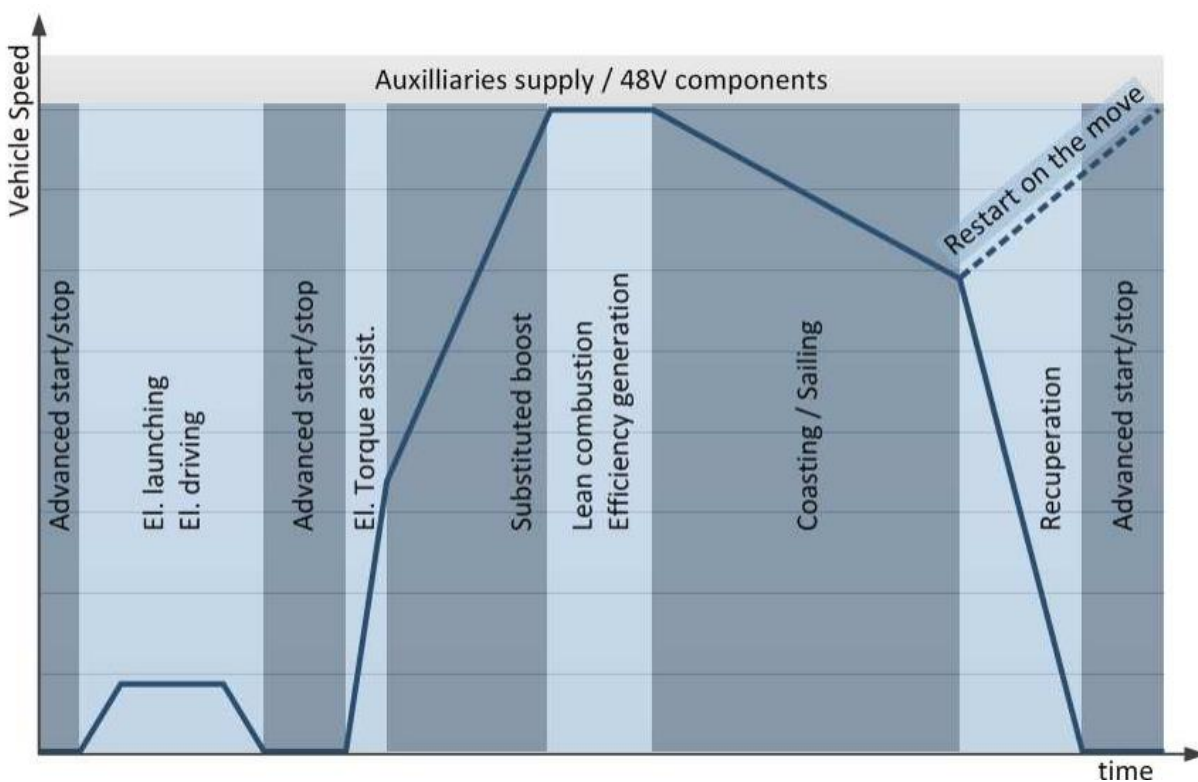


Figure 2.6 - Advanced 48 Volts functionalities and their application in urban driving environment [11].

New concepts using 48 Volts hybrid systems can also be used to provide power for small electric compressor motors within or without a turbocharger. These either directly boost the engine, or spin up the turbocharger to greatly reduce turbo lag. Improved boosting and reduced lag increase the ability to downsize and downspeed the engine. E-Boost allows the use of larger turbines with lower backpressure, for a direct reduction in brake specific fuel consumption in addition to the benefits from engine downspeeding and downsizing.

2.2 Ferrari S.p.A.

This work of thesis is based on an activity carried on entirely at the Powertrain Design & Development department of Ferrari S.p.A., the well-known Italian auto manufacturer based in Maranello (MO). This chapter gives a brief introduction to the factory and to the cars produced and highlights the main technological features adopted by latest Ferrari engines.

2.2.1 Cars Produced

Ferrari produces high performance and luxurious sports cars and it is the most successful racing team in Formula One's history. Its brand has become over the years the most powerful around the world. It was founded by Enzo Ferrari initially in 1929 in Modena as the Scuderia Ferrari, initially to race cars produced by Alfa Romeo, though by 1947 Ferrari had begun building its own cars. Nowadays, Ferrari produces a family of road cars that share more than 60 years of expertise in engineering and driving performance.

All current Ferrari models are equipped with a gasoline engine, V8 or V12. Models from the V8 line include the *488 GTB*, the *488 Spider* and the *California T*. The V12 line includes the latest *GTC4Lusso* (which is produced also with the V8 engine), the *F12 Berlinetta*, its "special" version *F12TDF* and the limited production hypercar *LaFerrari*, which is powered by an hybrid powertrain.





Figure 2.7 – Picture of Ferrari models produced in 2016.

2.2.2 Engines Produced

Ferrari cars are powered either by a V8 engine, either by a V12. All V8's adopted by Ferrari nowadays belong to the *F154* family (Figure 2.8, on the left), composed by twin-turbocharged, direct injected 90° V8 petrol engines designed and produced by Ferrari since 2013, while the V12 engines belong to the *F140* family (Figure 2.8, on the right), composed by naturally aspirated, direct injected 65° V12 petrol engines.

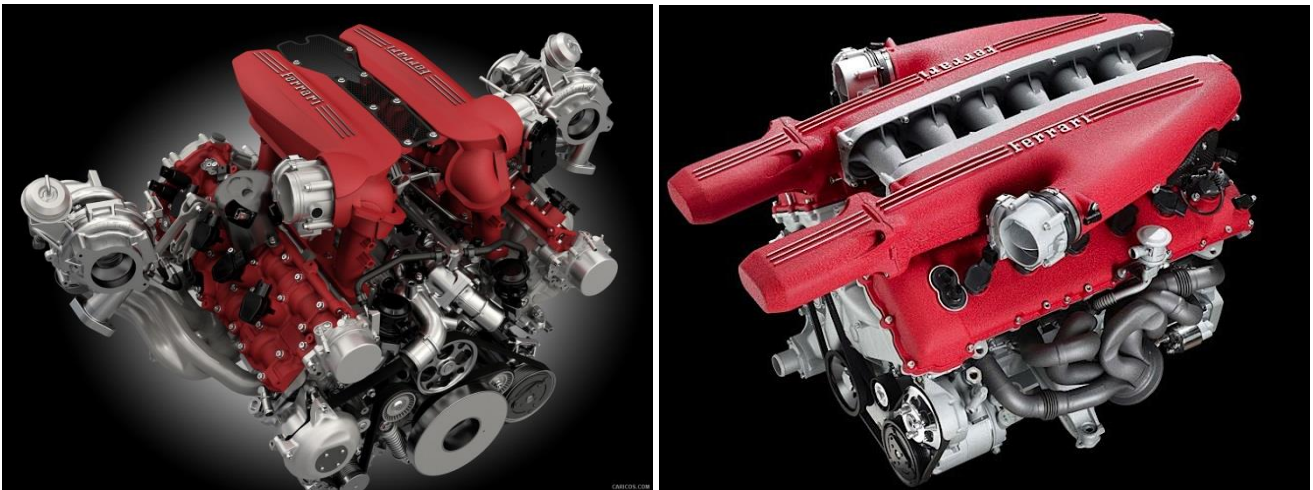


Figure 2.8 – Ferrari *F154CB* engine (*488GTB*) and *F140FC* (*F12 Berlinetta*).

The top performance V12 engine is the mid-rear mounted *F140* in the *LaFerrari*. With a 6262cc capacity, it produces 800 CV @ 9000 rpm and 700 Nm of torque @ 6,750 rpm, while the top performance V8 is the mid-rear mounted *F154CB* adopted by the *488 GTB*, with a 3902cc capacity and 670 CV @ 8000 rpm and 760 Nm of torque [12].

The main technical feature of the *F154* engine, elected International Engine of the Year 2016, comprehend: 200 bar gasoline direct injection, ion current measurement for combustion and ignition control (see Paragraph 2.5), variable displacement oil pump and dry sump lubrication, flat plane crankshaft and continuous variable valve timing system. The turbochargers, produced by IHI, feature a twin-scroll turbine, for more power extraction from exhaust pressure pulses, low-inertia titanium-aluminum turbine wheel and ball bearing to reduce friction, delivering the best engine's response in its class (Figure 2.9).

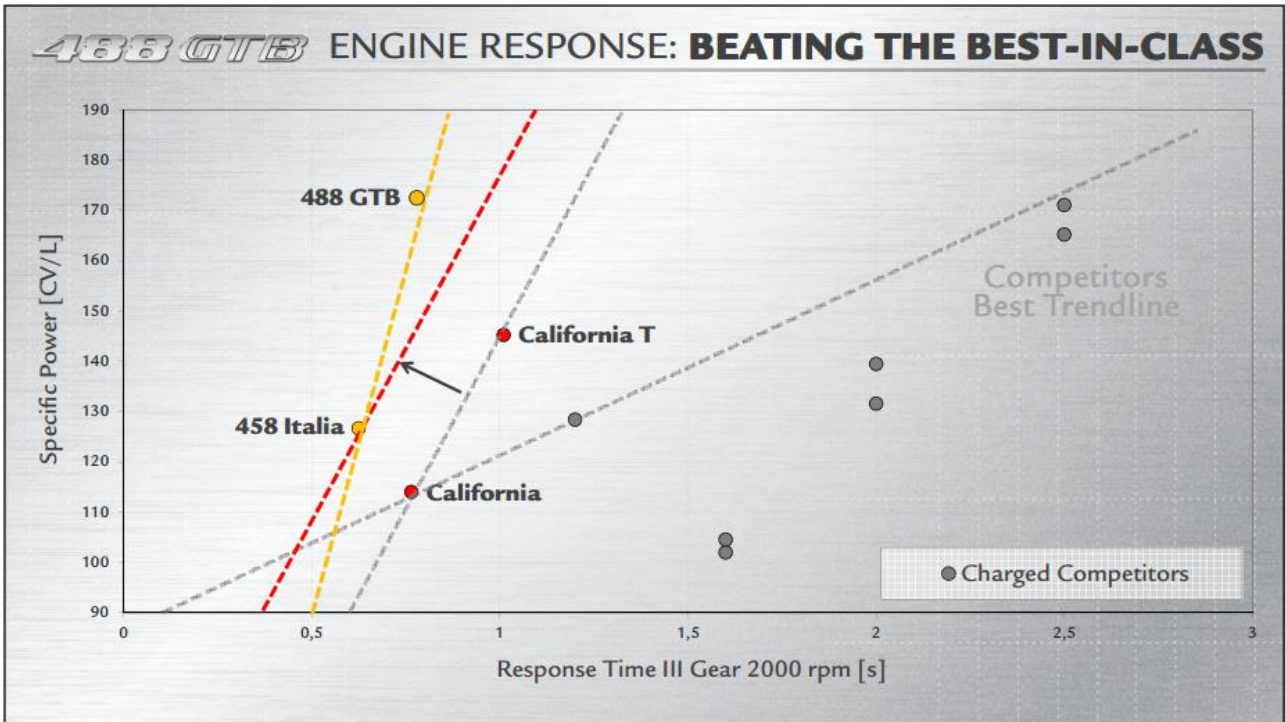


Figure 2.9 – 488 GTB engine response in 3rd gear against competitors [12].

2.3 Combustion in Spark-Ignition Engines

The combustion process releases the fuel's energy within the engine cylinder for conversion into useful work. What fraction of the fuel's energy is converted depends strongly on how combustion takes place. The Spark Ignition engine combustion processes therefore influence essentially all aspects of engine behavior. This section focuses on the combustion phenomena and on the main engine parameters adopted to evaluate its quality.

2.3.1 Physics of the Combustion Process

In a conventional Spark-Ignition engine, fuel and oxidizer are mixed together prior to their ignition. The combustion process is thus defined "premixed". Under normal operating conditions, combustion is initiated towards the end of the compression stroke through an electric discharge provided by the spark plug. The corresponding angular position is called "spark advance" and it's measured in degrees Before Top Dead Center ($^{\circ}$ BTDC).

The high-temperature plasma kernel created by the spark develops into a self-sustaining and propagating flame front, a reaction sheet where the exothermic combustion chemical reactions occur (Figure 2.10), so that fresh mixture and burnt products are sharply separated. The reaction zone propagates, since heat is transferred from reaction zone to fresh air mixture, which heats up, thus starting auto ignition.

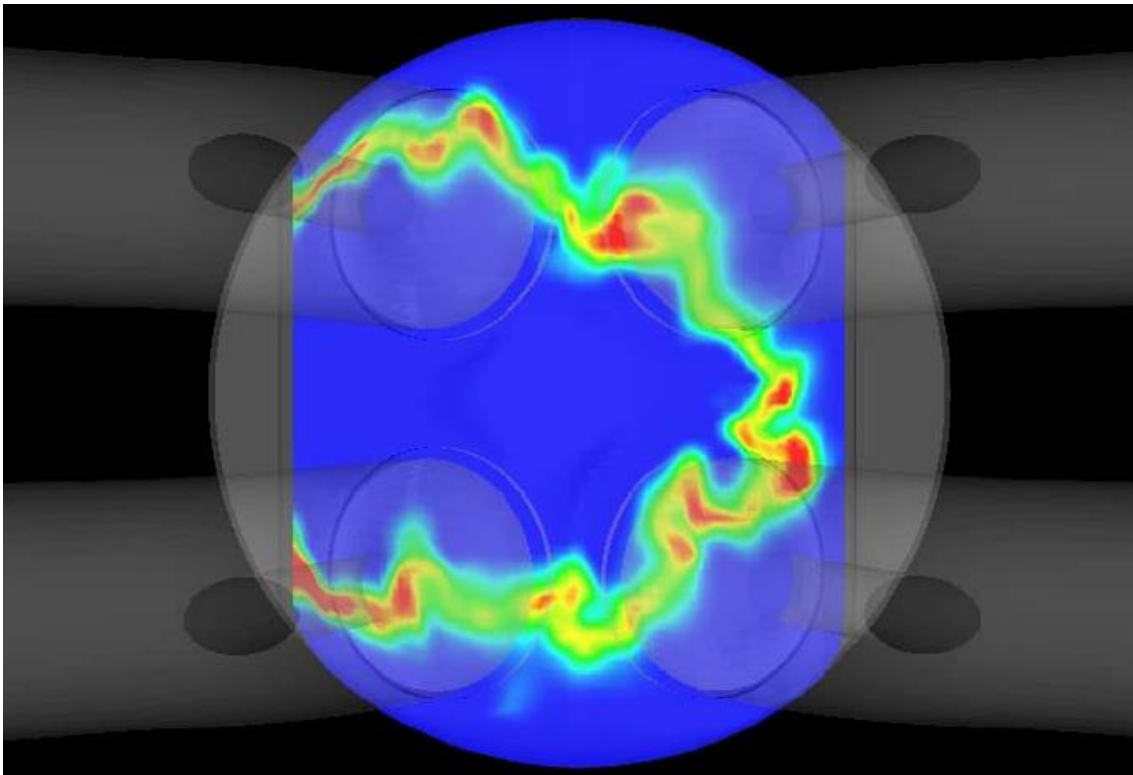


Figure 2.10 – Flame front propagation through combustion chamber, results of a CFD analysis [8]

The flame development and subsequent propagation vary cycle by-cycle. This is because flame growth depends on local mixture motion and composition. These quantities vary in successive cycles in any given cylinder and may vary cylinder-to-cylinder. Especially significant are mixture motion and composition in the vicinity of the spark plug at the time of spark discharge, since these govern the early stages of flame development. Cycle-by-cycle and cylinder-to-cylinder variations in combustion are important because the extreme cycles limit the operating regime of the engine.

The process described so far, in which the spark-ignited flame moves steadily across the combustion chamber until the charge is fully consumed, represents a normal combustion event.

However, several factors prevent this normal combustion process from occurring. Knock is the most important abnormal combustion phenomenon. Its name comes from the noise that results from the auto ignition of a portion of the fuel, air, residual gas mixture ahead of the advancing flame. As the flame propagates across the combustion chamber, the unburned mixture ahead of the flame is compressed, causing its pressure, temperature and density to increase. The unburned mixture may then auto ignite before the arrival of the flame front: when this abnormal combustion process takes place, an extremely rapid release of the chemical energy occurs, causing very high local pressures and the propagation of high frequency pressure waves of substantial amplitude across the combustion chamber, that produce the sharp metallic noise called "knock". Figure 2.11 shows the characteristics of a knocking combustion and how these are changing, from ignition up to the formation of a standing wave.

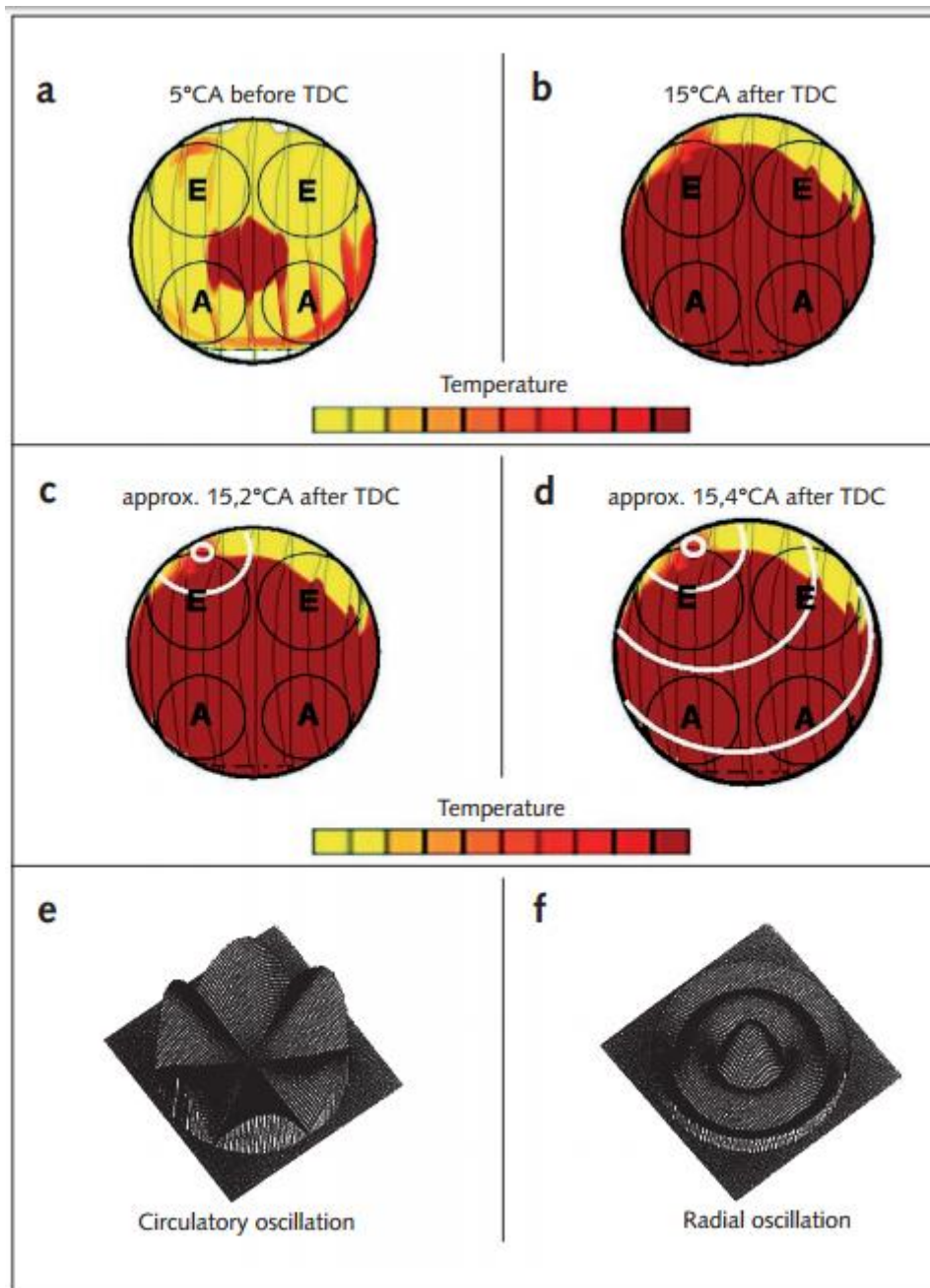


Figure 2.11 - Flame development, auto ignition and pressure wave propagation through the combustion chamber during a knocking combustion event [15].

Following ignition, the propagation of the primary flame front (Figure 2.11a and Figure 2.11b, border line between light and dark cylinder areas) takes place starting from the spark plug. The part of the mixture that remains unburned is called the "end gas zone", within which temperature gradients may exist and in which spontaneous ignition is liable to occur (Figure 2.11c). In the event of spontaneous ignition, the pressure in the ignition volume may not distribute fast enough over the whole combustion chamber, leading to the formation of a shock wave which propagates at the speed of sound through the surrounding un-burnt and already burnt mixture (Figure 2.11c, 2.11d). This

shock wave is reflected off the walls of the combustion chamber and moves around the combustion chamber again in the opposite direction, similar to an echo.

2.3.2 Pressure Signal

Combustion rate information can be obtained from in-cylinder pressure data. Cylinder pressure changes, as function of the crank angle, results from cylinder volume change, combustion process, heat transfer to chamber walls, flow into and out of crevice regions and leakage.

Cylinder pressure is usually measured with piezoelectric pressure transducers. This type of transducer contains a quartz crystal. One end of the crystal is exposed through a diaphragm to the cylinder pressure. As the cylinder pressure increases, the crystal is compressed and generates an electric charge which is proportional to the pressure. The piezoelectric pressure signal is synchronized to the crank angle position through an incremental encoder.

At the end of the compression phase, the spark ignites the gas mixture and the combustion begins. The combustion increases pressure and temperature in the cylinder. A typical pressure profile in the cylinder during the compression and expansion phase is shown in Figure 2.12. The dashed curve shows the pressure in the cylinder when no combustion occurs (motored cycle).

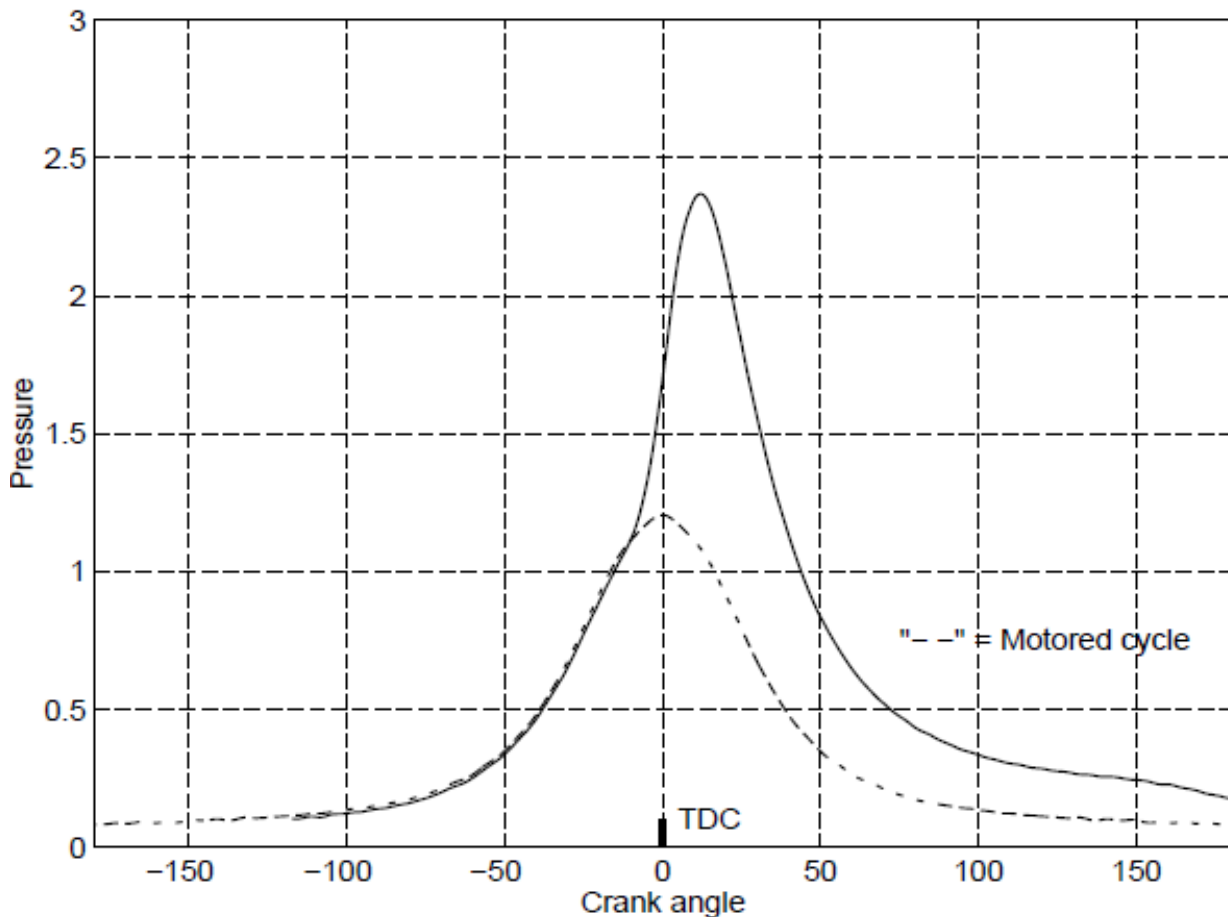


Figure 2.12 - Pressure development for a motored cycle and a cycle where combustion occurs. [16]

In case of combustion, before TDC the pressure begins to increase over the background pressure (continuous line in Figure 2.12). After the crank has passed TDC the volume starts to increase, still the pressure increases due to the combustion. At approximately 15°CA after TDC the pressure reaches its maximum. At this point the combustion is almost completed and the volume expands more rapidly, hence the pressure decreases.

The pressure versus crank angle curves shown in Figure 2.13a allow to understand why engine torque (at given engine speed and intake manifold conditions) varies as spark timing is varied. If the start of the combustion process is progressively advanced before top dead center, the compression stroke work transfer (which is from the piston to the cylinder gases) increases. If the end of the combustion process is progressively delayed by retarding the spark timing the peak cylinder pressure occurs later in the expansion stroke and is reduced in magnitude. These changes reduce the expansion stroke work transfer from the cylinder gases to the piston. The optimum timing which gives the maximum brake torque (called Maximum Brake Torque, or MBT timing) occurs when the magnitudes of these two opposing trends just offset each other. Timing which is advanced or retarded from this optimum gives lower torque. The optimum spark setting will depend on the rate

of flame development and propagation, the length of the flame travel path across the combustion chamber and the details of the flame termination process after it reaches the wall. These depend on engine design and operating conditions, and the properties of the fuel, air and burned gas mixture. Figure 2.13b shows the effect of variations in spark timing on brake torque for a typical Spark-Ignition engine. In order to control the combustion phase to produce maximum work, the spark advance must be varied with different working conditions for the engine. The spark advance for an engine depends on many different parameters, as engine speed, engine load, Air/Fuel ratio, fuel composition, air temperature, air humidity and several other factors. Modern engine controllers measure several of these parameters and then compute a spark advance based on these measurements, as reported in Section 2.4.

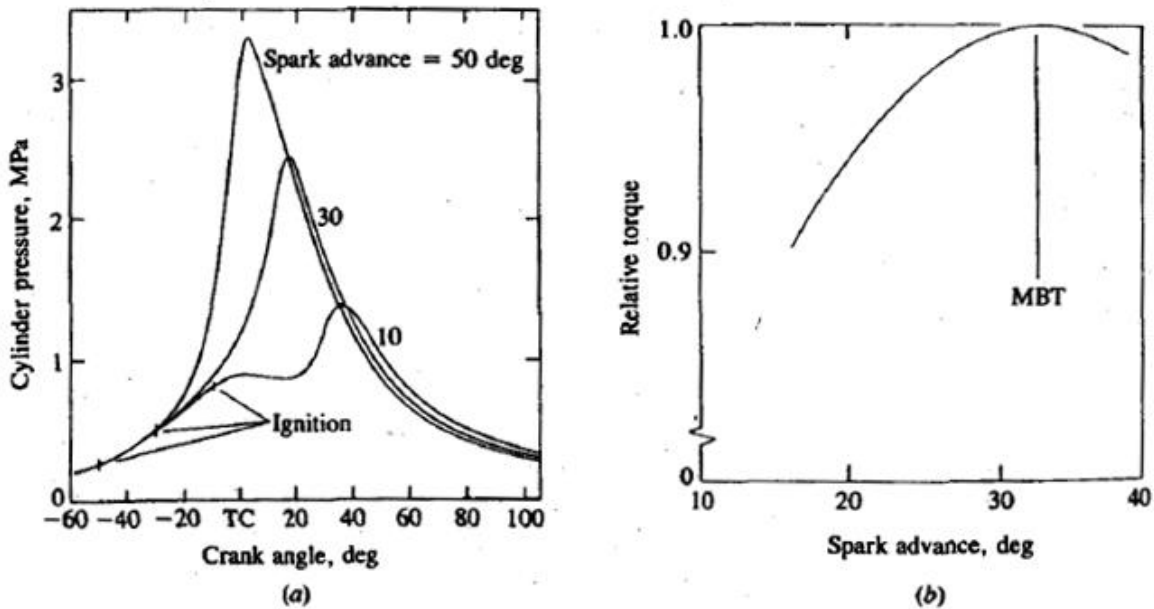


Figure 2.13 – (a) Cylinder pressure as function of the crank angle for over advanced spark timing (50°BTDC), maximum brake torque timing (30°BTDC), and retarded timing (10°BTDC). (b) Effect of spark advance on brake torque, normalized to its maximum value corresponding to MBT timing [13].

The in-cylinder pressure signal allows the calculation of certain combustion features, such as IMEP (Indicated Mean Effective Pressure), defined as follows:

$$IMEP = \frac{1}{V_{cyl}} \oint p(\theta) dV(\theta) \quad (2.1)$$

Where V_{cyl} stands for the displacement volume of the single cylinder. IMEP can be also defined as the uniform pressure that would be required throughout the power stroke of the cylinder to exchange the same amount of work done by the varying pressure that is in fact obtained during the stroke.

Observation of cylinder pressure for successive operating cycles shows the existence of important cycle-by-cycle variations. Since the pressure development is uniquely related to the combustion process, substantial variations in the combustion process, on a cycle-by-cycle basis, are occurring. These variations are important for two reasons. First, since the optimum spark timing is set for the "average" cycle, faster than average cycles have effectively over advanced spark timing, and slower cycles have retarded timing, resulting in losses in power and efficiency. Second, it is the extremes of the cyclic variations that limit engine operation, since the fastest burning cycles are most likely to knock under high-load conditions. Few cycles are those limiting spark advance from its optimal timing, thus limiting efficiency and performance. Figure 2.14 shows measured cylinder pressure for 100 consecutive engine cycles, on the same cylinder, with fixed engine operating conditions. The dispersion of the pressure curves is index of cycle-by-cycle variations.

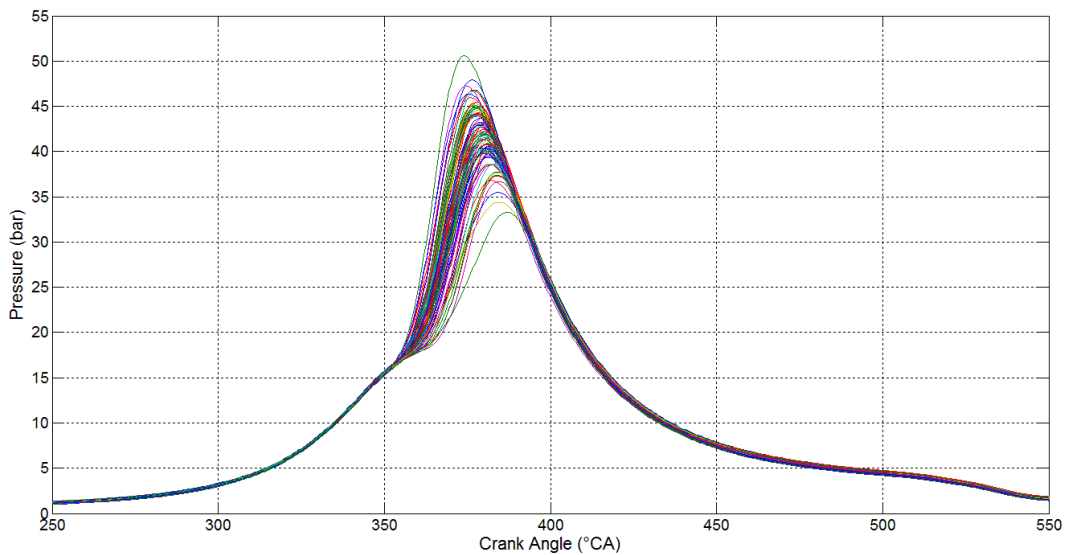


Figure 2.14 – An example of cycle-by-cycle variations on cylinder pressure for 100 consecutive engine cycles.

One important measure of cyclic variability, derived from pressure data, is the Coefficient of Variation of the Indicated Mean Effective Pressure. It is the standard deviation in IMEP divided by the mean IMEP, and is usually expressed in percent:

$$COV_{IMEP} = \frac{\sigma_{IMEP}}{\mu_{IMEP}} \cdot 100 \quad (2.2)$$

Another important information provided by the in-cylinder pressure is about the knocking condition. In case of a knocking combustion event, the cylinder pressure signal is overlaid with high frequency pressure oscillations; therefore the piezoelectric pressure transducer is the most useful monitoring device for knocking for research applications, because it can actually "see" the main

consequence of an abnormal combustion. In on-board applications, due to cost and reliability, nonintrusive sensors (accelerometers connected to the engine block) are mainly used.

Figure 2.15 clearly illustrates the effect of knocking combustion on in-cylinder pressure signal. Normal combustion, light knock and heavy knock conditions are respectively reported.

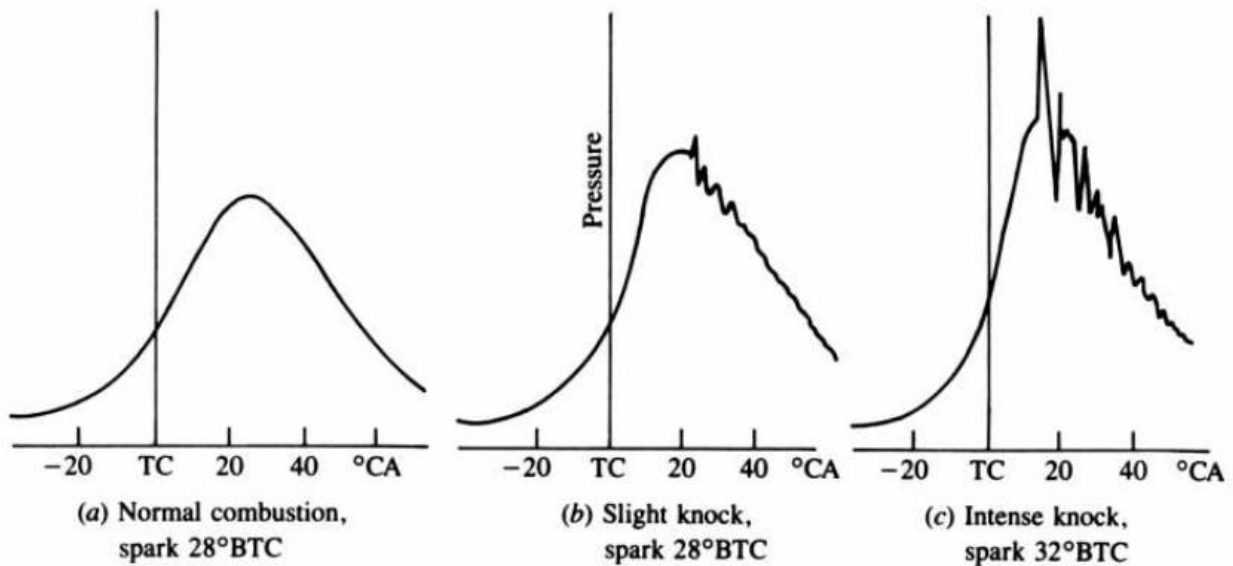


Figure 2.15 - Cylinder pressure versus crank angle traces of cycles with (a) normal combustion, (b) light knock, and (c) heavy knock [13].

Various algorithms are used to determine timing and intensity of knock. Signals generated by both accelerometer and pressure sensor are generally filtered in order to provide high frequency oscillations. MAPO (Maximum Amplitude Pressure Oscillation) is one of the most used pressure based knock index. It consists in filtering (band pass filter) the pressure curve and determining the maximum amplitude in a particular crank angle window:

$$MAPO = \max(|P_{bandpass}|) \quad (2.3)$$

2.3.3 Heat Release

As already mentioned, the main measurable effect of the combustion process is the rise of in-cylinder pressure. By using a heat release approach, based on the first law of thermodynamics, it is possible to relate directly the pressure changes to the amount of chemical energy released by the combustion. Figure 2.16 shows the open-system boundary (dotted line) adopted for the thermodynamic analysis of the combustion chamber.

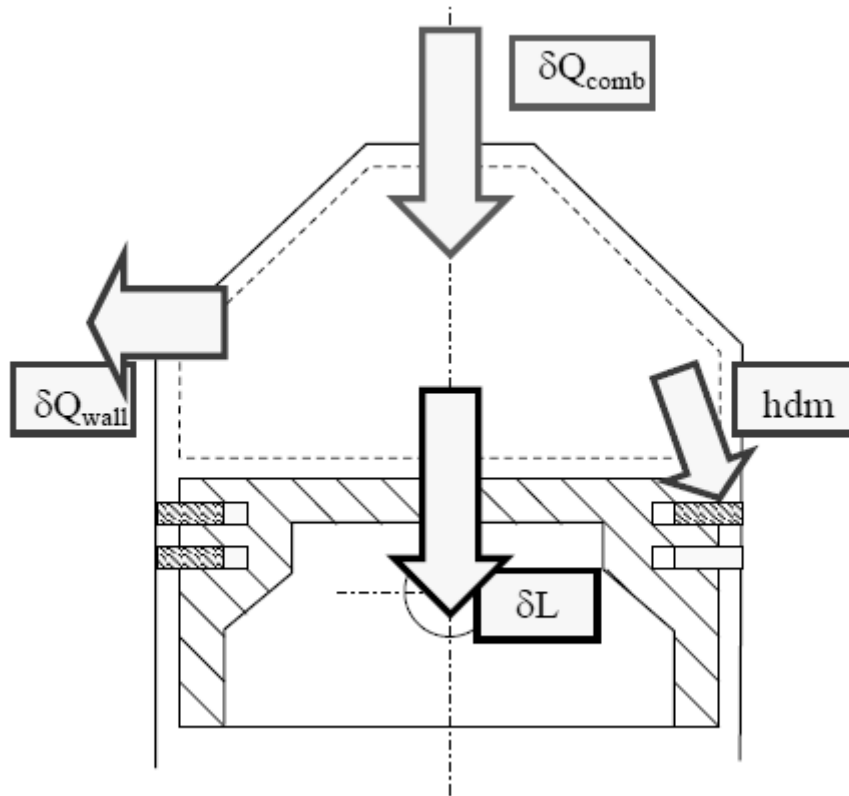


Figure 2.16 - Open system boundary for combustion chamber for heat-release analysis. Exhaust and intake valves are closed during combustion process. [14]

The first law of thermodynamics, applied to the control volume delimited by combustion chamber walls and considered as an open system, can be expressed as follow:

$$\delta Q_{comb} = dU_s + \delta Q_{wall} + \delta L + \Sigma_i h_i \cdot dm_i \quad (2.4)$$

Where:

- δQ_{comb} represents the heat released by the combustion process;
- δQ_{wall} is the heat exchanged with the chamber walls;
- dU_s is the variation of system's internal energy;
- δL is the work done by the gas on the piston;
- $h_i \cdot dm_i$ is the enthalpy variation relative to mass dm_i which pass through the control volume surface (blow by)

Assuming the gas in the cylinder to behave like an ideal gas, with constant and uniform temperature T (mass-averaged cylinder temperature during combustion since the molecular weights of the burned and unburned gases are essentially identical [13]), then:

$$U_s = m \cdot c_v \cdot T \quad (2.5)$$

Derived:

$$dU_s = m \cdot c_v(T) \cdot dT + u(T) \cdot dm \quad (2.6)$$

Where the second term is zero in case of no mass exchange through the contour surface ($dm = 0$). Substituting the expression of the work done by the gas on the cylinder ($\delta L = p \cdot dV$) in the Eq. (2.4):

$$\delta Q_{comb} = m \cdot c_v \cdot dT + u \cdot dm + \delta Q_{wall} + p \cdot dV + \sum_i h_i \cdot dm_i \quad (2.7)$$

And indicating with $dm_{cr}(= dm_i = -dm)$ the losses in mass due to crevice effects, and with h' their sensible enthalpy:

$$\delta Q_{comb} = m \cdot c_v \cdot dT + \delta Q_{wall} + p \cdot dV + (h' - u) \cdot dm_{cr} \quad (2.8)$$

This equation represents the gross heat released during the combustion process. The net heat release can be obtained from Equation (2.8), less heat lost to the walls and crevice effects:

$$\delta Q_{net} = \delta Q_{comb} - \delta Q_{wall} - (h' - u) \cdot dm_{cr} = m \cdot c_v \cdot dT + p \cdot dV \quad (2.9)$$

By expressing temperature as function of pressure and volume (under the hypothesis of ideal gas):

$$T = \frac{p \cdot V}{m \cdot R} \quad (2.10)$$

And considering the mass m constant:

$$dT = \frac{1}{m \cdot R} (p \cdot dV + V \cdot dp) \quad (2.11)$$

Substituting in the expression of Net Heat Release (2.9) and introducing $R = c_p - c_v$ and $\gamma = \frac{c_p}{c_v}$:

$$\frac{\delta Q_{net}}{\delta \vartheta} = \left(\frac{\gamma}{\gamma - 1} \right) \cdot p \cdot \frac{dV}{\delta \vartheta} + \left(\frac{1}{\gamma - 1} \right) \cdot V \cdot \frac{dp}{\delta \vartheta} \quad (2.12)$$

Expression (2.12) represents the Net Heat Release versus crank angle infinitesimal increment. This quantity is measurable starting from pressure signal and volume function and with a simple model for γ . "Net" because only the sensible energy change and work transfer to the piston is taken into account. The Gross Heat Release is thus higher, due to heat transfer to the wall and blow by effects.

In Figure 2.17, the Net Heat Release versus crank angle (indicated as ROHR – Rate of Heat Release (J/°CA)) is reported for different spark advance values, together with the corresponding pressure signal. Retarding the ignition results in slower combustion, with lower ROHR peak value.

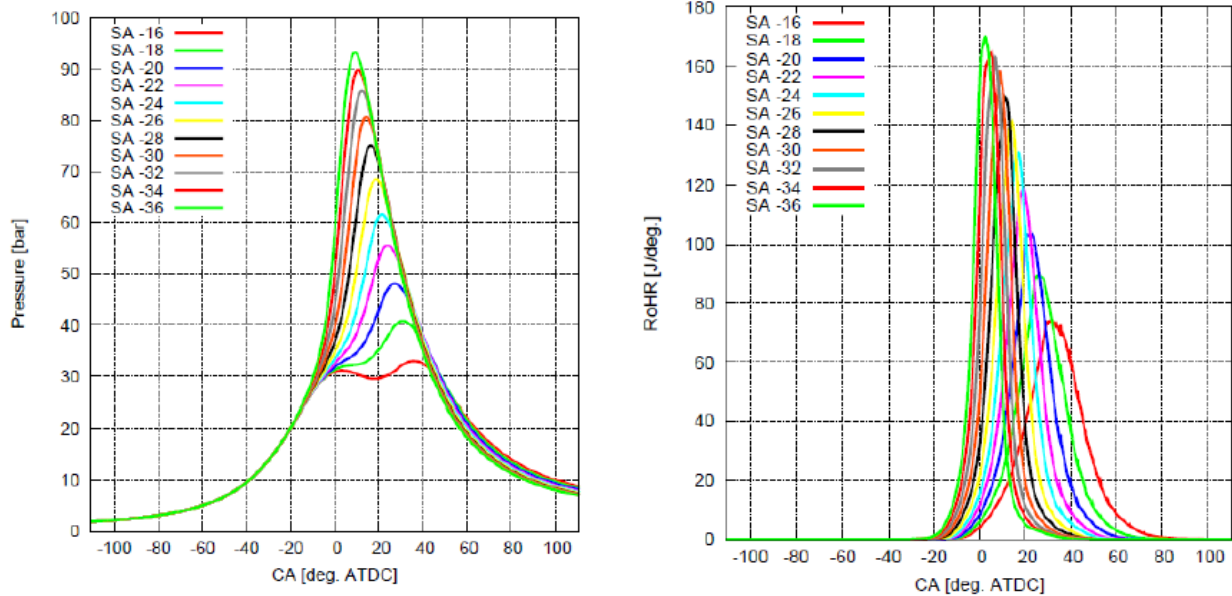


Figure 2.17 – Pressure signal on the left (bar) and corresponding net heat release profile on the right (Joule/°CA), calculated with Eq. (2.9), for different ignition timing versus crank angle [8].

Figure 2.18 shows, for different ignition timing, the Net Heat Release profile (ROHR) and its integration. The Net Heat Release profile obtained from integrating Eq. 2.12), normalized to give unity at its maximum value, is often interpreted as the burned mass fraction (or, more correctly, the energy-release fraction) versus crank angle profile.

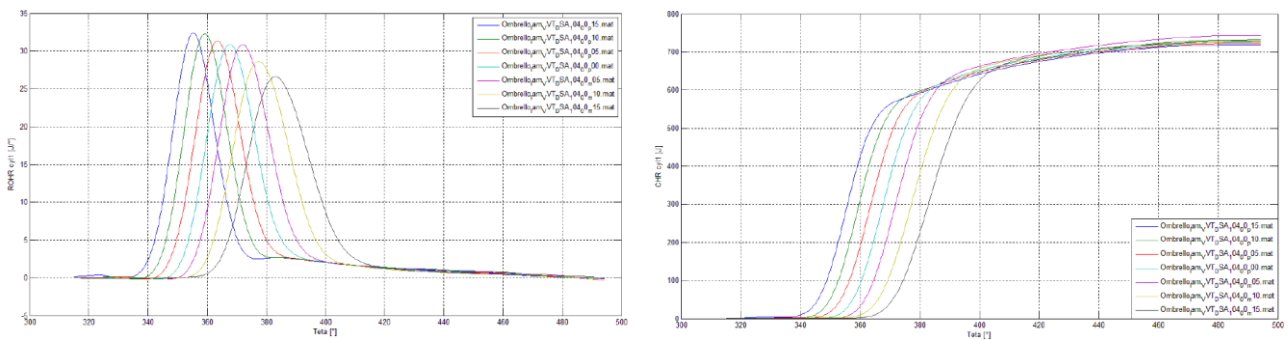


Figure 2.18 – On the left, Net heat release (Joule/°CA) versus crank angle and, on the right, its integrating profile, also known as Cumulative Heat Release (CHR), measured in Joule, for different ignition timing [14]

2.3.4 Combustion Phase Indicators

The Mass Fraction Burned profile as a function of crank angle can therefore be assimilated to the Net Heat Release integral curve, normalized to give unity at its maximum value. The rate at which fuel-air mixture burns increases from a low value, immediately following the spark discharge, to a maximum about halfway through the burning process and then decreases to close to zero as the combustion process ends. It is convenient to use these Mass Fraction Burned profiles to characterize different stages of the spark-ignition engine combustion process by their duration and position in crank angles.

Figure 2.19 reports the main MFB (Mass Fraction Burned) angles used to describe the combustion process development.

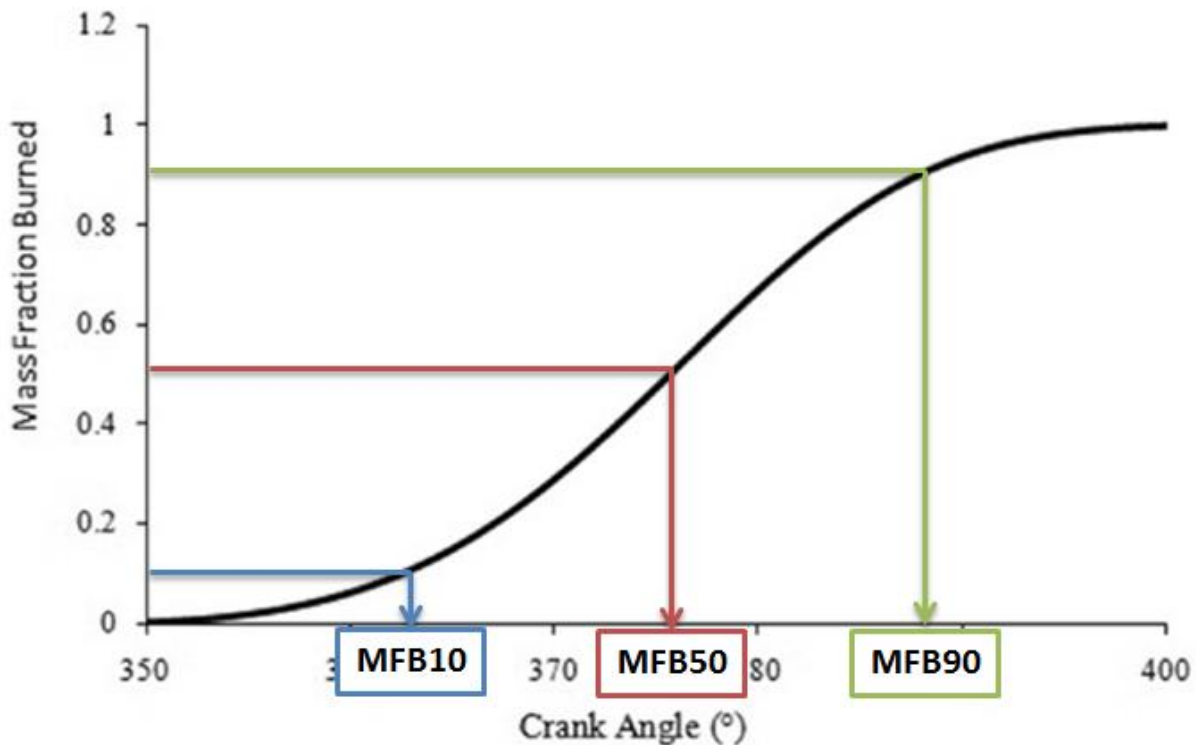


Figure 2.19 – Main Mass Fraction Burned angles.

The flame development process, from the spark discharge which initiates the combustion process to the point where a small but measurable fraction of the charge has burned, it's influenced primarily by the mixture state, composition, and motion in the vicinity of the spark plug. The duration of this first combustion stage can be identified by the MFB0-10 interval.

The stage during which the major portion of the charge burns as the flame propagates to the chamber walls is next. The MFB50 angle, corresponding to 50% mass fraction burnt, is the main combustion phase indicator used in this work of thesis. The spark advance well correlates with the MFB50 angle. In the final stage, the remainder of the charge burns to completion.

Another index for combustion phasing is APMAX. It expresses, in crank angle degrees, the position of the pressure signal peak and can be easily evaluated directly from the pressure curve without calculating the heat release function.

2.4 Engine Control Unit

In the last years, the development of electronic control systems in the automotive industry has been fundamental for innovation and to meet market's demand for low fuel consumption and emission. Engine control itself has taken over numerous additional responsibilities than just ignition and injection control. The main tasks of a modern engine control unit can be summarized as follows:

- control normal engine operations;
- reduce fuel consumption;
- reduce pollutant emission and diagnose of all emission related components ;
- diagnose malfunctioning;
- improve drivability;
- integrate with other vehicle control system.

In the next paragraphs an overview of a modern vehicle torque structure is given: the main inputs and outputs of a modern engine control unit are presented, along with the ignition angle control loop, important to better understand the main topic of this work of thesis.

2.4.1 Vehicle Torque Structure

All interventions for drivetrain and vehicle control can be converted in torque requests to the engine. Aim of a modern vehicle torque structure is to coordinate these demands and to provide a target torque value for the engine control unit. The engine control unit must then run the engine, through a series of actuators, to provide the desired torque in the most efficient way. Figure 2.20 summarizes the main torque requests from vehicle subsystems. Torque coordination is decentralized at different physical levels and it is engine independent. The interface between vehicle torque request and engine control unit is sharply defined.

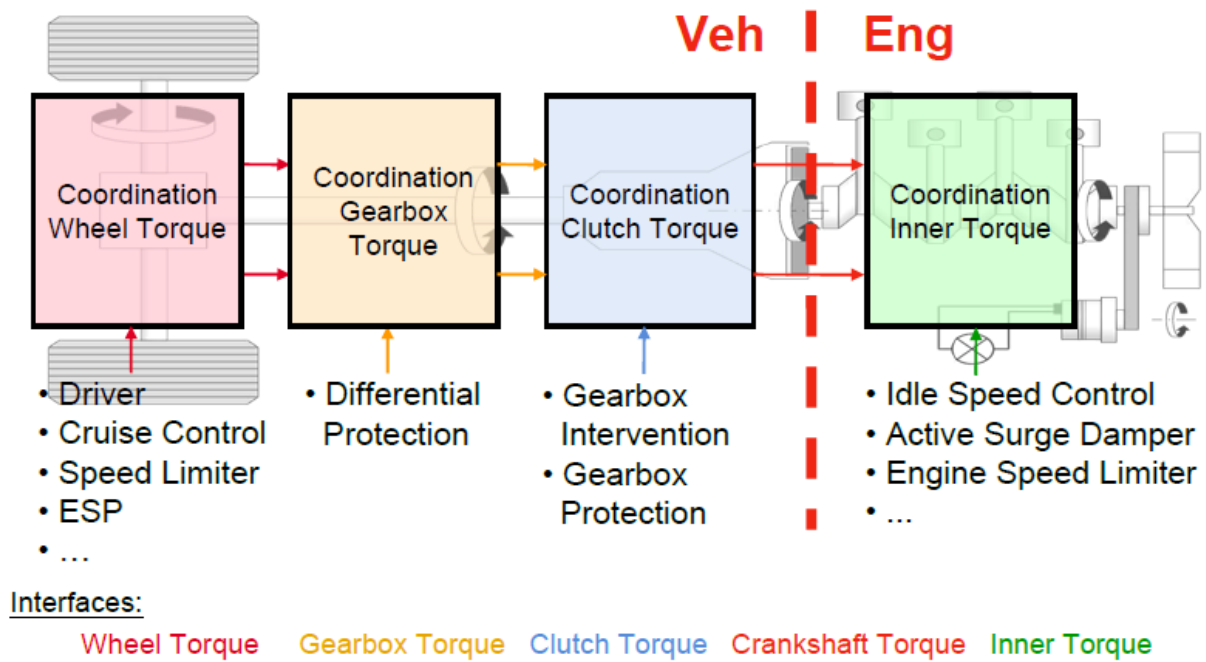


Figure 2.20 – Vehicle torque structure. All torque requests are coordinated at different physical levels and converted into a single torque request to the engine.

2.4.2 Sensor and Actuators of a Modern Engine Management System

The Engine Control Unit allows achieving, through the use of the calculation power, optimum efficiency, drivability and torque output targets. The idea behind the system is to fully integrate and regulate all engine system parameters, thereby enabling fuel delivery, spark timing and throttle control functions to be controlled by the same unit.

In a modern powertrain, through the extensive use of electrical components and sensors, always fewer are the mechanical connections between driver and engine. All requests are processed by the Engine Control Unit before they are converted into set values for different actuators. Focusing on the engine management system, Figure 2.21 illustrates the main sensors and actuators available to the Engine Control Unit. The layout presented refers to a modern Gasoline Direct Injected and turbocharged unit.

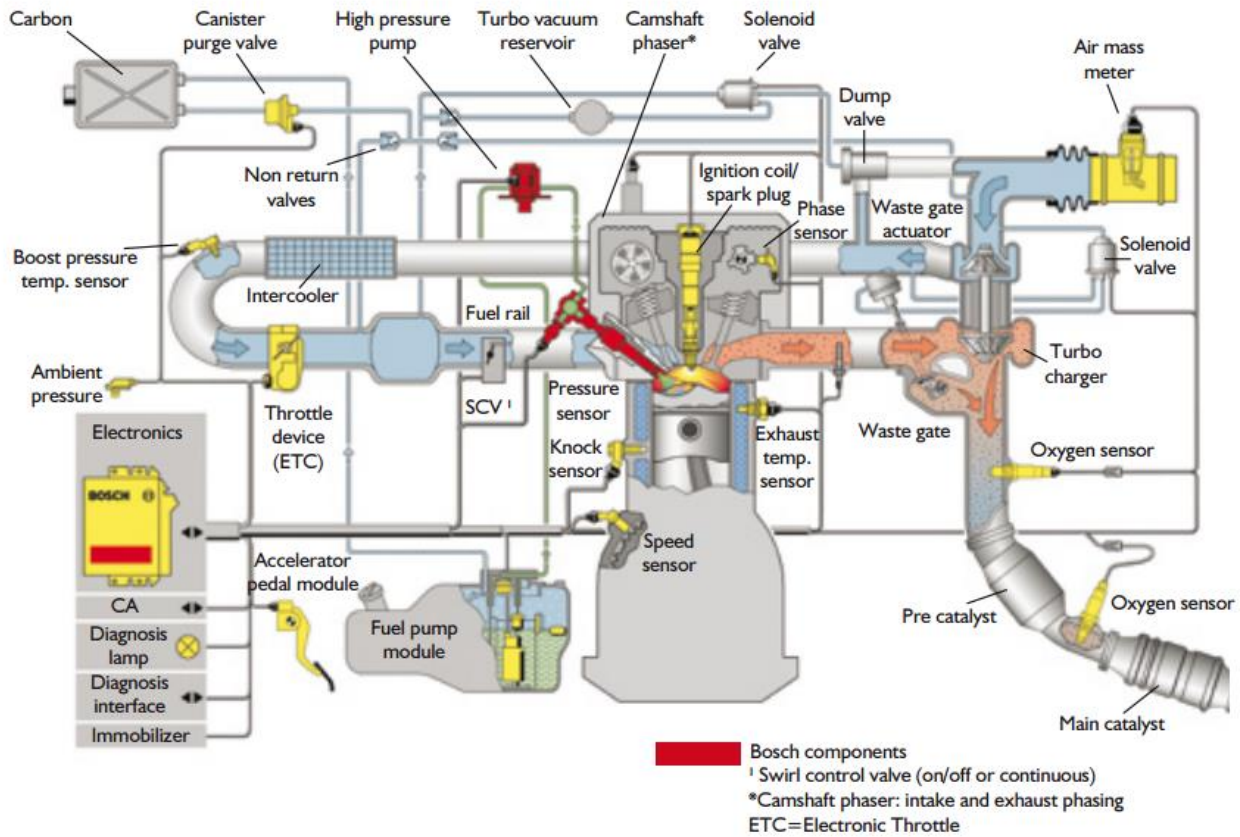


Figure 2.21 – Schematic view of a modern Engine Management System by Bosch.

Output torque is the main goal to be persecuted by the engine control unit. In a spark ignition engine, it is mainly influenced by the quantity of air and fuel introduced in the cylinders, which is primarily controlled by throttle (and waste gate, in turbocharged engines) position. Relation (2.13) express effective engine power output, where $V_c \frac{P_{coll}}{RT_{coll}} \eta_{vol}$ is the mass of air that takes part in the combustion process.

$$P_{eff} = V_c \frac{P_{coll}}{RT_{coll}} \eta_{vol} K' \eta_{tot} \frac{n}{2} \quad (2.13)$$

Besides throttle position, there are other variables that influence the delivered torque, such as ignition timing, air to fuel ratio, valve timing, engine temperature and so on. To manage all these variables, various control functions are implemented in the ECU. Among them, four of the main control loops implemented in the engine control unit are [17]:

- the fuel-injection feed forward loop;
- the air/fuel ratio feedback loop;
- the ignition angle feed forward loop;
- the knock feedback loop.

2.4.3 Ignition Angle Control Loop

One of the most important parameters affecting internal combustion engine efficiency is represented by the combustion phase, which in a Spark Ignition engine is mainly controlled by phasing the spark discharge, or spark advance timing. The Engine Control Unit, hence, performs an open-loop control of the combustion phase on the base of proper spark advance maps predetermined on bench tests and stored in memory.

Figure 2.22 provides a simplified overview of the ignition angle control loop. The final result is the ignition angle, or $zwout$.

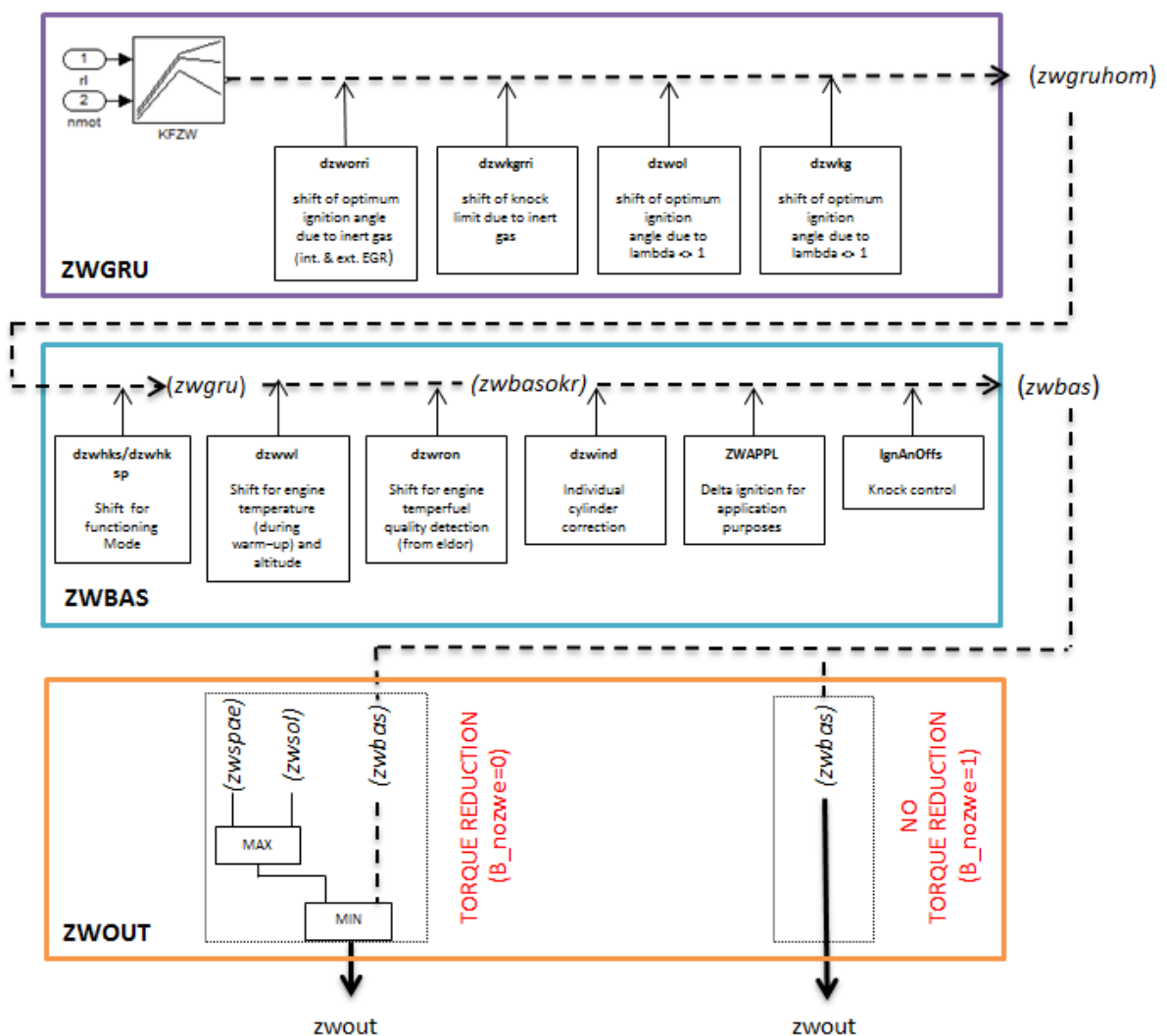


Figure 2.22 – Spark advance calculation path

Task of the functions *ZWBAS* is to provide the earliest possible ignition angle, starting from the base ignition angle provided by the function *ZWGRU*. Starting from a pilot control map for ignition timing (*KFZW*), function of relative air charge (*rl*) and engine speed (*nmot*), the spark advance value is then modified through a series of corrections. Influence of air/fuel ratio, residual gas,

functioning mode, engine temperature, ambient pressure, fuel quality and presence of abnormal combustions is taken into account. If no request for torque reduction via an ignition angle intervention is present ($B_{nozwe}=1$), the spark advance value provided by the function *ZWBAS* is enabled. Otherwise, the spark advance carried out is provided by the engine torque structure (*zwsol*). Torque reduction through an ignition angle variation can be applied in the case of catalyst heating, when higher exhaust temperature are requested, anti-jerk intervention or idle torque reserve.

It shall be noticed that this fundamental engine parameter is currently controlled in open-loop by means of lookup tables. With the ionization current system adopted by Ferrari, described in the next paragraph, it is already possible to close the spark advance control loop under abnormal or critical conditions (knocking, misfire, pre-ignition...) with feedback on the combustion process derived from the ion current signal: purpose of this work is to evaluate the feasibility of a closed loop control under normal operating condition.

2.5 Ionization Current for Ignition Control

The ionization current signal is strictly related to many parameters of the combustion and among them the pressure, which is an important possible feedback for spark advance control. One advantage with measuring the ionization current, instead of the pressure, is that it makes use of already existing equipment, commercially available in cars, such as the spark plug and electronics [18]. Measuring the ionization current inside the cylinder is thus an alternative to measuring the pressure signal.

Ion current measurement system is currently employed by all production Ferrari engines, and features of the ion signal are made available at every combustion event by a dedicated control unit.

In this Paragraph, a brief literature study is performed and presented to give a background about the ionization current signal. The principle for measuring ion current is described, along with the signal's main features. In the last paragraph, the actual applications on Ferrari engines are presented.

2.5.1 Ion Generating Process and Measurement

The ionization process can shortly be described as follows. The heat in the flame front ionizes the gas in the combustion chamber and the gas becomes conductive. An electric field is applied in the combustion chamber and the generated current is measured. The ionization degree depends on the temperature in the cylinder, which is strongly connected to the pressure inside the cylinder. The result is that the ionization current contains information about the pressure and the combustion process.

The measurement system for ion current employed by Ferrari uses the spark plug as a probe for detecting the ionization levels. The spark plug has the advantage that it is already mounted (no extra costs). A potential disadvantage is the spark ignition itself, since no useful ionization signal is retrieved during this phase. When the ignition ends, the spark plug is again available for measurement during the remaining part of the combustion.

The principle for measuring, as described earlier, is to create an electric field in the combustion chamber and measure the current through the spark plug gap. The measuring equipment, shown in Figure 2.23, is positioned at the high voltage side of the ignition coil, which implies that the circuits must be protected from the high voltage pulse that generates the spark through high voltage diodes. As reported in Figure 2.23, during the spark phase, the energy associated to the spark is used to charge a capacitor. Once the ignition process is completed, the energy stored in the capacitor is

gradually discharged, due to the generation of the ion current between the spark gap. The signal is measured in voltage through calibrated resistances.

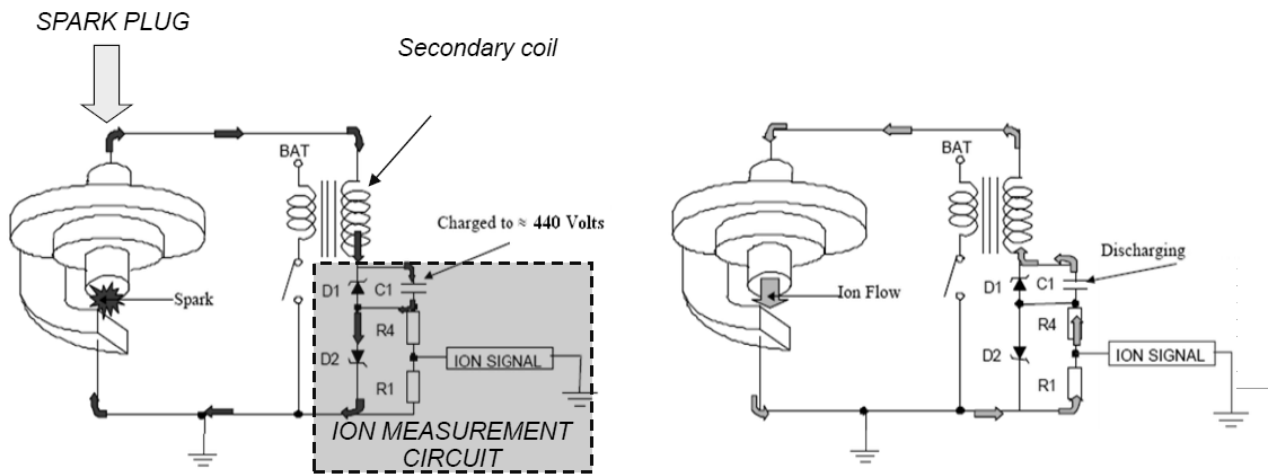


Figure 2.23 - Ionization measurement circuit at the high voltage side of the ignition coil. Electric current flow during spark discharge (left) and during ion current measurement phase (right). The spark plug is the ion current sensor inside the combustion chamber. [19]

2.5.2 Ionization Current Feature

In Figure 2.24, a characteristic ionization signal is reported, together with the corresponding pressure signal measured through a piezoelectric sensor. The ion signal is characterized by three main phases: ignition, chemical and thermal phase.

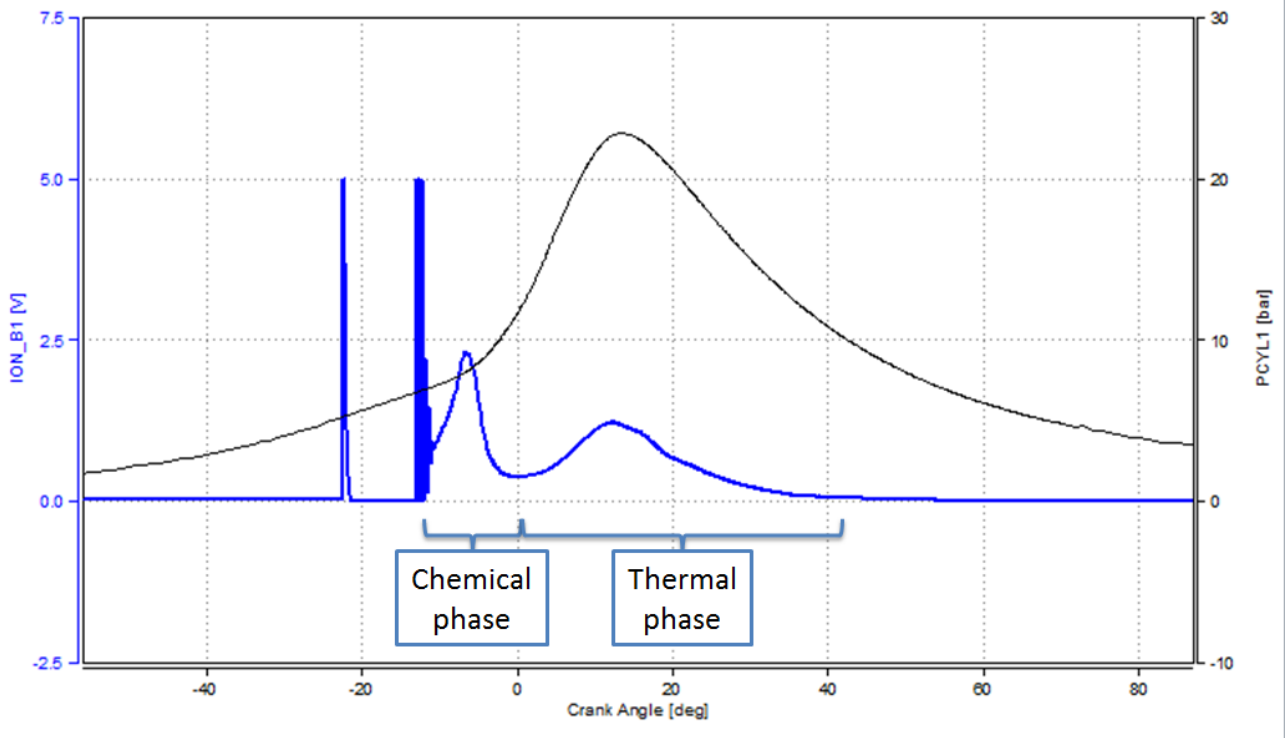


Figure 2.24 - Ionization current (in blue), with the chemical and thermal phase highlighted, and pressure signal (in black). The Ionization current follows the pressure signal in the thermal phase.

In the ignition phase the ion signal is disturbed by the ignition pulse generated by the coil (the spike just before the chemical phase). Immediately following the spark discharge, the ion signal is characterized by the presence of two main peaks: the first one is associated to chemical ionization, while the latter to thermal ionization.

The first peak, called chemical peak, is caused by ions generated in the flame front. The flame front is only close to the spark plug for a short period, then it propagates through the combustion chamber, causing the ionization of the gas between the spark plug electrodes to decrease.

The ion current then rises again, leading to the second peak, or thermal peak. Here the ionization is associated with the high temperature resulting from the combustion, due to its effects on the ion concentration. Since temperature and pressure are closely related, ideally $pV = nRT$, the ionization signal follows the pressure signal (reported in black) to some degree in this latter phase.

2.5.3 Ionization Current Applications for Ferrari

The ion measurement system is currently adopted on all new Ferrari engines. Ionization current for every cylinder is measured and processed in real-time by a dedicated control unit. Through the analysis of the ion current it's possible to obtain important information about the combustion for each cycle and for each cylinder, without the installation of pressure sensors. The main applications for ion current system in Ferrari concern:

- Knock detection and control;
- Misfire detection and control;
- Mega knock detection and control;
- Octane rating detection.

As the ion signal is strongly correlated to the temperature and therefore to the pressure in the combustion chamber, information from ion current signals can be used to identify and quantify knocking combustion events.

To prove this correlation, Figure 2.25 reports both the pressure and the ion signal during a knocking combustion. High frequency oscillations, symptoms of abnormal combustion, can be seen on both signals.

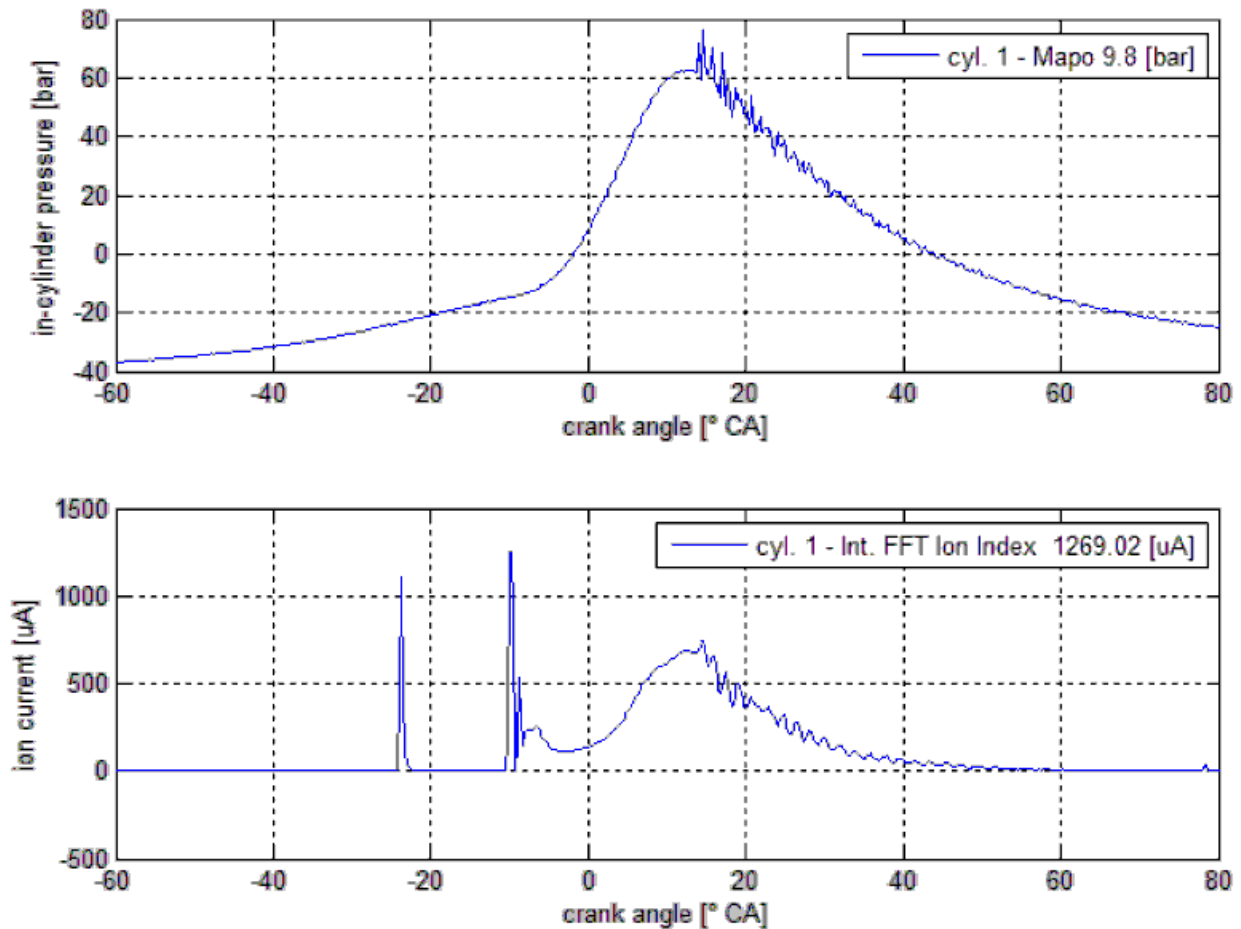


Figure 2.25 – Effect of a knocking combustion on in-cylinder pressure signal (upper diagram) and ion current signal (lower diagram). High frequency oscillation are visible in both signals.

To detect the knock level, the first step is the definition of a knock index, derived from the ion signal, that well correlates with a reference knock index evaluated from the pressure signal. The most used (and reliable) knock index is the MAPO, which is the Maximum absolute Amplitude of the Pressure Oscillation due to a knock event (see Paragraph 2.3).

Most of the calibration process consists in the determination of the optimal frequency window for the calculation of the ion derived knock index. The choice of these parameters is made through an optimization process, whose target is the maximum correlation with MAPO. Once the knock index from ion current signal is available, it can be used as a feedback for knock control. In case of knocking combustion, the control requires, cylinder by cylinder, individual spark advance corrections, with different strategies depending on the intensity of the event.

A particularly dangerous event, due to the great amount of energy released in a small time interval, is the ignition of the whole mixture charge before the spark discharge. This phenomenon, called pre-ignition or “Mega knock”, can be identified through the measurement of the ion current during

the coil charge phase. In fact, an ion current before the ignition spark can be measured only in case of pre-ignition. If a Mega knock is detected, the engine control unit can take different actions to prevent successive Mega knock events, such as mixture enrichment, variable valve timing overlap reduction or load reduction.

Figure 2.26 shows a further application of the ion current signal. In this case, it is used to recognize the so called “misfire”, or missing combustion.

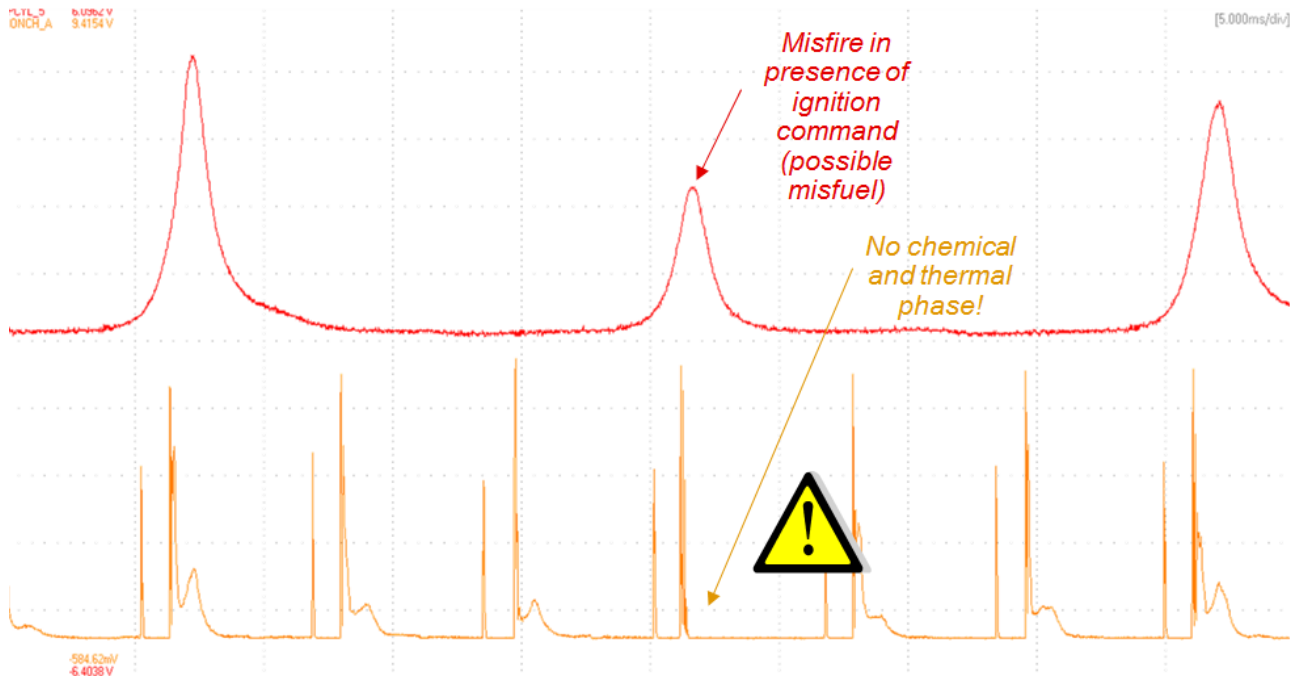


Figure 2.26 - Pressure signal (red) and ion current signal (orange) for normal and misfiring cycle. Chemical and thermal phase are absent, index of missing ionization inside the cylinder (i.e. no combustion).

It is possible to define an index for the mean amplitude of the chemical and thermal signal phase and use the difference between this index and a calibrated threshold to identify a misfiring cycle. In the specific case of Figure 2.26, the ion signal highlights the presence of the spark ignition, while the chemical and thermal phase are absent, since no combustion occurs (as confirmed by the corresponding pressure signal, reported in red).

3 Correlation Analysis

The results of an experimental measurement campaign at the engine test bench are presented in this Chapter. Aim of the experimental activity is to quantify the correlation level between combustion features derived respectively from the pressure signal and from the ionization current signal. Since the physical phenomenon to be controlled is the combustion phase, the following indicators are measured and analyzed: the pressure peak location and the Mass Fraction Burned angles, derived from the pressure signal, and the thermal phase peak position evaluated from the ionization current signal. This last index is chosen since a strong correlation is reported by various authors ([20],[21],[22]) with the pressure based phase indicators. The experimental activity is carried on entirely at the test bench on a Ferrari turbocharged engine.

Experimental results from a post-processing correlation analysis, based on the “raw” signals of pressure and ionization current, are presented in Paragraph 3.1.

Paragraph 3.2 focuses on the performance evaluation of a real time algorithm for ion thermal peak detection. The results from the real time analysis are compared with the results from a post processing analysis based on “raw” ionization current signal. An error in the conversion process from the sample based system of the Ion Control Unit to the angle-based system is identified, together with a possible solution. Further combustion features, that can be found both on the pressure and on the ionization signal, are presented in Paragraph 3.3.

3.1 Offline Processing of Raw Signals

The results from a post-processing analysis of the “raw” pressure and ionization current signals are presented in this Section. The indicators for combustion phasing are evaluated through a specific post-processing script, whose inputs are the high frequency sampled pressure and the ion current signal, measured for every cylinder and every engine cycle. The analysis based on the raw signals helps evaluating the physical correlation between the two sources of information, neglecting the performance of the real-time algorithm for ion current processing (see Paragraph 3.2).

3.1.1 Offline Algorithm

The ion current feature to be extracted from the signal is the location of the thermal phase peak (see Paragraph 2.5). To define the corresponding angle in an efficient way, the ion signal is windowed around the angular position corresponding to the maximum of the pressure signal, “APMAX”, as reported in Figure 3.1. This procedure presumes the availability of the pressure signal, therefore it cannot be used for real-time on-board applications, but just for a preliminary correlation analysis.

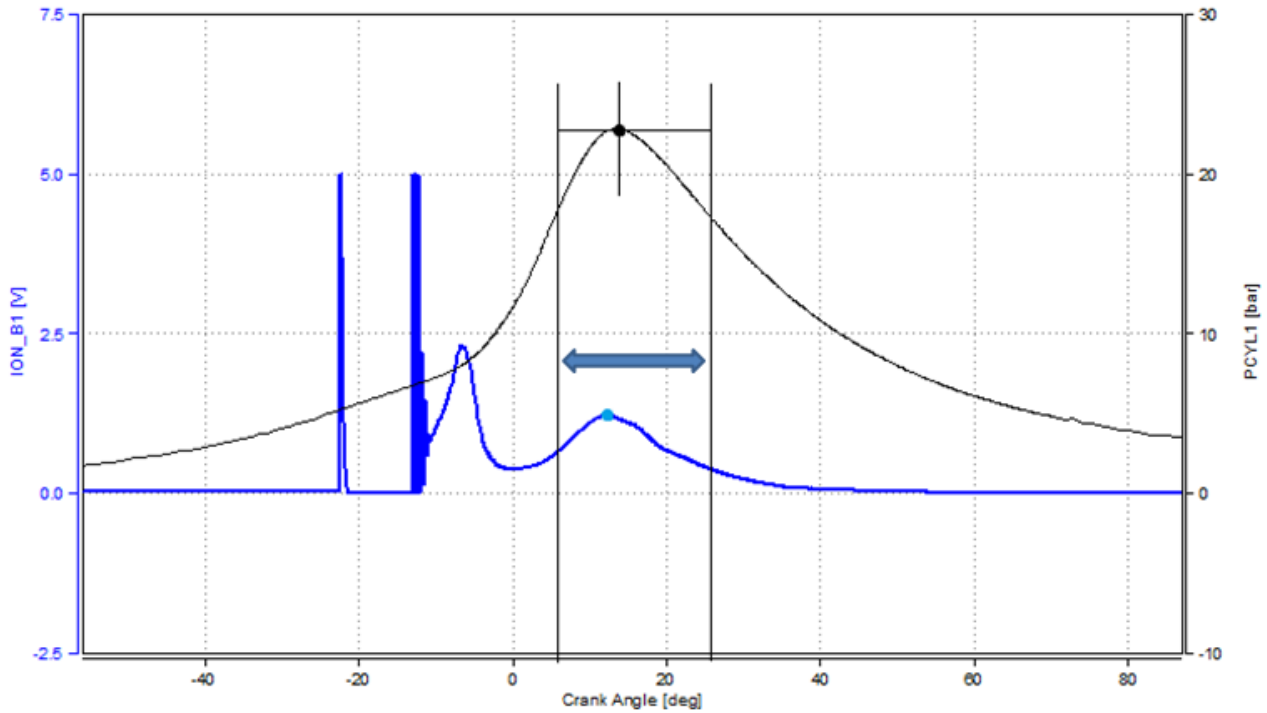


Figure 3.1 - Thermal phase peak position on ion raw signal (blue). The location algorithm starts from the maximum pressure angle position APMAX.

In case the ion current peak is not found in the window defined around APMAX, the algorithm iteratively shifts the ion observation window on the basis of the ion signal gradient. In case the algorithm does not converge to the thermal peak location, the corresponding engine cycle for the specific cylinder is excluded from the analysis.

3.1.2 Experimental Activity

The pressure and ion signals have been measured during a series of steady state tests conducted for 18 different spark advance values (each test comprises 500 engine cycles at constant spark advance). The investigated engine operating conditions, reported in Table 3.1, comprehend different loads and temperatures.

Table 3.1 - Engine operating conditions for test bench data collection. The combustion phase is changed by adjusting the applied spark advance (18 different values for each operating condition).

		Engine Speed (rev/min)	
		1000	
BMEP (bar)	1	T_H2O=75°C	
	3	T_H2O=30°C T_H2O=53°C T_H2O=75°C	
	6	T_H2O=75°C	

The raw signals, both ion and pressure, are acquired with a fixed angular resolution of 0.1°CA, which, at 1000 rpm, corresponds to 60 kHz sampling frequency. During the steady state measurements, all the main actuators of the engine are fixed to the reference calibrated conditions (with no spark advance correction): air to fuel ratio, camshaft position, injection phase and pressure and throttle position. This last actuator is used to regulate the engine to produce the desired BMEP with the reference spark advance value set.

3.1.3 Raw Signal Correlation Results

In this paragraph the correlation results between raw pressure and ion signal are presented. The analyzed indicators are:

- APMAX (°CA): angular position of the peak of pressure signal;
- MFB50 (°CA): angular position corresponding to 50% Mass Fraction Burned, derived from the pressure signal through the heat release analysis (see Paragraph 2.3);
- AThPeak (°CA): ion current thermal phase peak location, evaluated from the raw signal (see 3.1.1).

To measure how well the linear regression line approximates the real data points, the coefficient of determination, denoted R^2 , is used:

$$R^2 = 1 - \frac{\sum_{i=1}^n (y_i - \hat{y}_i)^2}{\sum_{i=1}^n (y_i - \bar{y}_i)^2} \quad (3.1)$$

Where y_i are the observed values of the dependent variable, \bar{y}_i their mean value, and \hat{y}_i are the fitted values.

R^2 equal to 1 indicates a perfect fit, while a zero value indicates that there is no correlation between the two signals.

Correlation diagrams respectively between MFB50 and AThPeak, and between APMAX and AThPeak, are reported in Figures 3.2 and 3.3. All data refer to Cylinder 2, BMEP 3 bar and 1000 rpm. For each stationary test at fixed spark advance, 500 engine cycles have been measured.

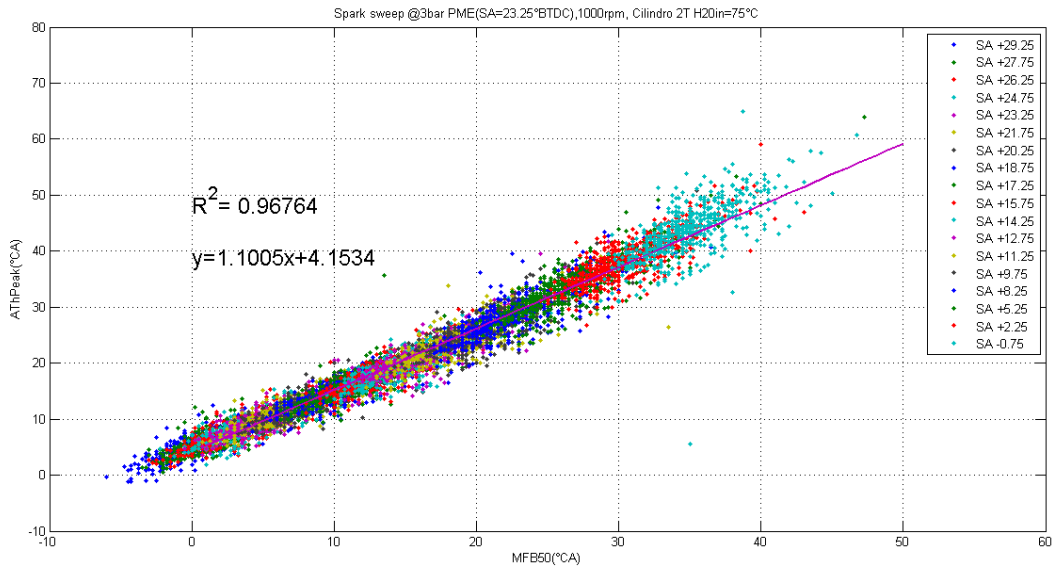


Figure 3.2 – MFB50 (from heat release analysis of the pressure signal) and AThPeak (from ion current signal). Only data from Cylinder 2 are shown.

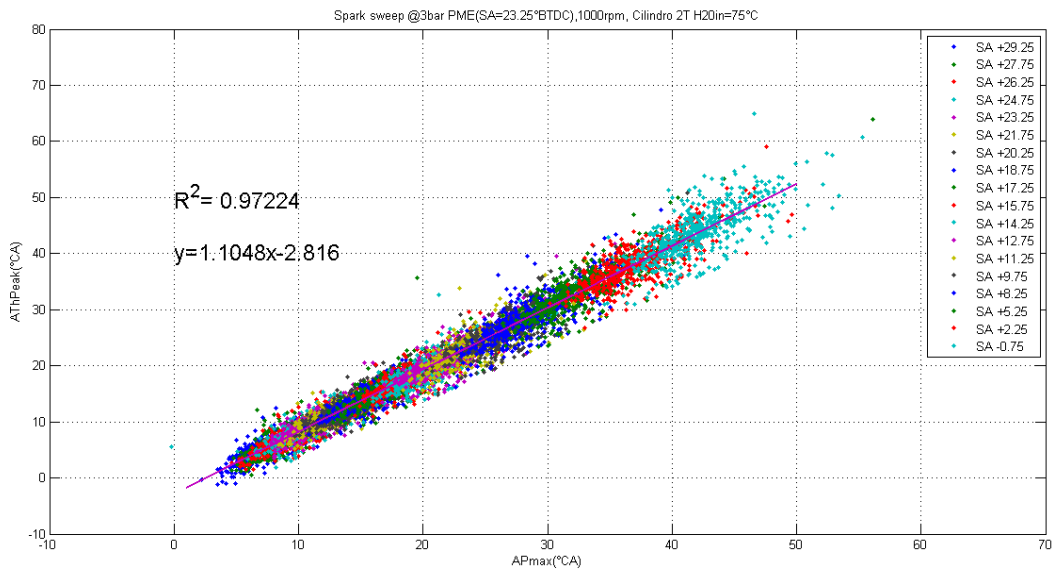


Figure 3.3 – APMAX (from pressure signal) and AThPeak (from ion current signal). Only data from Cylinder 2 are shown.

Results from all 8 cylinders are reported in Figure 3.4, in terms of MFB50 versus AThPeak, while results for different operating conditions are summarized in Table 3.2. Data from all 8 cylinders are considered.

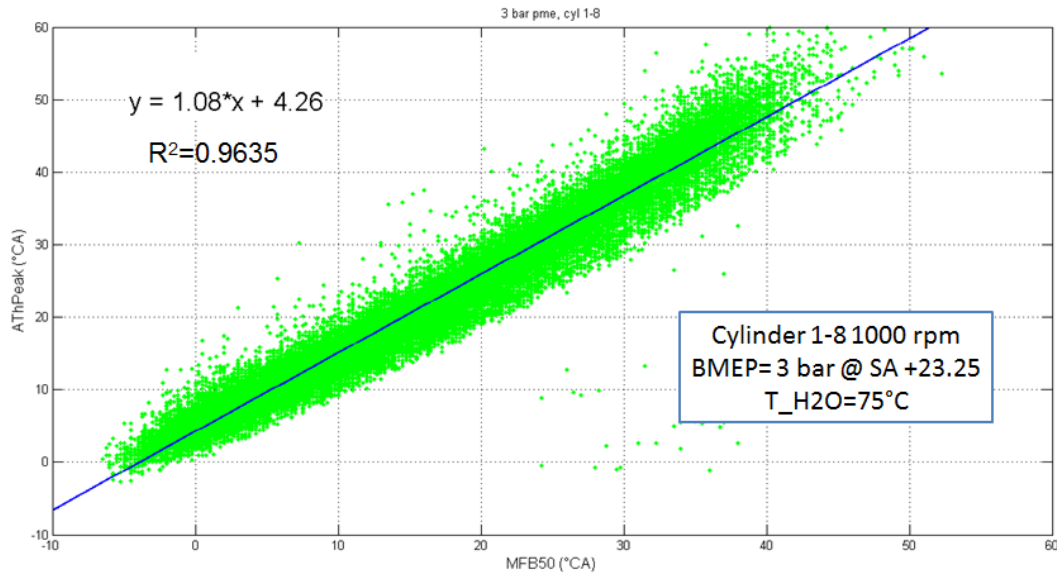


Figure 3.4 - MFB50 (from heat release analysis of the pressure signal) and AThPeak (from ion current signal) for all cylinders and 18 different ignition timings.

Table 3.2 – Summary of correlation results for different operating conditions (1000 rpm, IMEP 1-3-6 bar) in terms of MFB50 versus AThPeak.

BMEP (bar)	Linear Regression MFB50(°CA) / AThPeak(°CA)	R ²
1	AThPeak = 1.01*MFB50 + 5.21	0.9244
3	AThPeak = 1.08*MFB50 + 4.26	0.9635
6	AThPeak = 1.03*MFB50 + 4.55	0.9712

Since MFB50 and AThPeak show a very high correlation level, even their variation is linked: when the combustion development varies due to cycle-to-cycle variation, a higher dispersion on both MFB50 and AThPeak angles is observed. Figure 3.5 illustrates the correlation diagram between the standard deviation of MFB50 and AThPeak. Every point represents the behavior of a single cylinder over a steady state measurement of 500 engine cycles. This relation could be deepened with measurements in operating conditions characterized by high cycle-to-cycle variations (for example, cycles with retarded spark advance timing).

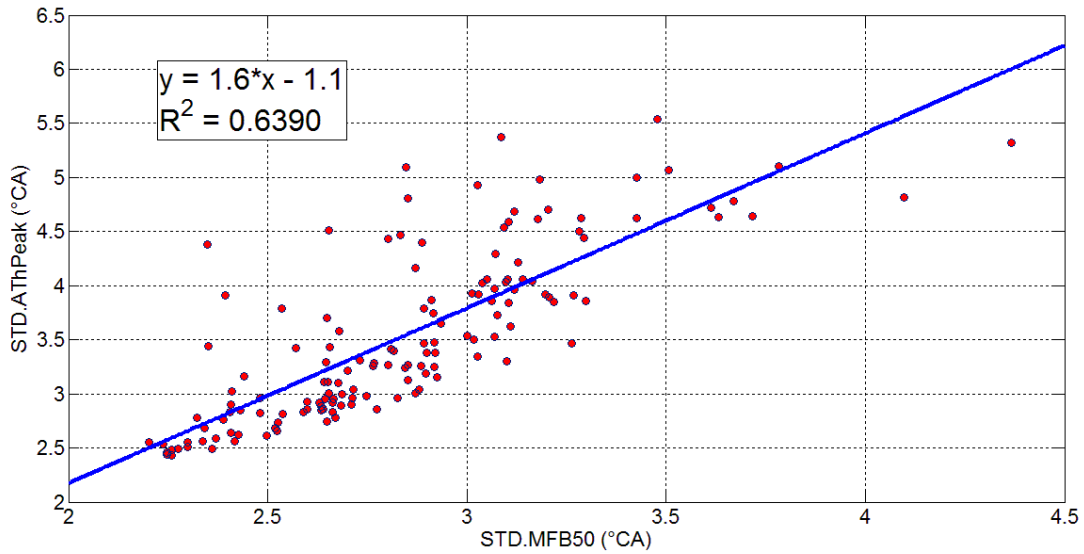


Figure 3.5 - Relation between MFB50 variability and AThPeak variability, evaluated over 500 consecutive engine cycles with given SA. The Standard Deviation is used to quantify the dispersion of the data.

Influence of engine temperature is taken into account at the engine operating conditions of 3 bar BMEP and 1000 rpm. The tests are made by varying the cooling water temperature entering the engine block. Results from complete spark sweeps at 3 different temperatures are summarized in Figure 3.6. No significant differences in terms of correlation between MFB50 and AThPeak are observed.

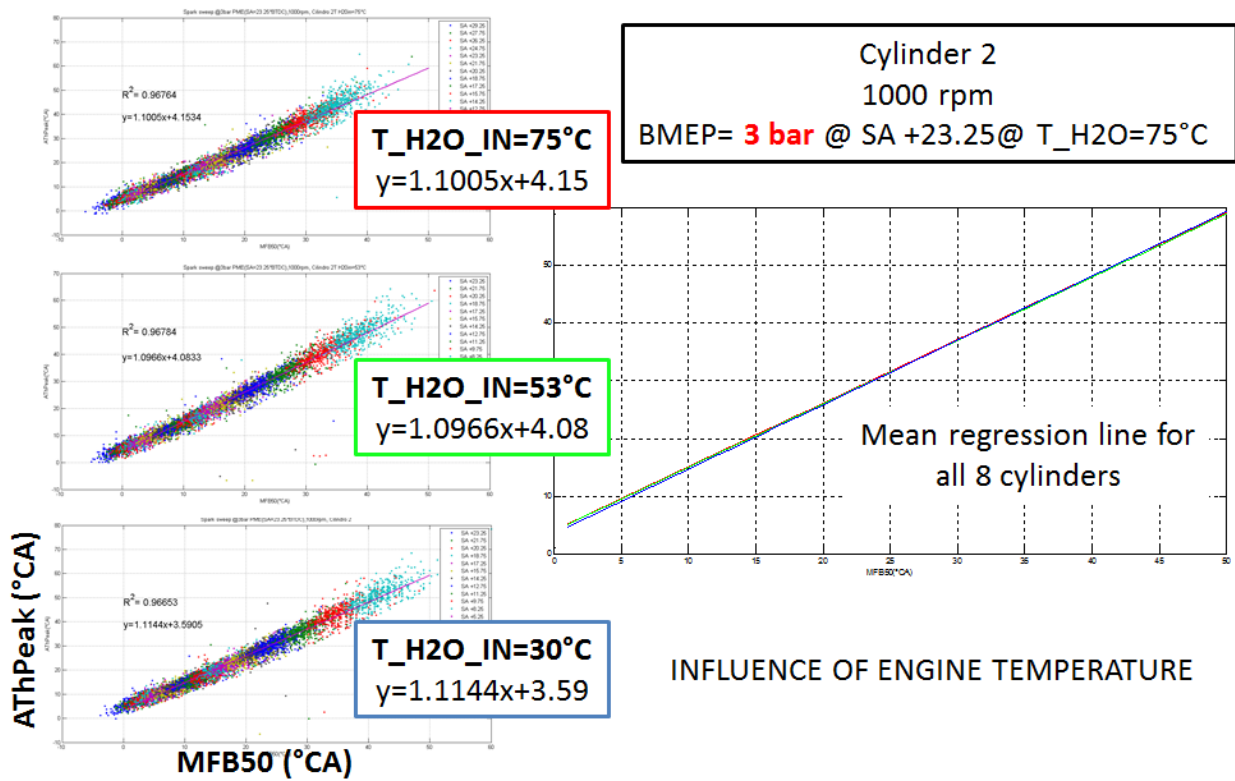


Figure 3.6 – Correlation between MFB50 (from heat release analysis of the pressure signal) and AThPeak (from ion current signal) at different engine temperatures. Engine operating conditions of 3 bar BMEP and 1000 rpm (at 75°C water temperature)

3.2 Real Time Processing of Ion Signal

In this Section the results from the real time processing of the ionization current signal are presented. As a consequence of the high correlation levels presented in Paragraph 3.1, the software of the ion current control unit has been modified in cooperation with the manufacturer. The developed software prototype allows the evaluation of the thermal peak location every combustion event and for every cylinder. This value is called “ThPeakAngle”, to distinguish it from the one evaluated in post-processing from the raw ion current signal (AThPeak).

The identification algorithm is no longer based on the peak pressure signal location, since this measure is not usually available on-board. “ThPeakAngle” can be indeed used for control purposes, since it makes use of hardware structure already present on every Ferrari engine.

An experimental campaign is made at the test bench to evaluate the performance of the real time algorithm for ion thermal peak location. The results are compared with the ion thermal peak location evaluated from the post-processing analysis of the raw signal (Section 3.1).

3.2.1 Experimental Activity Requirements

Target of the experimental activity is the validation of the algorithm for the ion current thermal peak identification. The data to be collected can be summarized as follows:

- AThPeak for every cycle and cylinder, measured from the raw ion signal, and several combustion parameters extracted from the pressure signal (APMAX, IMEP, MBF...);
- The corresponding ThPeakAngle for every cycle and cylinder, calculated by the ion current control unit every combustion, together with other features calculated by the ion current control unit;

To obtain a perfect correspondence, a complex post processing alignment operation is requested, since:

- Ion raw signal (and so the corresponding AThPeak) and ThPeakAngle, evaluated real time, are sampled with different frequencies, with different measurement systems and different delays: a time-based resampling is thus not possible.
- In stationary tests with given spark advance, the variation in AThPeak and ThPeakAngle does not allow to define if a correct alignment is reached. Dynamic spark sweeps, with great variation of spark advance in the same acquisition, and thus on both AThPeak and ThPeakAngle, are necessary for a correct alignment (the step is used as reference).

- No correspondence between cycles definition: for the indicating system one cycle corresponds to all cylinders fired in geometric order, while for the ion system one cycle means all cylinders fired in firing order. Need to re-sample the cyclic combustion parameters (APMAX, IMEP, MFB...).

The raw ion signals are sampled through the combustion analysis system with a 0.1°CA angular resolution as in Section 3.1. Since electrical noise on the ion signal is generated while measuring ion current with the ordinary combustion analysis system, causing detection fault in the ion control unit, an alternative On-Board Indicating system is used for this application (Alma Automotive OBI M2).

The ThPeakAngles are calculated by the ion current control unit every combustion, published via CAN as soon as the calculation is completed and then sampled every 5ms by the measurement software (INCA). The acquisition system layout is schematized in Figure 3.7.

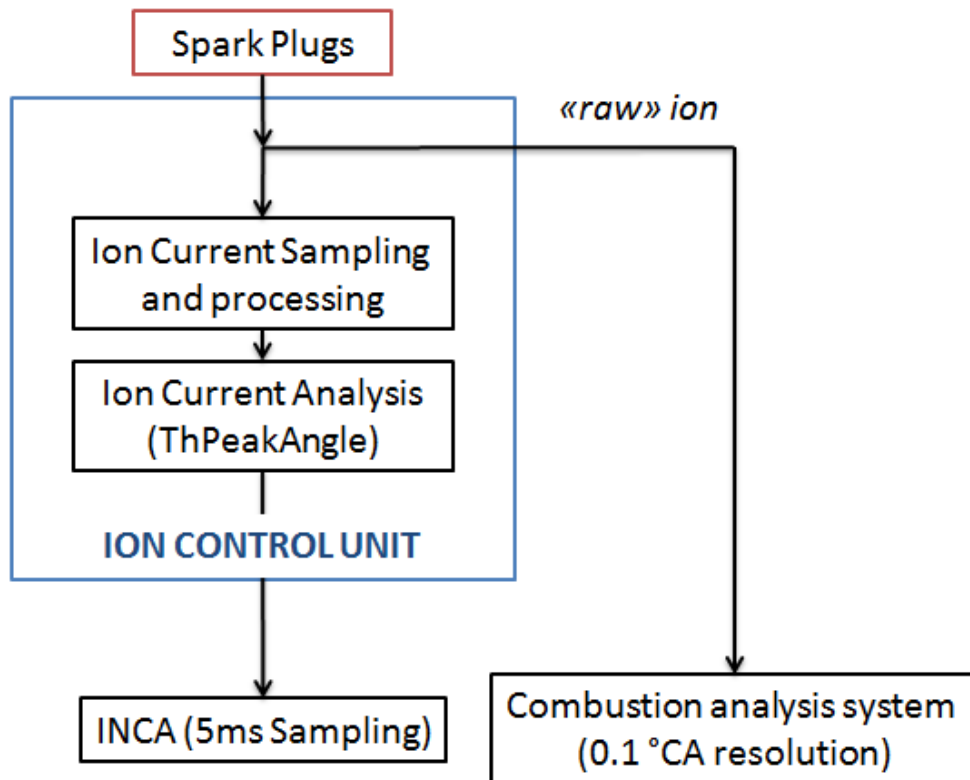


Figure 3.7 - Schematic layout of the experimental setup for measuring both the ion raw signal and ion real-time feature, evaluated by the ion control unit.

The “raw” ion signals are sampled through analog outputs placed on the ion control unit, as visible in Figure 3.8. Only 4 analog outputs are visible, since each of them is used for 2 cylinders.



Figure 3.8 – Ion current control unit with additional analog outputs for raw ion signal measurement.

3.2.2 Dynamic Spark Sweep

During this part of the activity, the correlation with the MFB50 from the pressure signal is not considered, since only the performance of the real-time algorithm are investigated. The first set of measures consists in the execution of dynamic spark sweeps: during a unique acquisition of around 740 engine cycles, the spark advance is initially varied with steps of 30°CA , then with smaller variations (see the effect on ThPeakAngle and AThPeak in Figure 3.9 and 3.10). The idea is to use the steps to perfectly align each ThPeakAngle with the corresponding AThPeak , and to verify whether the correct alignment is maintained throughout the end of the acquisition (no “mistakes” during the re-sampling process). Figures 3.9 and 3.10 report the results for cylinder 3 and 5. The upper diagrams confirm the correct alignment between the two quantities (AThPeak and ThPeakAngle) for the given cylinder. The correlation diagram is reported below.

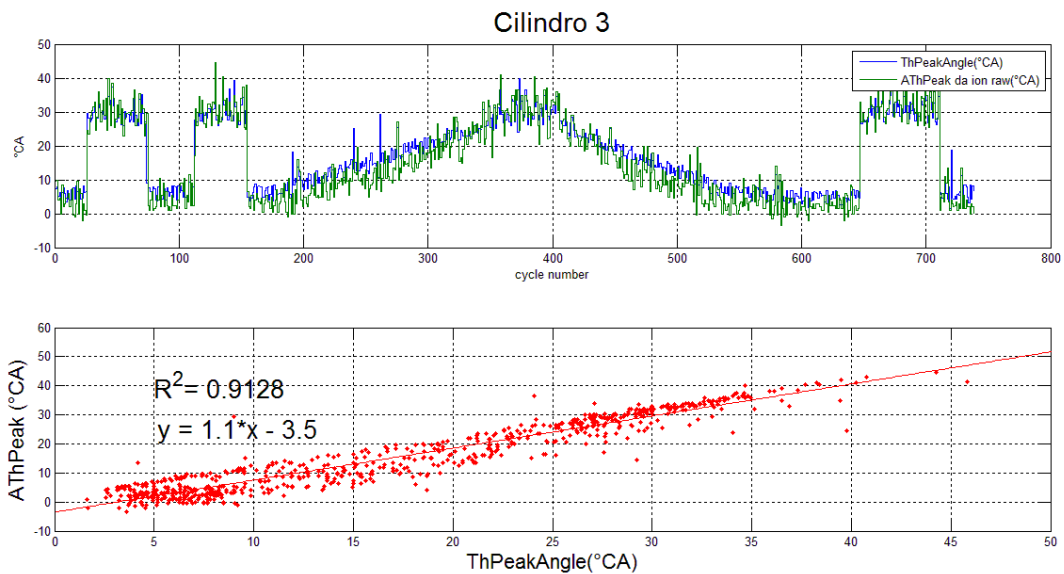


Figure 3.9 – Angular position of the ion thermal peak for cylinder 3, as evaluated from the raw ion signal analysis (AThPeak) and from the real time algorithm implemented in the ion control unit (ThPeakAngle). The test condition are 1000 rpm and 3bar of BMEP.

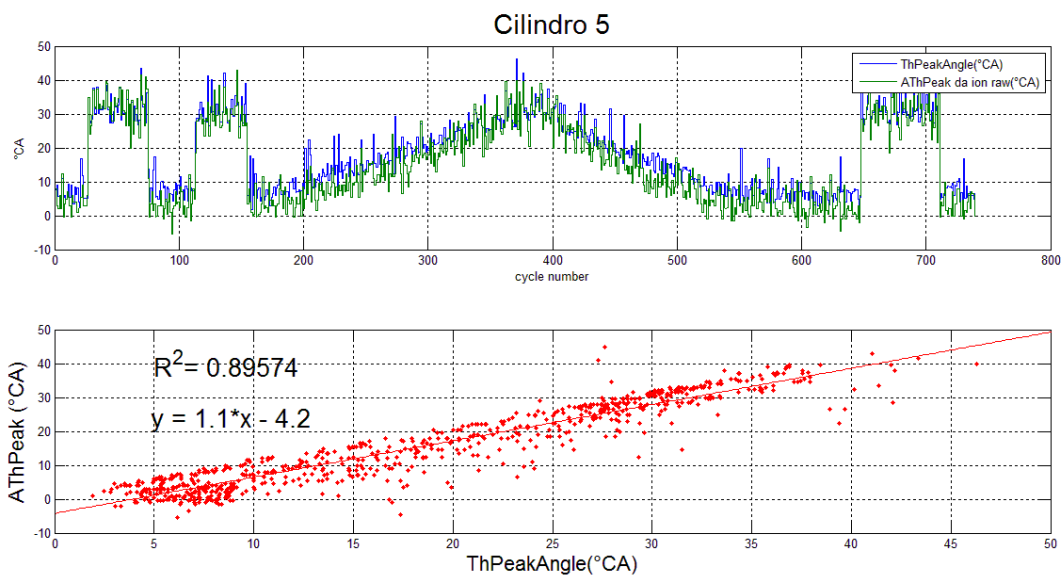


Figure 3.10 - Angular position of the ion thermal peak for cylinder 5, as evaluated from the raw ion signal analysis (AThPeak) and from the real time algorithm implemented in the ion control unit (ThPeakAngle). The test condition are 1000 rpm and 3bar of BMEP.

An “ideal” result would give a correlation one to one between ThPeakAngle, evaluated real time by the ion control unit, and its reference value AThPeak, evaluated in post-processing from the raw ion signal, since they refer to the same physical quantity (the ion current thermal peak location).

Because the correlation level it is not as high as expected (the ThPeakAngle does not correspond perfectly to the physical AThPeak) and the data seems to fit two main regression lines, a further analysis is developed.

3.2.3 Conversion from Sample Based to Angle Based

This section resumes the procedure adopted to identify the causes of the apparently inaccurate ThPeakAngle real time evaluation.

The idea is to compare the raw ion signal sampled by the combustion analysis system with the ion signal sampled by the ion control unit. This is possible since few ion cycles (31 out of 740), sampled by the ion control unit and stored in a buffer, are published via CCP and measured for debugging purposes.

The analysis allows to compare directly what is actually “seen” by the ion control unit to the corresponding physical phenomenon. An example is reported in Figure 3.11.

On the upper diagram, in blue, the raw ion signal is reported. With the green marker, the position of the thermal peak, properly located by the offline algorithm (AThPeak) is highlighted, while in red is the apparently “wrong” location of the thermal peak (ThPeakAngle) evaluated by the real time algorithm implemented in the ion control unit. In the specific cycle reported in Figure 3.11, ThPeakAngle is evaluated to be 7.125°CA while the correct value, AThPeak, is 9.5°CA .

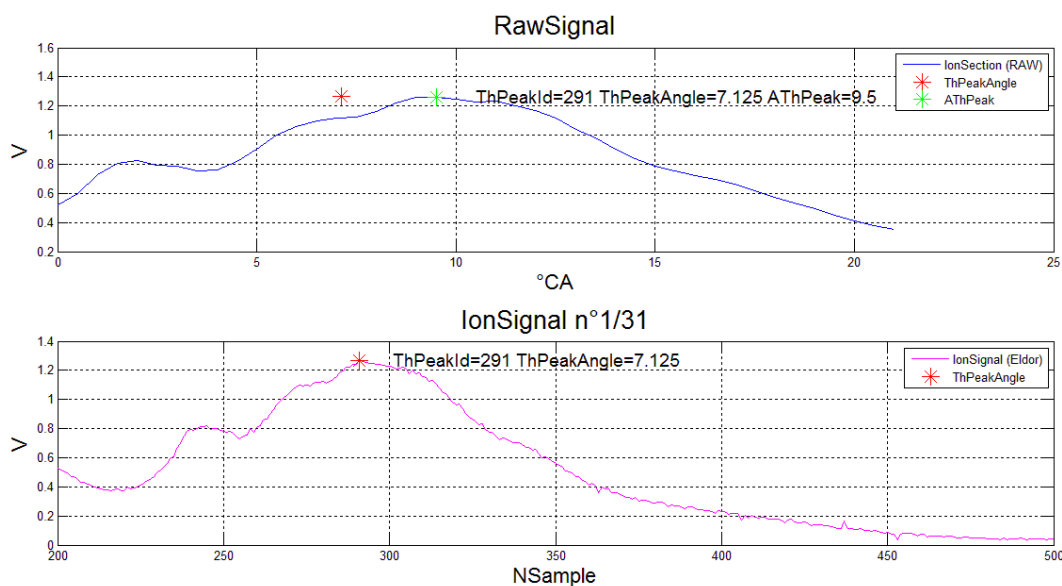


Figure 3.11 – Raw signal ionization thermal phase signal (angle-based) and ionization thermal phase signal sampled by the Ion Control Unit (sample based). The identification of the Thermal Peak in the sample based system is correct (lower diagram), while the estimated angular position is wrong, as highlighted in the upper diagram.

The lower diagram makes clear how the error occurs. The purple line represents the ion signal as it is sampled by the ion control unit. It must be noticed that the x-axis reports the sample number and not the angular position. The location of the thermal peak in the sample based system is correct, as

confirmed by the sample number corresponding to the thermal peak, called “ThPeakId”. What it is not precise is the conversion from the sample-based to the angle-based coordinate system.

The analysis of the remaining cycles highlights this behaviour. On 23 cycles out of 31 examined, the thermal peak location in the sample based coordinate system is correct, while the value converted to the corresponding angular position results imprecise. Therefore the algorithm is able to identify the thermal peak location with good precision, while the evaluation of the corresponding angular position seems to be imprecise.

An analysis of the conversion process is made. The formula used to convert the thermal peak position from the sample-based system (ThPeakId) to the angle-based system (ThPeakAngle) takes into account the Spark Advance value, the dwell time (the amount of time required to charge the inductive coil) and the DTheta, which is the angular step corresponding to the ion sampling time step. Since the angular position of the spark discharge is known, and since the sample number ‘one’ corresponds to the start of the coil charge, the algorithm uses those informations to convert ThPeakId into ThPeakAngle on the basis of the angular step DTheta. Tests conducted at constant spark advance, dwell time and speed are supposed to give a perfect correlation between ThPeakId and ThPeakAngle. Figure 3.12 shows the relation between ThPeakId (sample number) and ThPeakAngle (°CA) measured during a stationary test with fixed spark advance and dwell time.

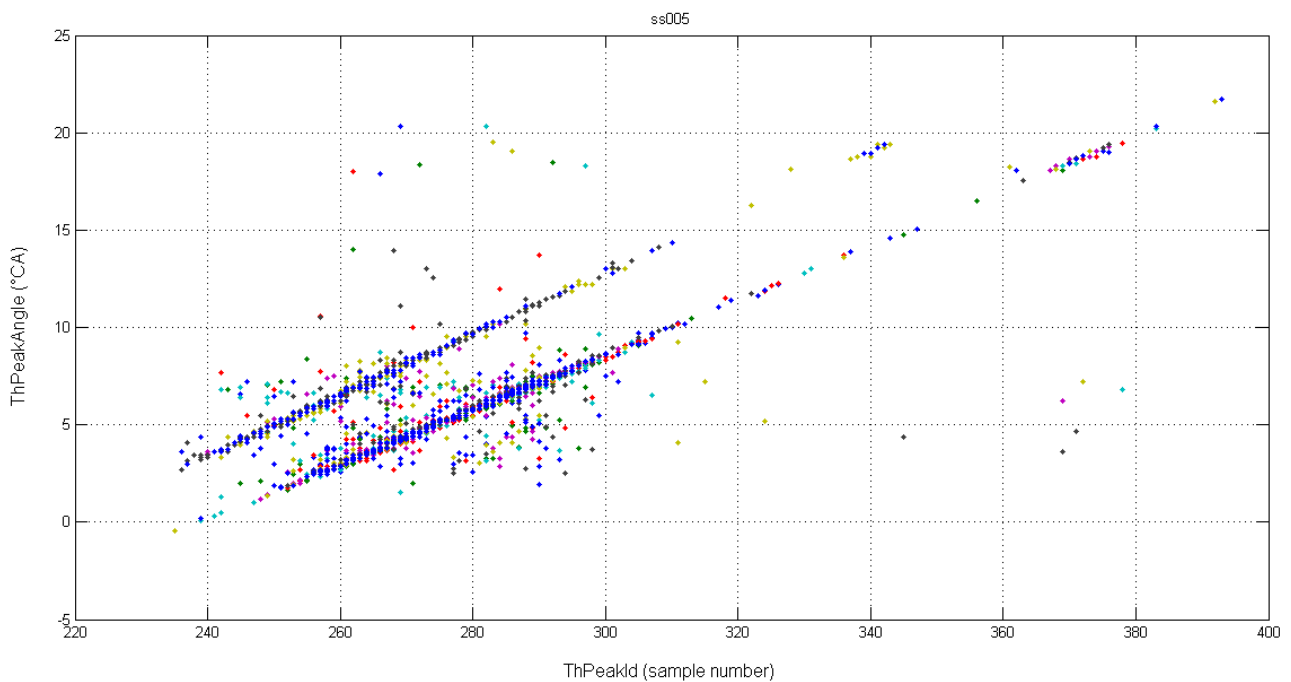


Figure 3.12 – ThPeakAngle (angle based thermal peak location) and ThPeakId (sample based thermal peak location) for fixed spark advance and dwell time. The quantization of the angular step DTheta causes ThPeakAngle to vary, for given ThPeakId, in steps of around 3-4°CA.

Two main lines are sharply visible. The cause of this behaviour is found to be in the quantization of the quantity DTheta starting from the sample time DT. Since the speed presents small oscillations, the sample time of the ionic current, which is function of Rpm, varies. The quantization of the corresponding angle step DTheta causes an important 3-4°CA degrees oscillation in the resulting ThPeakAngle value. The proposed solution to improve the result is to execute the quantization at the end of the calculation chain so that a higher precision can be achieved. This improvement is currently under development.

3.2.4 Real Time Algorithm Performance

The correlation results presented in this section refer to a steady state tests conducted for 18 different spark advance values (each test comprises 500 engine cycles at constant spark advance) at 1000 rpm and 3 bar BMEP. The test procedure is the same as the one described in Paragraph 3.1.2.

The ion thermal peak position evaluated by the real-time algorithm implemented in the ion control unit, ThPeakAngle, is compared with the MFB50, evaluated from the pressure signal. The results are affected by the quantization effect presented in the previous section: the correlation diagrams in Figure 3.13 and 3.14 distinctly highlight this behaviour, since two main correlation lines are visible due to the quantization problem in the conversion from ThPeakId (sample based) to ThPeakAngle (angle based). The solution to this problem is currently under development.

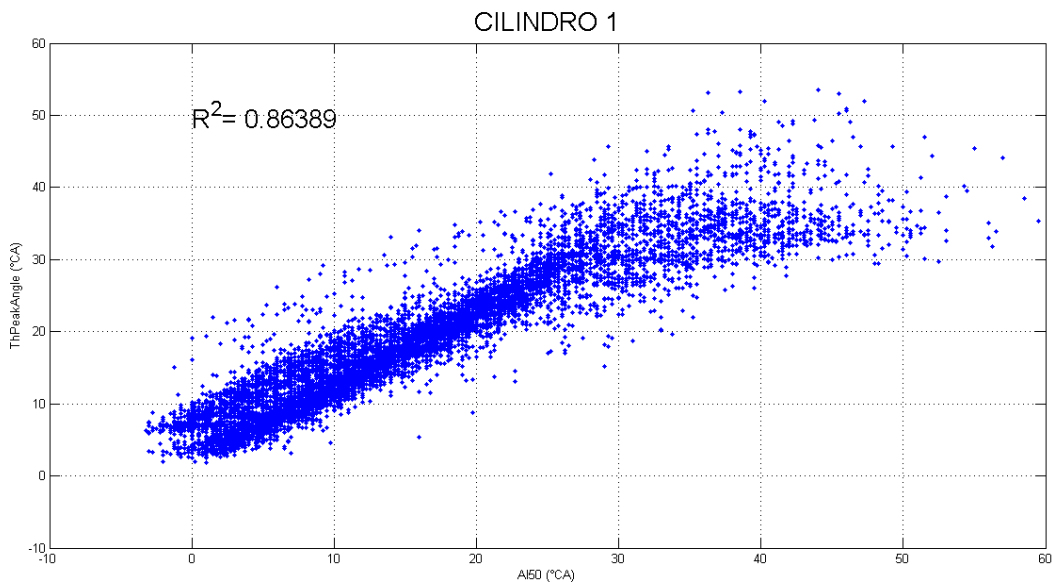


Figure 3.13 - MFB50 (from heat release analysis of the pressure signal) and ThPeakAngle (from ion control unit) for Cylinder 1. Results affected by the quantization phenomenon.

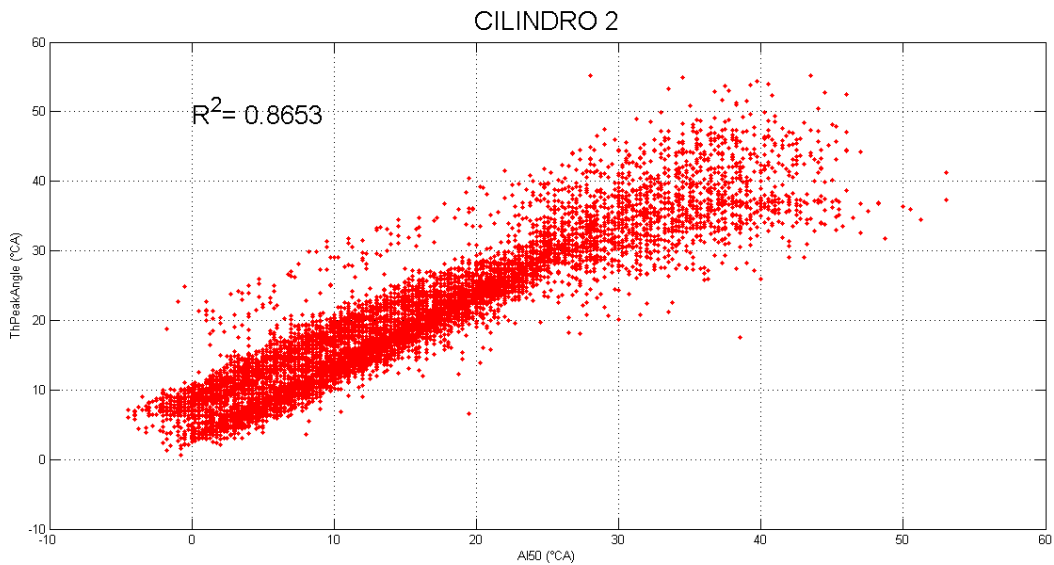


Figure 3.14 - MFB50 (from heat release analysis of the pressure signal) and ThPeakAngle (from ion control unit) for Cylinder 2. Results affected by the quantization phenomenon.

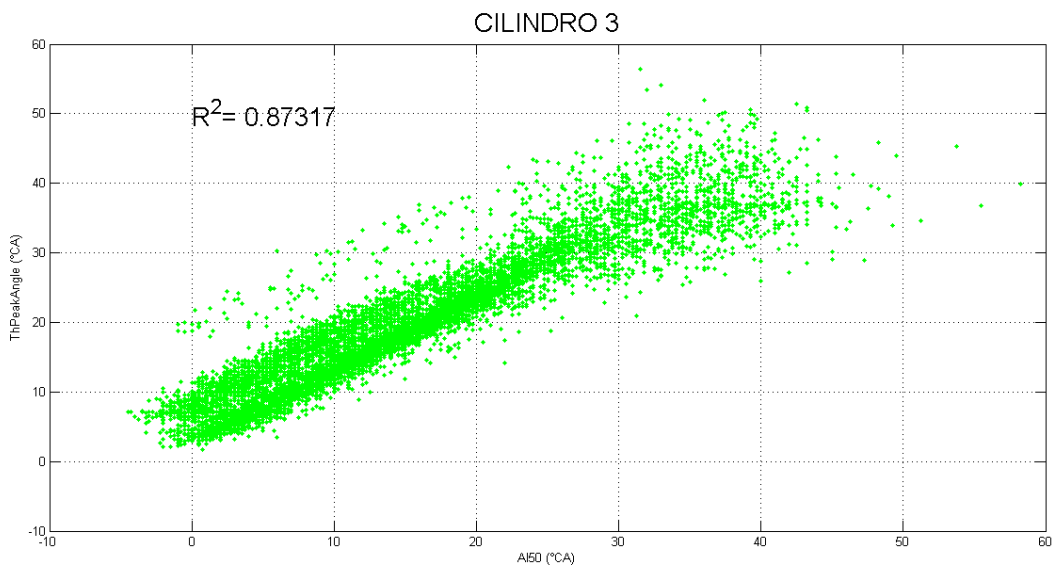


Figure 3.15 - MFB50 (from heat release analysis of the pressure signal) and ThPeakAngle (from ion control unit) for Cylinder 3. Results affected by the quantization phenomenon.

3.3 Other Combustion Features from Steady State Tests

Besides the correlation between pressure and ionization signal, the spark sweeps allow the evaluation of further combustion features.

It must be noticed that during the spark sweep, IMEP (and BMEP) varies in accordance with the ignition timing, as explained in Section 2.3. Figure 3.2 shows this behavior for the measurements at 1000 rpm and 3 bar of BMEP, produced with an ignition timing of 23.25°BTDC. When the MFB50

(Mass Fraction Burned 50%) is at optimum (maximum IMEP), the variations in the output IMEP (i.e. torque) are minimal.

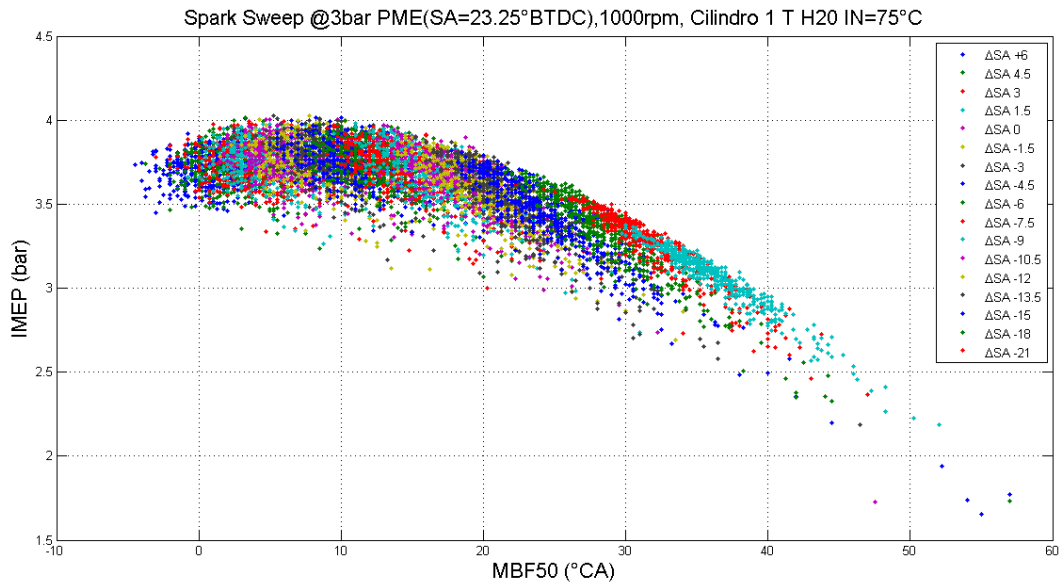
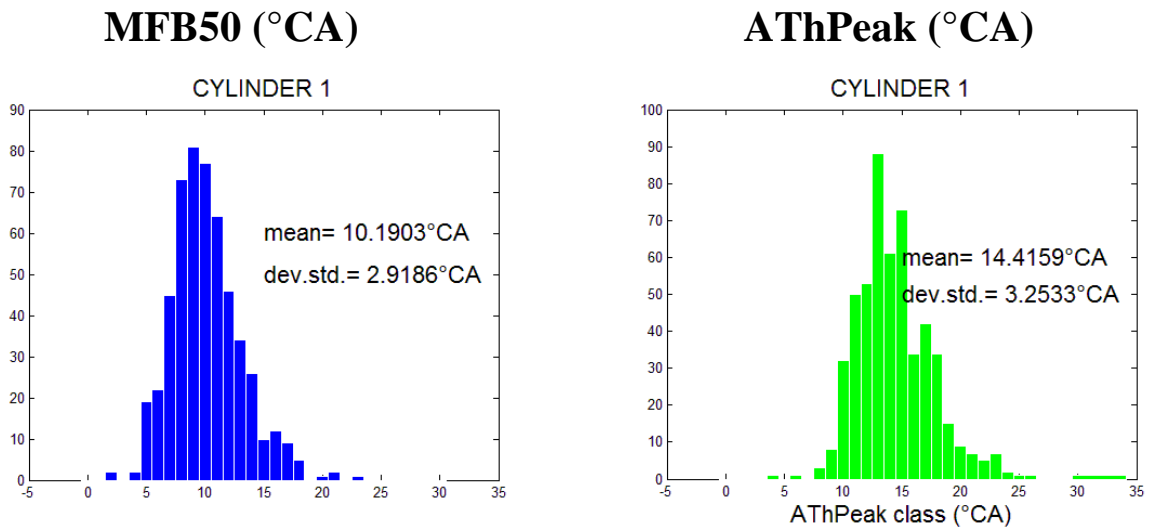
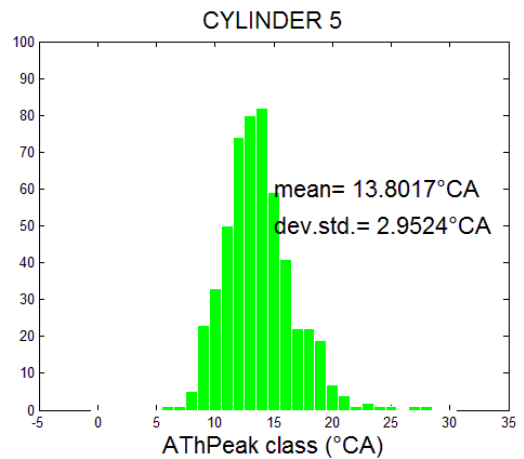
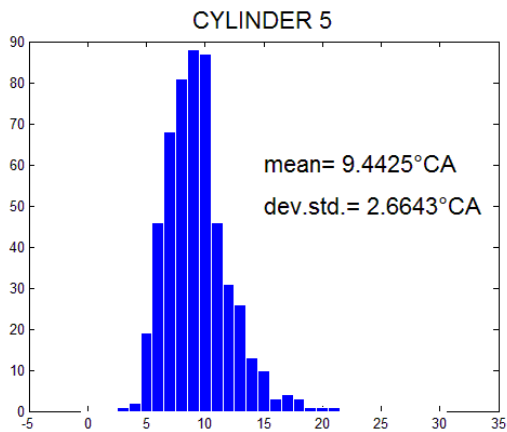
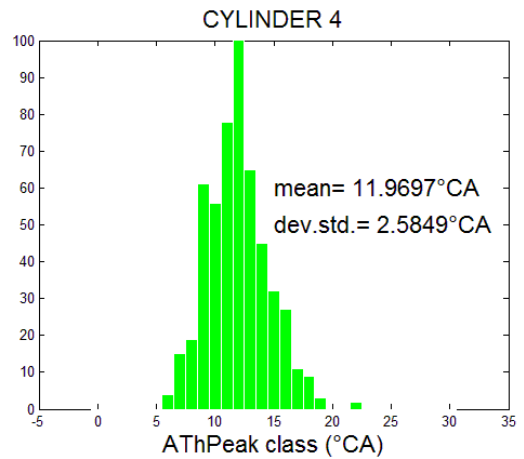
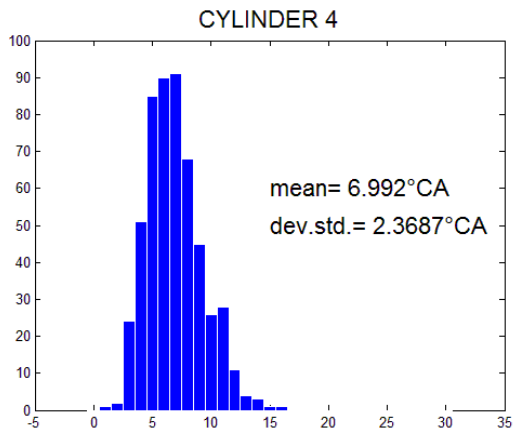
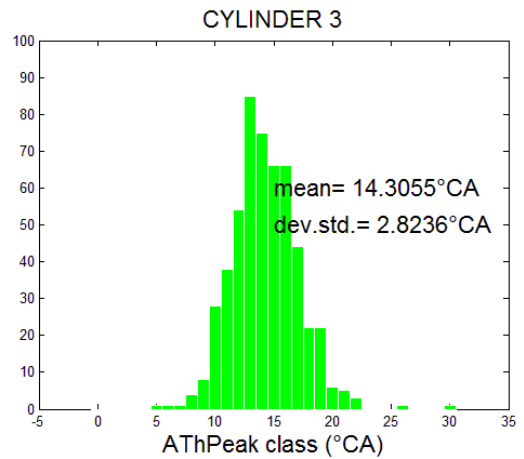
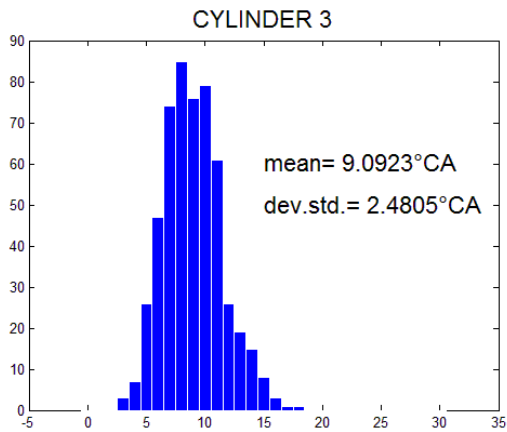
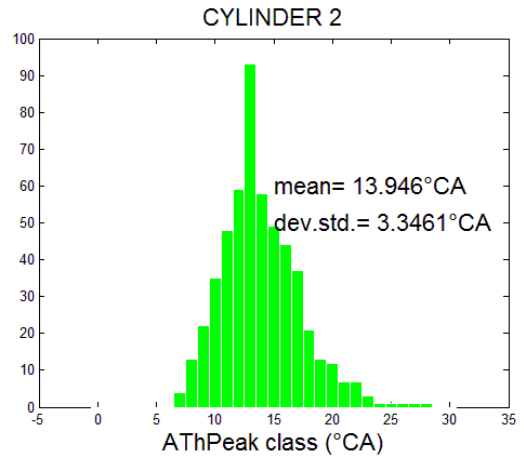
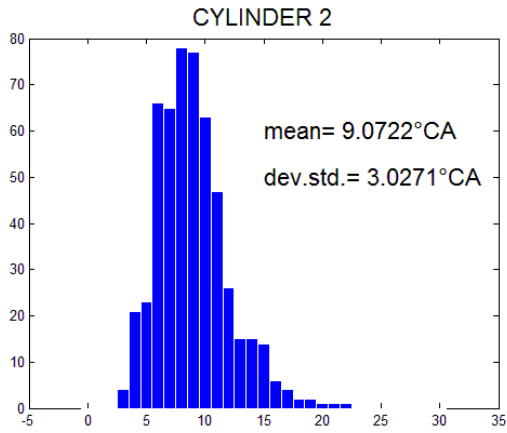


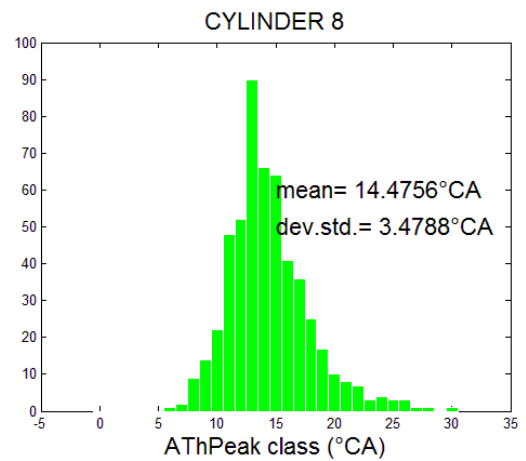
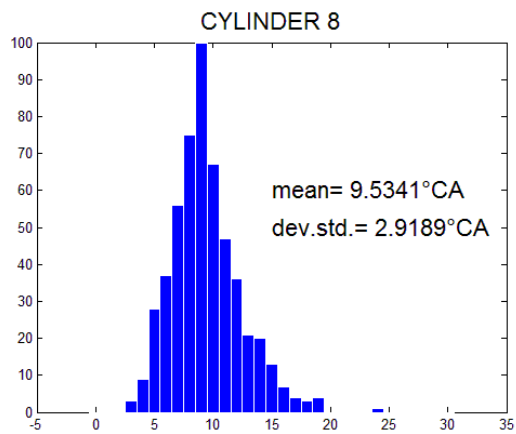
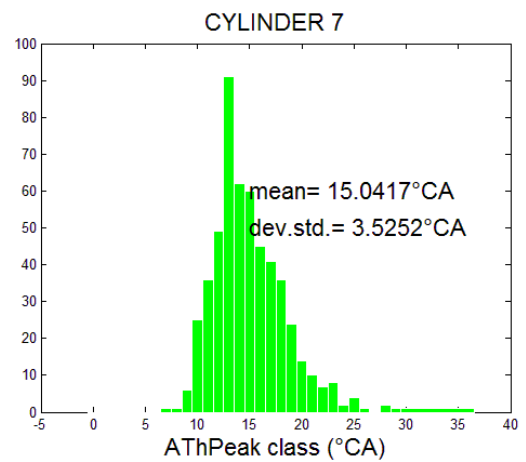
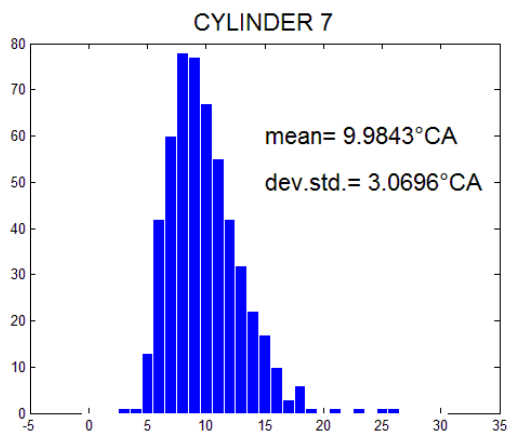
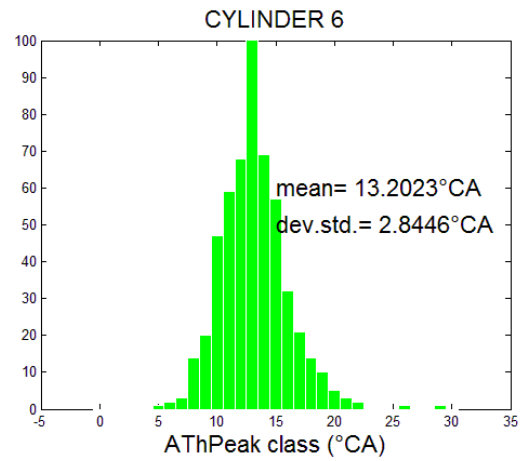
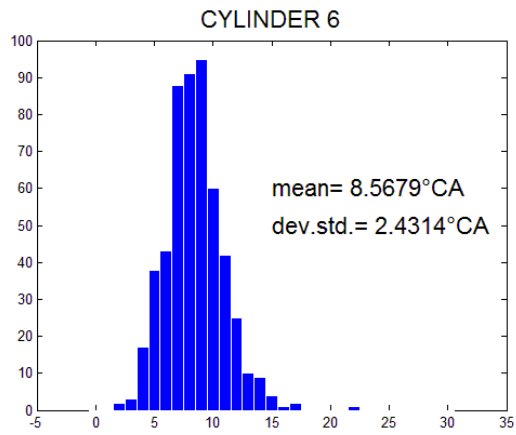
Figure 3.16 – IMEP (Indicated Mean Effective Pressure) variations as function of MBF50. The data reported refer to the 1000 rpm and 3 bar of BMEP produced with 23.25°BTDC ignition timing. Only data from cylinder 1 are reported.

The execution of a steady state test highlights also the differences in the combustion process development between the engine cylinders. Table 3.3 sums up the statistical distribution of MBF50 and AThPeak for every cylinder, while the statistics are summarized in Figures 3.17 and 3.18. The ignition timing is fixed and common for all cylinders.

Table 3.3 – MBF50 dispersion and AThPeak dispersion. The cycle-to-cycle variability is visible both on the pressure and on the ionization current signal, as well as the cylinder-by-cylinder differences. SA=23.25°BTDC.







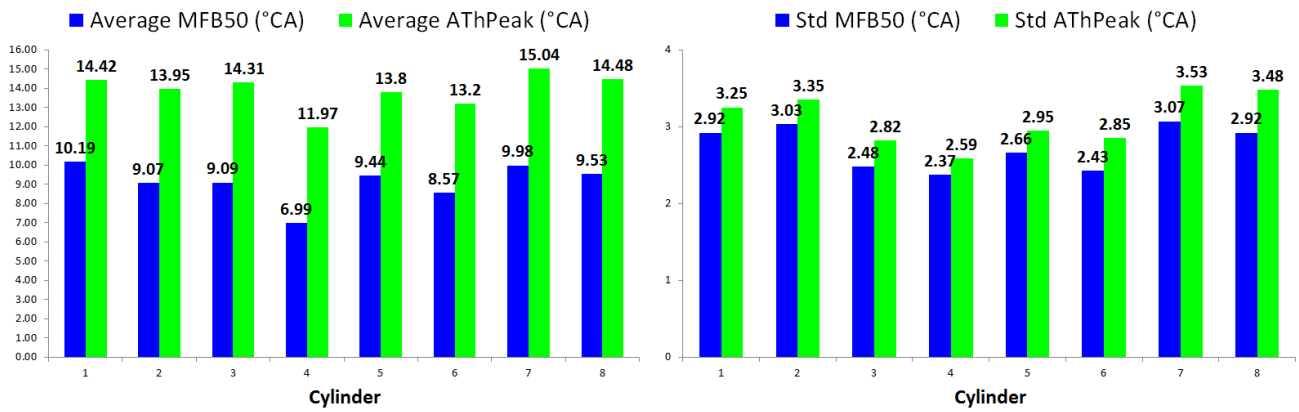


Figure 3.17, 3.18 - Average MFB50 and average AThPeak and Standard Deviations for 500 consecutive engine cycles, SA=23.25°CA. The strong correlation allows the individuation of cylinder-to-cylinder differences in the combustion process using the ionization current thermal peak. A high variability in the combustion process phase corresponds to high variability of the ion thermal peak location.

4.1 Combustion Analysis

The analysis of the combustion phase is limited to those engine cycles where no request for a torque reduction via an ignition angle intervention is present. In those sections, the applied spark advance equals the “base” value calculated by the Engine Control Unit (the condition of no torque reduction is identified by TRUE value of the bit B_nozwe).

In the upper diagram of Figure 4.2, the speed profile of the vehicle during the execution of the test is reported as a function of time. In the diagram below, the corresponding value of the applied spark advance angle, $zwout$, and its base value, $zwbas$, are reported as function of the engine cycle progressive number. The sections of the NEDC cycle where no request for a torque reduction via an ignition angle intervention is present are highlighted in red in the top plot. About half of the measured engine cycles meets this condition.

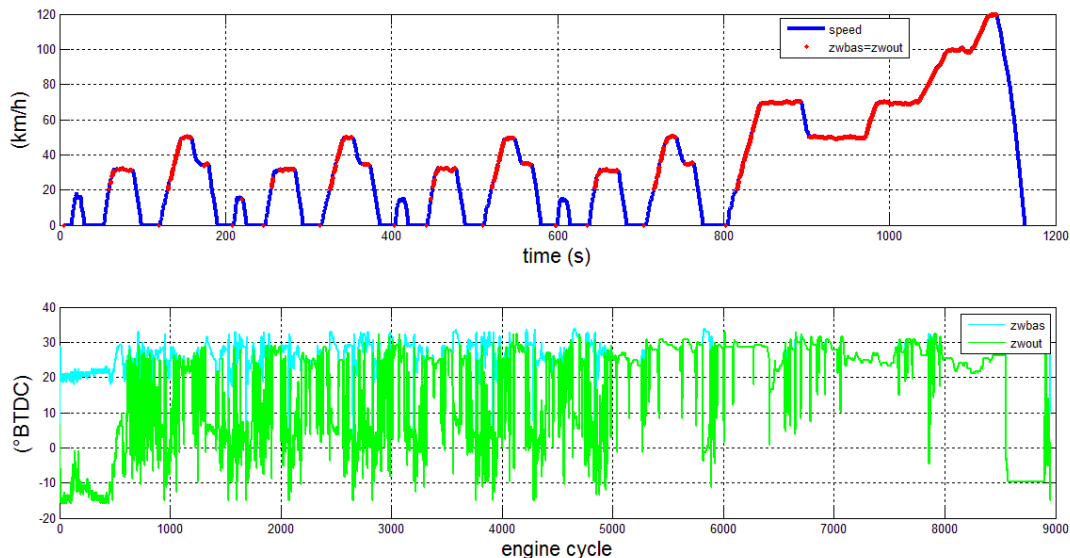


Figure 4.2 - Speed profile (km/h) and ECU’s parameters $zwbas$ and $zwout$ (°BTDC) measured during NEDC driving cycle. Sections where no torque reduction through ignition angle is requested are highlighted in red.

Several factors contribute to spark advance deviations from the base values (see Section 2.4).

For example, in the lower diagram of Figure 4.2, it can be noticed that the ignition angle in the first engine cycles is retarded compared to its base value. Late ignition timing during cold start is a common strategy for fast catalyst warm-up, since the catalytic converter has to be warmed up sufficiently to be fully effective. Retarded combustion reduces work transfer from cylinder gases to the piston resulting in higher exhaust temperature. For constant engine torque, the reduced fuel conversion efficiency associated with late combustion requires greater fuel and air flow rate as it can be seen in Figure 4.3, where the fuel consumption for every engine cycle is reported. Thus late

ignition leads to greater engine-out sensible enthalpy flow due to both higher temperatures and greater mass flow rates.

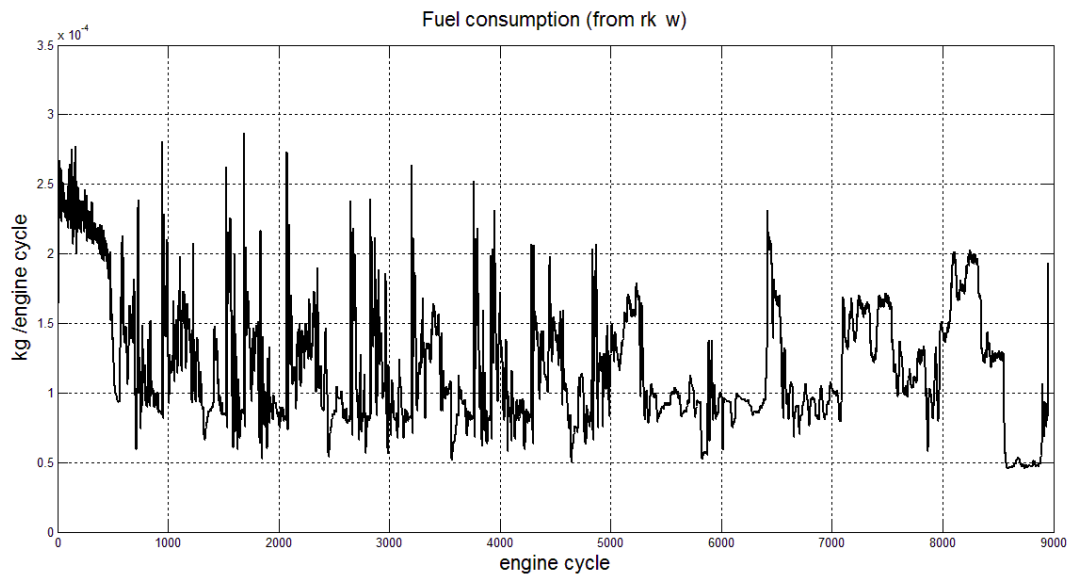


Figure 4.3 – Fuel consumption (kg/engine cycle) estimated by the ECU’s mixture control function during NEDC. During catalyst heating, the ignition retard is limited by excessive engine-out HC emissions, due to incomplete combustion as well as misfire. An open loop retard calibration needs to provide enough margins to avoid misfire at all conditions, therefore it is inherently conservative. The results that can be achieved with the open loop control are presented in Figure 4.4: during the catalyst heating, the combustion is phased at around 80°CA MFB50. Other events that lead to a retarded ignition timing are in case of anti-jerk intervention, during gear shifts (as it can be seen in Figure 4.4, once the catalyst heating phase is completed) and at idle speed, when a torque-reserve is requested for controlling purpose.

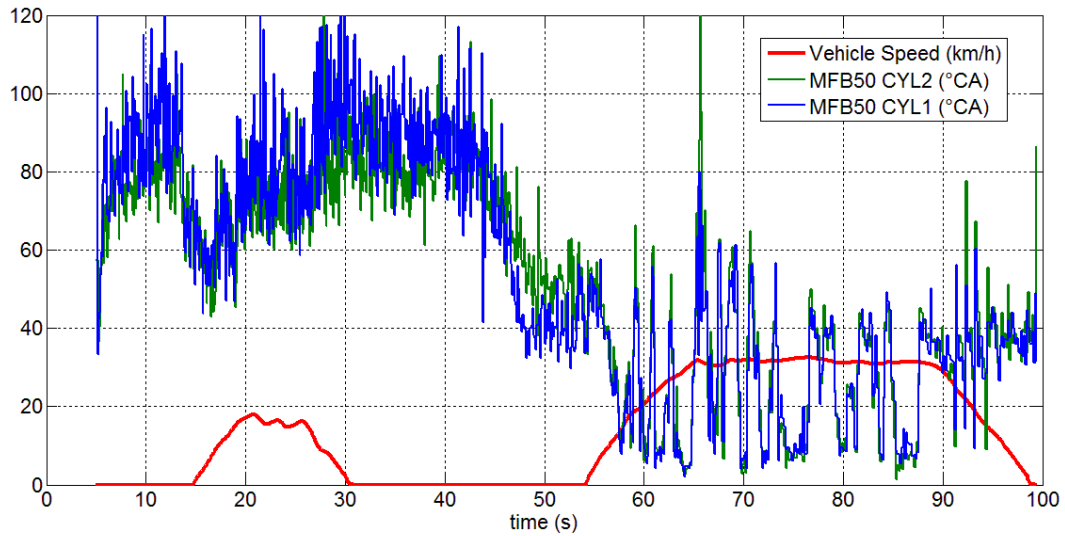


Figure 4.4 – Combustion phase and vehicle speed during the first 100s of the NEDC driving cycle. Retarding the combustion phase is a common strategy to reduce the light-off time of the catalytic converter.

A potential benefit of a closed loop control could be an improved start-up strategy to reduce cold-start HC emissions by reducing the time required to increase the catalysts temperature to its light-off level. The closed loop nature of the system could provide maximum usage of the possible ignition timing range in the retard direction at any given operating condition, while assuring that misfire is avoided [23].

The results of the combustion analysis, limited to engine cycles where no retarded ignition is requested, are presented in Figure 4.5 and 4.6. Only two pressure signals are measured (from Cylinder 1 and 2). The combustion phasing is represented by mean of the 50% Mass Fraction Burned angle (MFB50).

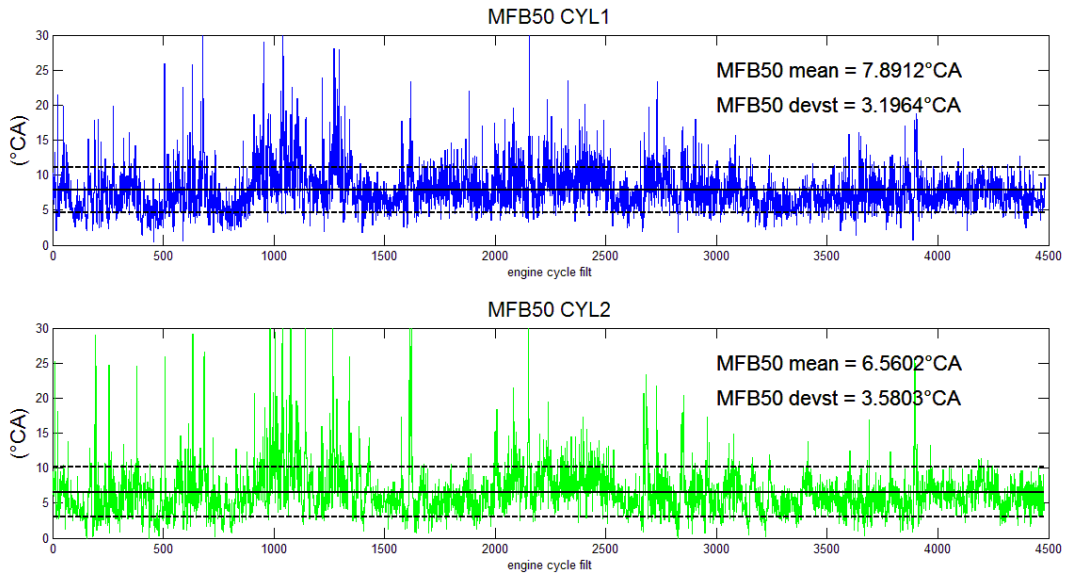


Figure 4.5 – MFB50 for Cylinder 1 and Cylinder 2 during NEDC with open loop spark advance control. Only cycles with base ignition timing are shown.

The open loop control cannot compensate the differences between the two observed cylinders in terms of combustion phase mean value (Figure 4.6).

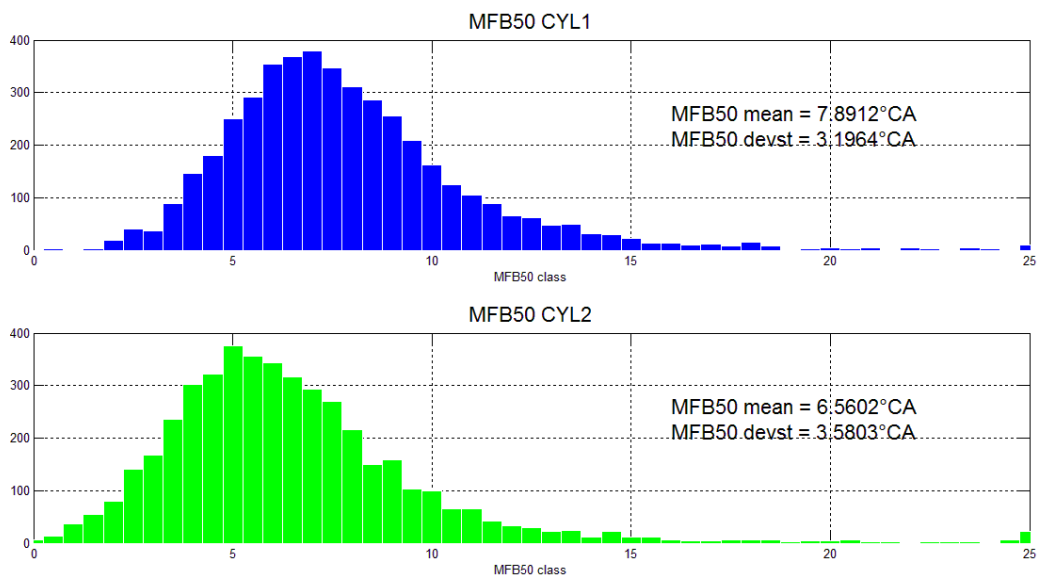


Figure 4.6 – MFB50 distribution for Cylinder 1 and Cylinder 2 during NEDC with open loop spark advance control. Only cycles with base ignition angle are shown.

4.2 Evaluation of Possible Improvements in Fuel Economy

An evaluation of the possible improvements in fuel consumption is made, based on the results of the combustion analysis and on the fuel mass consumption evaluated by the mixture control function implemented in the Engine Control Unit (reported in Figure 4.4).

Starting from the fuel consumption evaluated by the Engine Control Unit, an hypothetic optimum value corresponding to a perfectly phased combustion is calculated through the function reported in Figure 4.7. Such figure, derived from experimental data previously collected (Spark Sweep), reports the percentage variation of BSFC (Brake Specific Fuel Consumption) as function of the difference between MFB50 and its optimal value (i.e. of minimum BSFC).

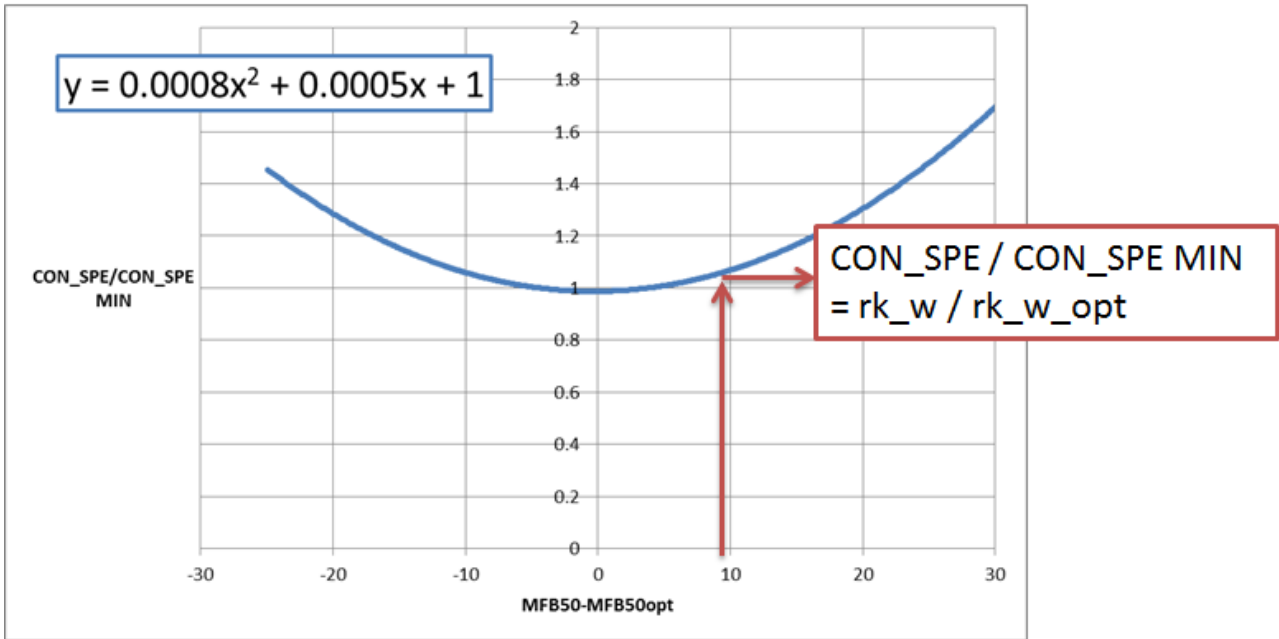


Figure 4.7 – Variation in BSFC (Brake Specific Fuel Consumption) as function of the combustion phase.

The fuel consumption evaluation at the optimal combustion phasing is based on the following approximation:

- The MFB50 optimum value is hypothesized to be 8°CA, with no regard for the specific load/speed condition.
- Only one curve delta BSFC/delta MFB50 is used for all the engine cycles. A small variation in the shape of the curve has great influence on the result.
- The effective fuel consumption is not measured through an high precision fuel consumption measurement system, but integrating the value estimated by the engine control unit for every engine cycle (see Figure 4.3)
- Only two cylinders are analyzed. All other cylinders are assumed to behave in the same way.

The equations used to evaluate fuel consumption are reported below:

$$CONS (kg/cycle) = rk_w * KUMSIRL * (1/14.17) * (2/60); \quad (4.1)$$

$$CONS_OPT (kg/cycle) = rk_w_opt * KUMSIRL * (1/14.17) * (2/60); \quad (4.2)$$

where *KUMSIRL* is the conversion constant from mass flow to relative air charge and *rk_w* is the relative fuel mass for the relative air charge predicted by the Engine Control Unit. The results obtained through the described procedure are summarized in Table 4.1.

Table 4.1 – Evaluation of fuel consumption improvement in case of perfectly phased combustions on the NEDC (only cycle with no torque intervention via ignition angle).

	Fuel consumption	Fuel consumption @ MFB50_Opt	Variation	
			Kg	%
CYL 1	0.5436	0.5398	-0.0038	-0.70%
CYL 2	0.5436	0.5382	-0.0054	-1.00%

5 Closed Loop Combustion Control

Purpose of this work of thesis is to evaluate the feasibility of a closed loop control of the ignition timing under normal operating condition. This particular application focuses on the possibility of controlling the combustion phase for all engine cylinders to the desired reference value. The feedback parameter must then be an indicator of the combustion phasing, either evaluated from the ionization current signal, either directly from the in-cylinder pressure signal.

In this Section, the proposed control structure is presented. An offline simulation environment is adopted to test the performance of the controller. The development phase is followed by the implementation of the combustion controller prototype on a Ferrari turbocharged engine. Measurements are conducted at the engine test bench and at the vehicle roller bench. An evaluation of the potential benefits is made.

5.1 Controller Structure and Feedback Selection

The schematic structure of the proposed feedback control is represented in Figure 5.1. The controller compares the actual value of the controlled variable with its set point and obtains an error, on the base of which it performs an adjustment on the output spark advance that, in turn, causes a change on the engine combustion process and, hence, on the combustion phase indicator value.

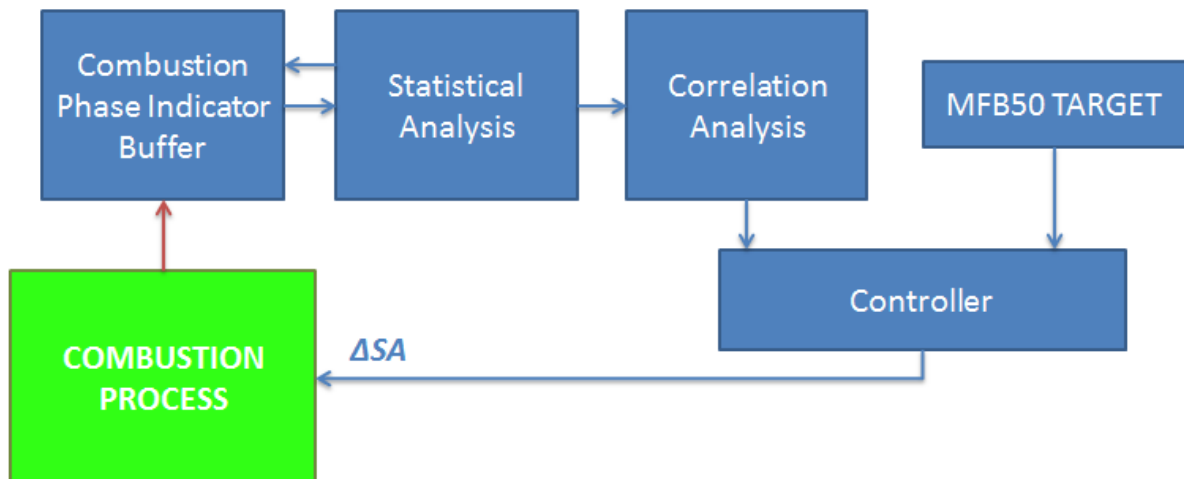


Figure 5.1– Feedback control structure for combustion phase regulation.

A proportional integral (PI) controller is chosen among the feedback control structures for its simplicity. The output of a general PI controller is directly proportional to the error by the constant K_P and to the integral of the error by the constant K_I , hence:

$$SA = KP \cdot e(t) + KI \cdot \int e(t) \quad (5.1)$$

where $e(t)$ is the error (function of time t) between the controlled variable and its set point. The contribution of a derivative action, which should have a predictive effect, is not implemented since, due to combustion cycle-to-cycle variations, engine combustion behaves similar to a random process and cannot be predicted on a cycle-to-cycle base. The variability of the combustion process, visible both on the pressure and on the ionization current signal for a given spark advance, is highlighted in Figure 5.2.

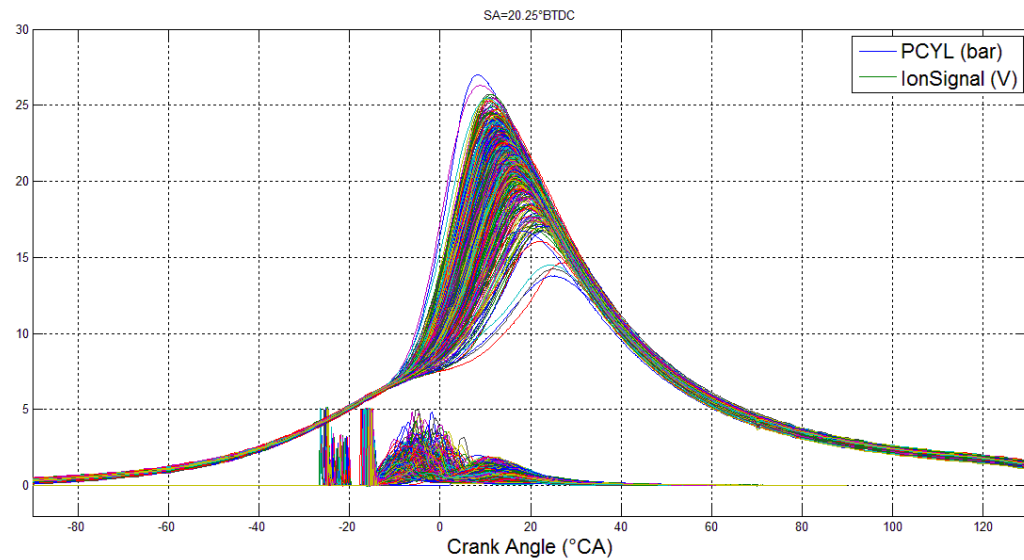


Figure 5.2 - Cycle to cycle variations effects on in-cylinder pressure and ionization current for given spark advance. 500 consecutive cycles, SA=20.25° BTDC, Cylinder 1.

The effect of SA on combustion is stochastic, due to the cycle-to-cycle variation: maintaining a given SA value, the MFB50 shows a given statistical distribution. Figure 5.3 reports the MFB50 dispersion relative to the engine cycles presented in Figure 5.2. The spark advance is fixed at 20.25° CA. A similar distribution is visible on the corresponding ion thermal peak location (A_{ThPeak}).

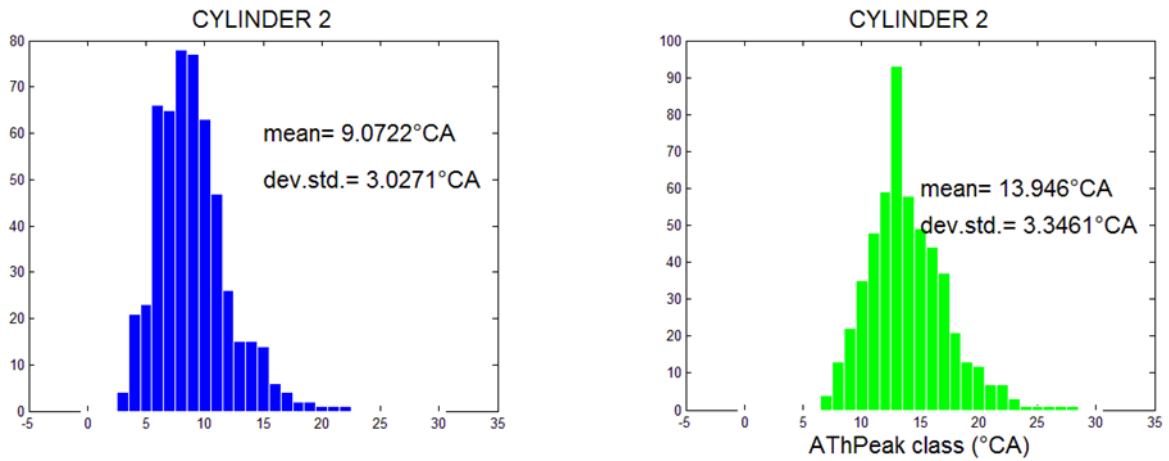


Figure 5.3 – MFB50 and AThPeak dispersion. 500 consecutive cycles, SA=20.25°BTDC, Cylinder 2.

While the single MFB50 cannot be used for controlling purpose, due to the cycle-by-cycle variability of the combustion process, its mean value over a certain number of cycles shows a more stable behavior, as highlighted in Figure 5.4. The MFB50 moving average, and the AThPeak moving average, can indeed be used as a feedback for controlling the combustion phase.

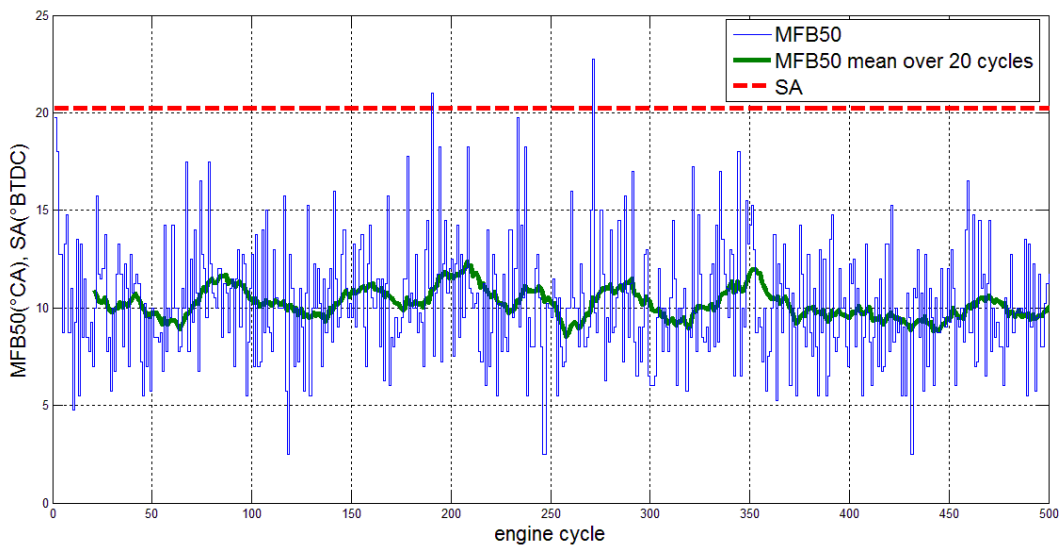


Figure 5.4 – MFB50 and MFB50 moving average over 20 consecutive engine cycles. SA=20.25°BTDC. The MFB50 moving average can be used as feedback for controlling purpose.

The chosen feedback parameter in the developed control structure is then the moving average of the ion thermal peak position, over the last 10, 20 or 30 engine cycles. The “buffer size” represents a parameter that needs to be tuned, together with the controller gains: with a lower number of cycles, the controller is expected to be faster during transient conditions, while, with a higher number of stored cycles, the controller is expected to be more stable and precise in stationary conditions.

5.2 Offline Controller Performance Evaluation

The performance of a combustion controller based on the position of the ion current thermal peak are evaluated “offline” in this part of the activity, using data previously collected at the test bench. Aim of the activity is to verify the accuracy that can be achieved with such controller and to provide a first tuning of the working parameters. The offline simulation environment for testing the combustion phase controller performance and the results obtained are presented in Paragraph 5.2.1 and 5.2.2.

5.2.1 Engine Simulation Environment

In order to test the controller performance in a very time and cost efficient way, a specific environment is developed to simulate the on-board operation of the algorithm. Such software environment allows evaluating the ability of the given controller to achieve the pre-defined indicating value. The main idea behind this approach, presented in [24], is that the stochastic nature of combustion can be reproduced by using a limited set of previously acquired experimental data. Considering a given cylinder and a specific engine operating condition, the same set of data acquired during the calibration tests can in fact be used in this validation phase as input to the controller, by randomly selecting, for a given SA value (output of the controller), an in-cylinder pressure cycle (and the corresponding ionization current signal) belonging to the cylinder-specific group of pressure cycles (and ion current cycles) measured in the very same SA conditions.

Data collected from the spark sweep at 1000 rpm and 3 bar of BMEP from the previous correlation analysis (Section 3.1) can be used for this purpose. The data are organized in a structure containing around 9500 engine cycles, measured during steady state tests at 18 different spark advance values. For each cycle and for each cylinder, combustion features based on pressure and ion signal are stored.

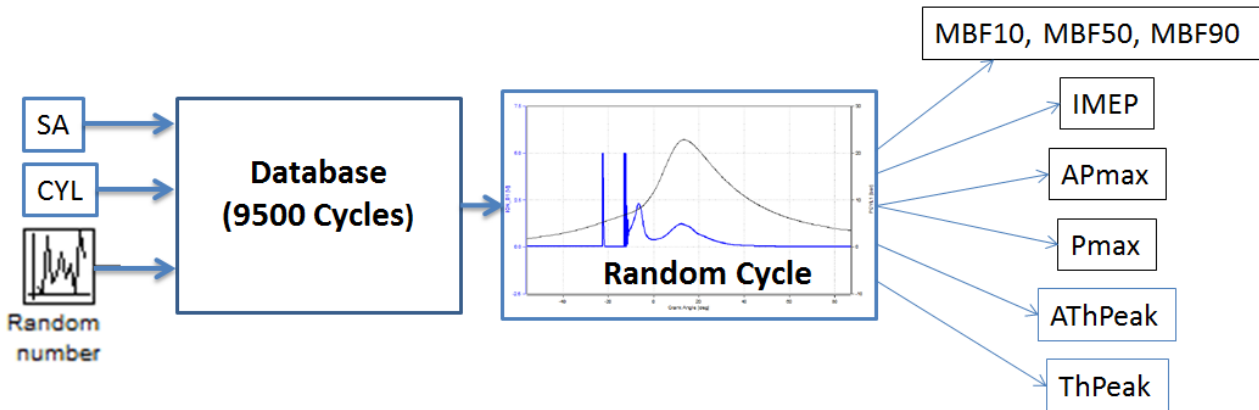


Figure 5.5 – Engine simulation environment used for offline performance evaluation. The Engine behavior is emulated using a set of acquired pressure and ionization current cycles.

The feedback loop is used to regulate the mean value of the stochastic feedback parameter to a mean target value. The controller is structured as a Proportional Integral. Despite the variability of the stochastic feedback, its mean value is a well-behaved signal for regulation purposes. The regulation controller needs to be tuned to provide the desired settling time and steady-state accuracy for the response. A summary of how the simulation environment works is reported in the following list:

- A random cycle with the given spark advance set by the controller is picked from the database.
- From the acquired ion signal, the position of the thermal phase peak (AThPeak) is computed for every cylinder.
- The thermal peak position is stored in a buffer, containing the values corresponding to the last 10, 20 or 30 cycles. Each cylinder has its own buffer, so that individual spark advance corrections can be applied.
- A statistical analysis of the buffer is made. The mean value of AThPeak is evaluated, along with its standard deviation.
- Corresponding mean MFB50, for each cylinder, is estimated through the regression line obtained from the correlation analysis (Chapter 3).
- The estimated mean MFB50 is used as feedback for the PI controller action, comparing its value with the predefined set point.
- The output of the controller is an individual cylinder spark advance correction, to be added to the “base” spark advance, which is constant for all 8 cylinders.

5.2.2 Offline Simulation Results

The performance of the combustion controller, evaluated through the offline simulation environment introduced in the previous paragraph, are presented in this Section. The emulated engine operating conditions refers to 1000 rpm and 3 bar BMEP. The combustion phase feedback for the controller is the position of the ion thermal peak, AThPeak, while the error with the reference value is evaluated on the moving average over the last 20 cycles. Figure 5.6 shows the system's response to a step in the MFB50 reference value. The combustion phase of each cylinder, represented by means of the MFB50 moving average, is reported together with its reference value. The controller is able to keep the combustion phase close to the target value, with different individual spark advance corrections on each cylinder, as visible in Figure 5.7.

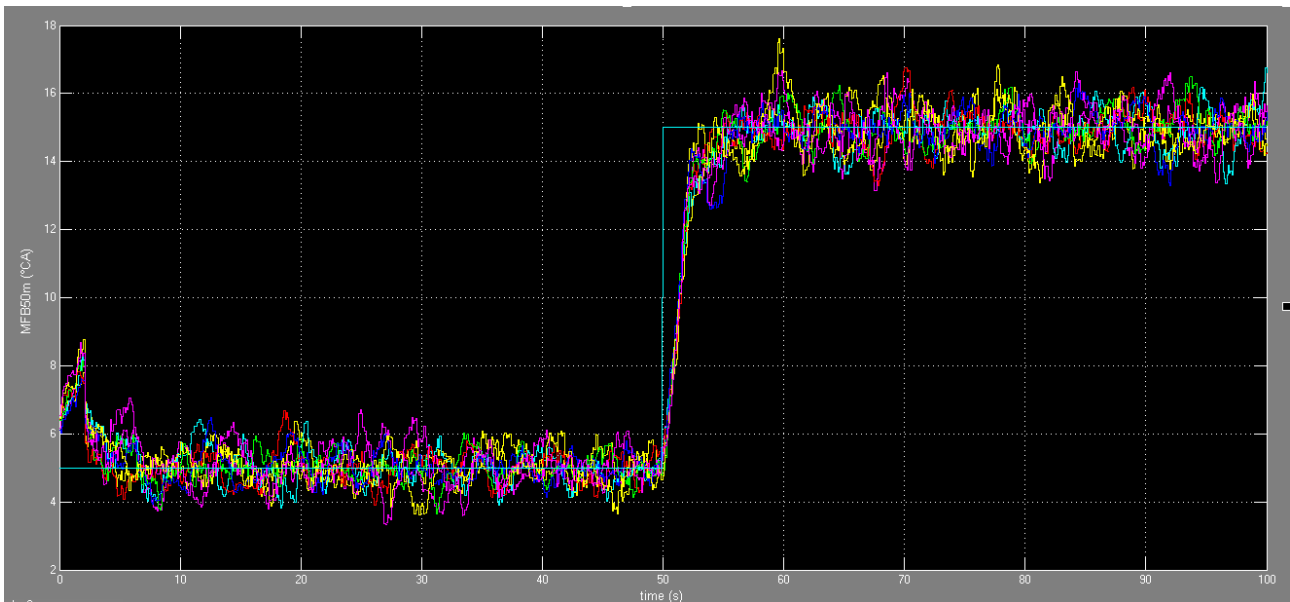


Figure 5.6 – Mean MFB50 angles (over 20 consecutive cycles) as function of time (each time step correspond to the cycle duration at 1000rpm). Results from offline controller performance simulation.

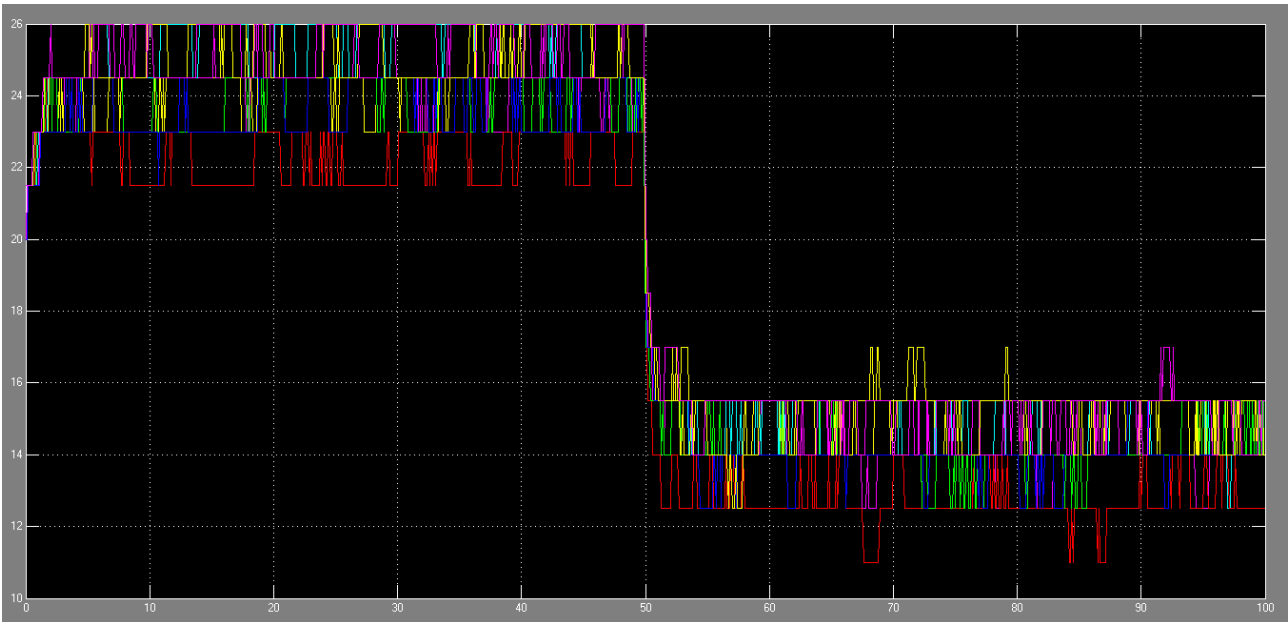


Figure 5.7 – Individual spark advance correction requested by the controller action. The effect on the combustion phase is reported in Figure 5.6. Results from offline controller performance simulation.

Test with different MFB50 reference value for each cylinder highlights the possibility of individual cylinder correction. Figure 5.8 shows the controller performance in case different individual combustion phase targets are requested.

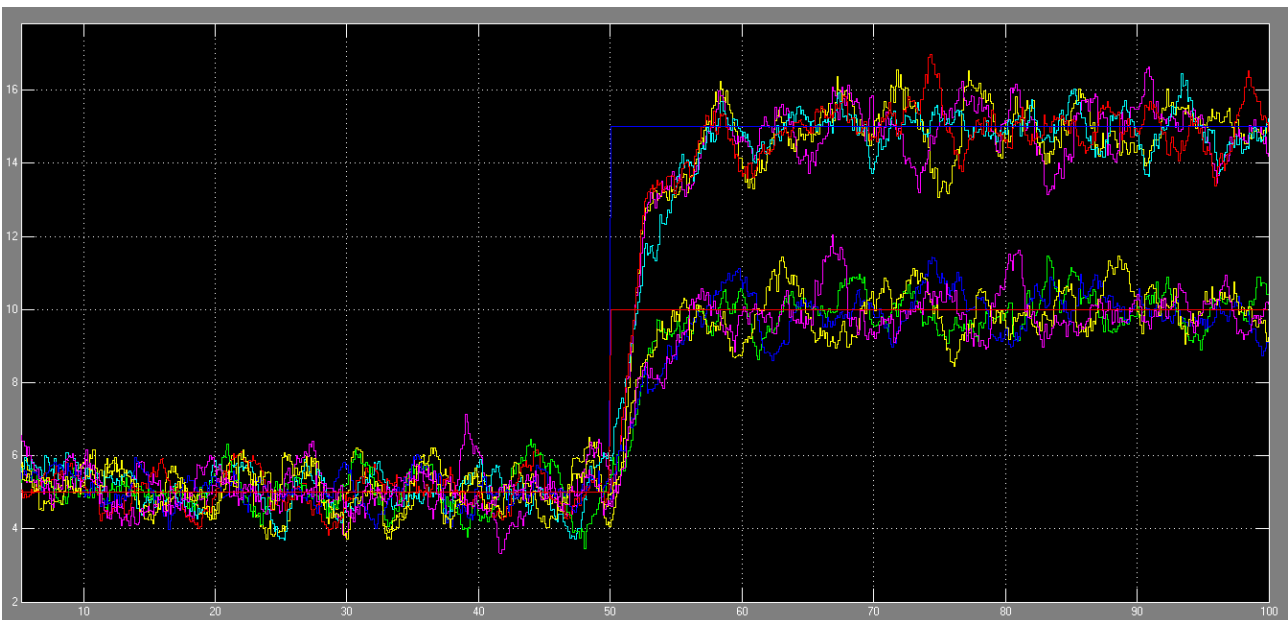


Figure 5.8 - Mean MFB50 angles (over 20 consecutive cycles) as function of time (each time step correspond to the cycle duration at 1000rpm) for different MFB50 reference values (15°CA for cylinders 1 to 4 and 10°CA for cylinders 5 to 8)

5.3 Real Time Combustion Controller with Pressure Signal Feedback

The real-time spark advance controller structure presented in Paragraph 5.2 has been implemented and tested on a Ferrari F154CB engine. Ignition timing is the actuation to be controlled in order to set the combustion phase to the desired target value. Since the strategy cannot be implemented directly in the Engine Control Unit, a specific hardware layout is developed to test in a fast and efficient way a prototype of the controller system. The controller layout is presented in this Section, together with the measured results. The feedback parameter, represented by the MFB50 combustion angle, is in this phase evaluated directly from the pressure signal, while the controller structure based on the ion current signal is presented in Paragraph 5.4.

5.3.1 Controller Layout

Figure 5.9 shows the hardware layout implemented in order to individually control the spark advance actuation without modifying the Engine Control Unit software.

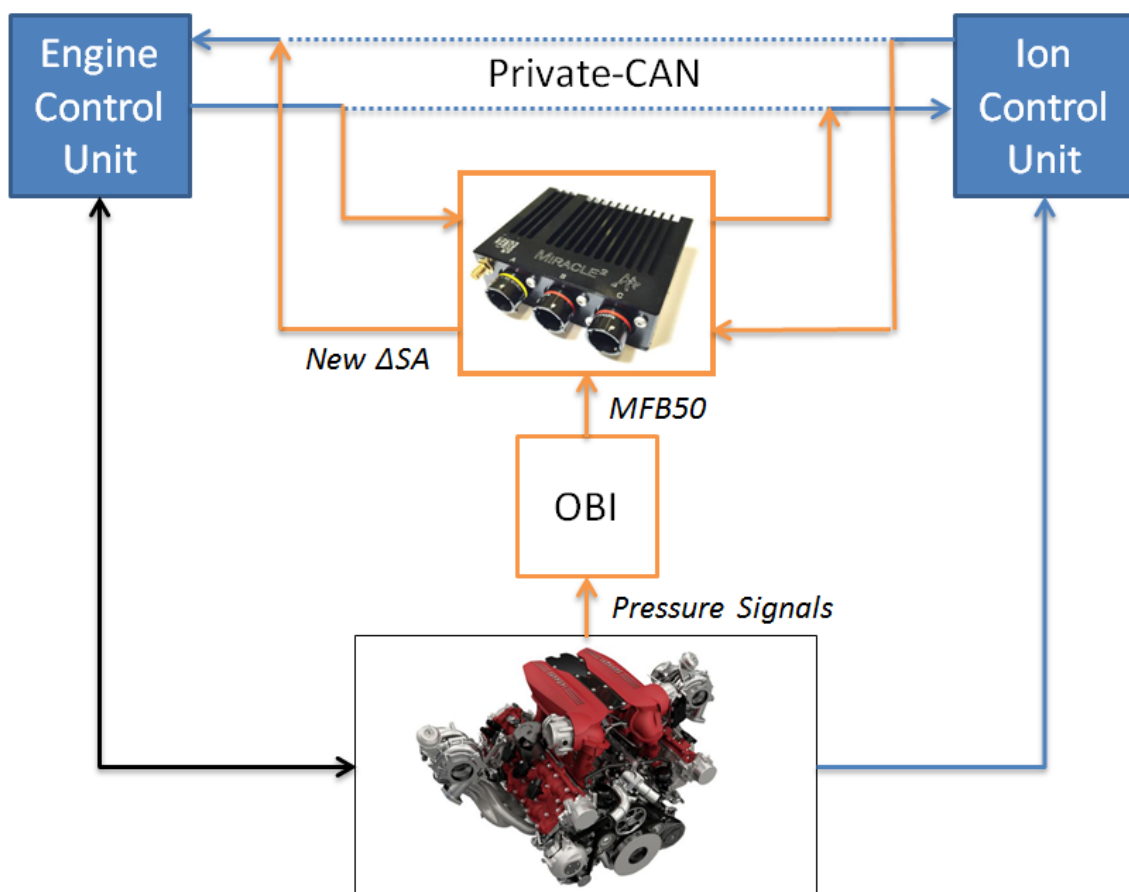


Figure 5.9 – Layout used for spark advance control with pressure signal feedback. The individual cylinder spark advance corrections are overwritten on the private CAN line.

The private CAN line between the engine control unit and the ion control unit is intercepted by means of a Rapid Control Prototyping platform. The line is “Private” because, compared to the

vehicle CAN line, only two nodes have access to it: the Engine Control Unit and the Ion Control Unit, both with the authority of reading and writing messages.

The private CAN messages exchanged by the two control units refer to engine status parameters, like load, speed, temperature (sent by the ECU) and information and control action derived from the analysis of the ion current signal (sent by the ion control unit). Among these, individual spark advance corrections are sent every combustion event by the ion control unit. Their value is zero in case of normal combustion events, while spark advance corrections are required to the Engine Control Unit in case of knock, mega knock or other abnormal combustion events detected by the ion current analysis (see Section 2.5).

In the layout shown in Figure 5.9, the CAN messages containing the spark advance corrections are intercepted and overwritten with the spark advance corrections evaluated in real time by the control algorithm, based on measured in-cylinder pressure, while the other messages are just read and copied in both directions. The Engine Control Unit interprets the spark advance corrections and applies them, as if an abnormal combustion was occurring. Since only negative corrections are permitted by the engine control unit (spark advance reduction), the spark advance needs to be manually increased with reference to corresponding map value in order to make the control action effective.

The algorithm performs the control strategy on the basis of the MFB50 angles, evaluated in real-time by a dedicated unit (On Board Indicating system) through the heat-release analysis of the pressure signals. Therefore, this control system is based on the pressure signal analysis and requires piezoelectric pressure sensors on every cylinder and the use of a combustion analysis unit. The control action based on the ion (ThPeakAngle) feedback evaluated by the ion control unit is currently under development (see Paragraph 5.4).

5.3.2 Controller Algorithm

A high-level representation of the controller structure developed in MathWorks Simulink and implemented on the Rapid Control Prototyping platform is reported in Figure 5.10. Every combustion event the MFB50 value is received as input and sent to the corresponding cylinder calculation block, which is triggered by the combustion event itself.

The structure, developed for the combustion control based on the ThPeakAngle, can be used directly on the MFB50 value evaluated from the pressure signal by excluding the correlation analysis calculation block. The low level structure that runs on the Rapid Control Prototyping

platform is developed in National Instrument LabVIEW. Its task is the interpretation of the CAN messages and their management.

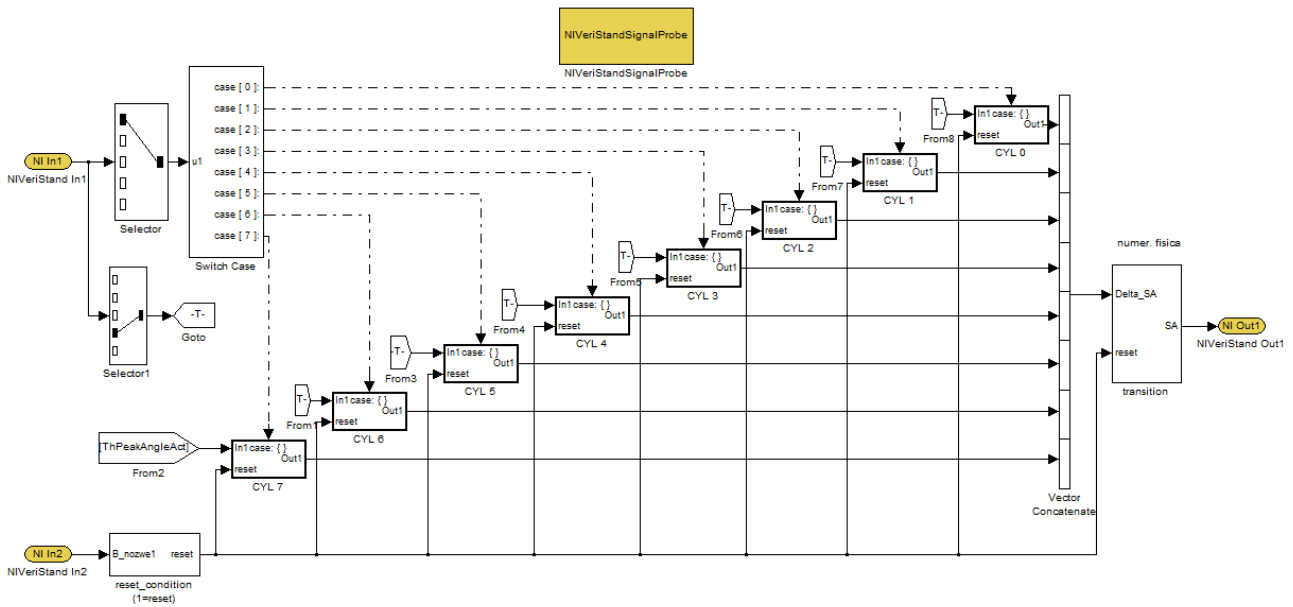


Figure 5.10 – Controller structure developed in MathWorks Simulink. The calculation block corresponding to a single cylinder is executed when the corresponding cylinder combustion process ends. The cyclic indicating parameters are sent by the On-Board Indicating system.

5.3.3 First Set: Step Response

A series of steady state tests is conducted at the test bench in order to verify the controller behavior. The engine operating condition is 1000 rpm and 6 bar BMEP. Figure 5.11 and 5.12 show the controller response with slow and aggressive PI settings. The controller action on the spark advance is reported in green, while the controlled variable, MFB50, is reported in blue. The MFB50 target is a square wave with 20 °CA amplitude.

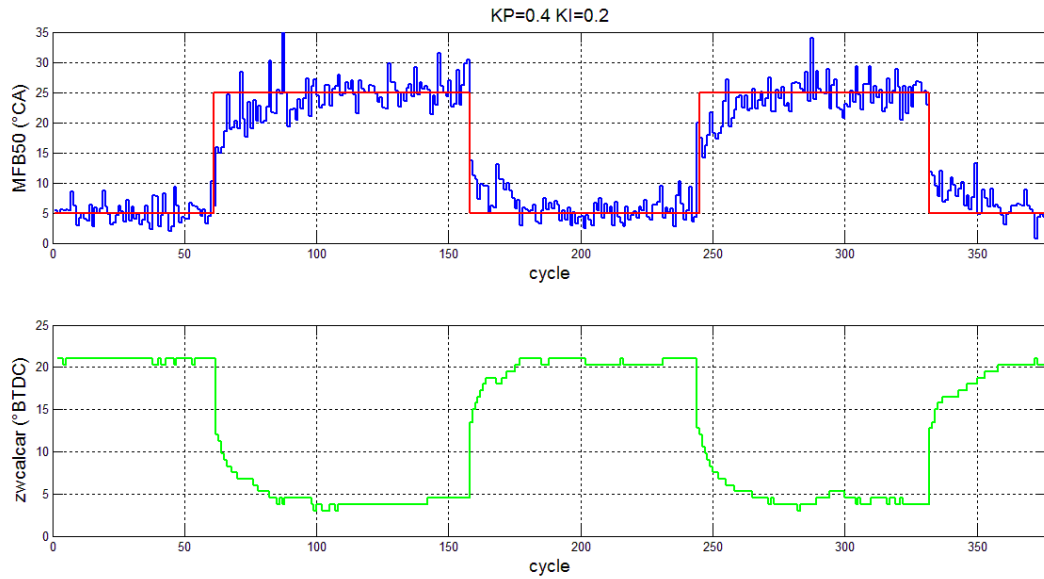


Figure 5.11 – Closed loop control action on spark advance, when changing MFB50 reference value. Controller gains are $K_P=0.4$ and $K_I=0.2$, Cylinder 2. The controller is able to control the combustion phase to its target value.

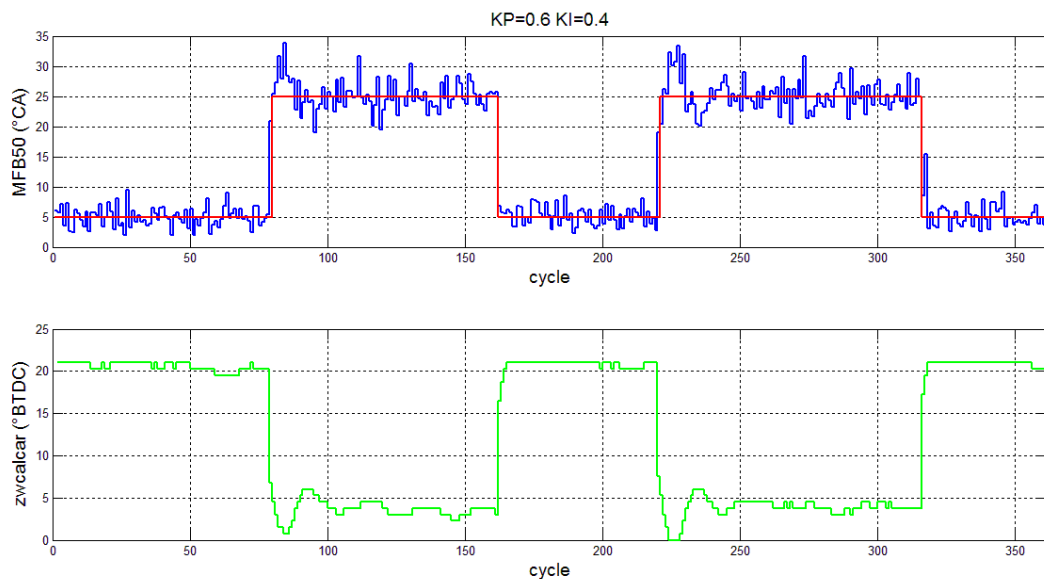


Figure 5.12 - Closed loop control action on spark advance, when changing MFB50 reference value. Controller gains are $K_P=0.6$ and $K_I=0.4$, Cylinder 2. High K_I 's values cause overshooting.

Test with faster control action (Figure 5.12) highlights an excessive overshooting caused by the integral windup. This behavior can be limited by preventing the integral term from accumulating above or below pre-determined bounds, or by excluding the integral action during rapid transients. The results reveal that the proposed layout and controller system is robust and that spark advanced actuation can be managed in closed-loop with the cyclic indicating parameters.

5.3.4 Second Set: Steady State Tests

A measurement campaign is made at the engine test bench in order to evaluate the controller performance on a high number of cycles in steady state conditions: the capability of keeping the combustion phase next to its target value is taken into account, together with the effects on the overall engine efficiency. The working conditions are summarized in Figure 5.13.

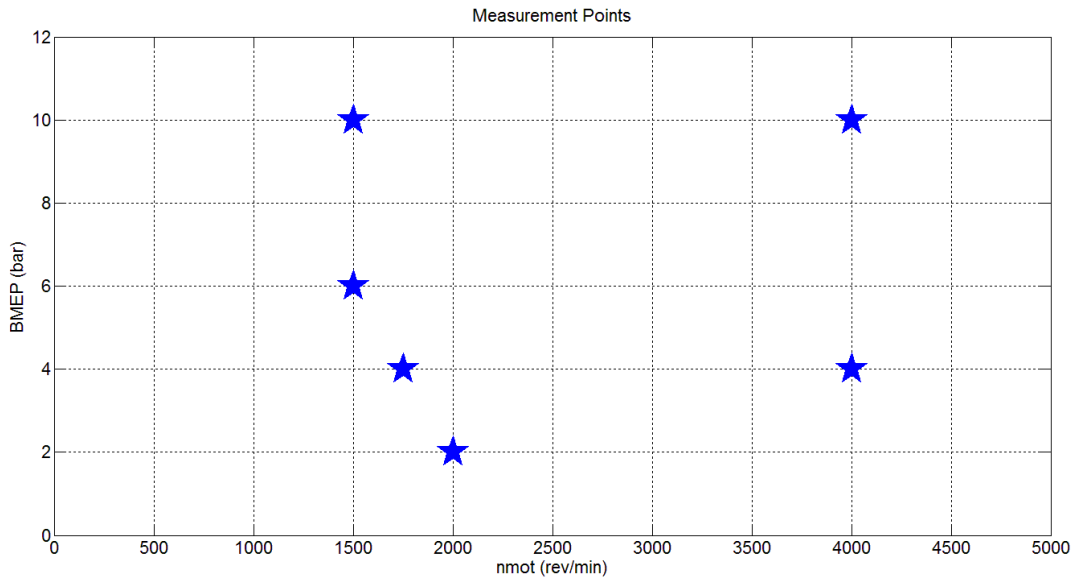


Figure 5.13 - Engine Operating Conditions for Steady State Measurements

For each operating condition, defined by engine speed and Brake Mean Effective Pressure (BMEP), acquisitions of pressure signal, test bench data and Engine Control Unit actuations are performed over a time interval of 60 seconds. The measurements are repeated in each operating point with the standard open loop spark advance calibration and with the developed combustion control activated, setting different MFB50 reference values for the combustion phase.

To make the controller action effective, the map based spark advance is manually increased by 10.25°CA during tests with closed loop ignition control, since only spark advance reductions are permitted by the Engine Control Unit for knock control (see Paragraph 5.3.1). The controller action is therefore applied through negative ignition timing corrections over the map based spark advance value, voluntarily over-advanced.

The air mass flow processed by the engine is maintained constant for each working point by forcing throttle, valve timing, air to fuel ratio and waste gate position to the calibrated value. Otherwise, a variation in the applied ignition timing would be interpreted by the Engine Control Unit as a variation in the combustion efficiency, causing a compensation in the intake air quantity.

The controller action on the ignition timing of each cylinder is clearly shown in Figure 5.14 and 5.15. The spark advance and the measured MFB50 for each cylinder are reported for the operating point at 1500 rpm and 10 bar of BMEP.

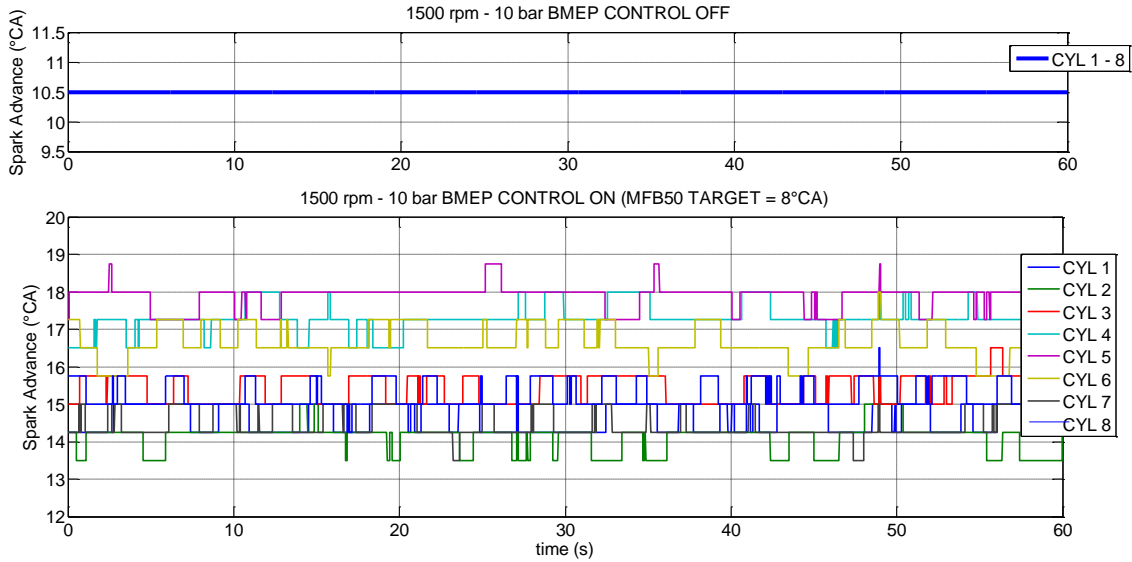


Figure 5.14 – Ignition timing with open loop (upper diagram) and closed loop combustion control (lower diagram), MFB50 target set to 8°CA. The closed loop control allows individual corrections on each cylinder.

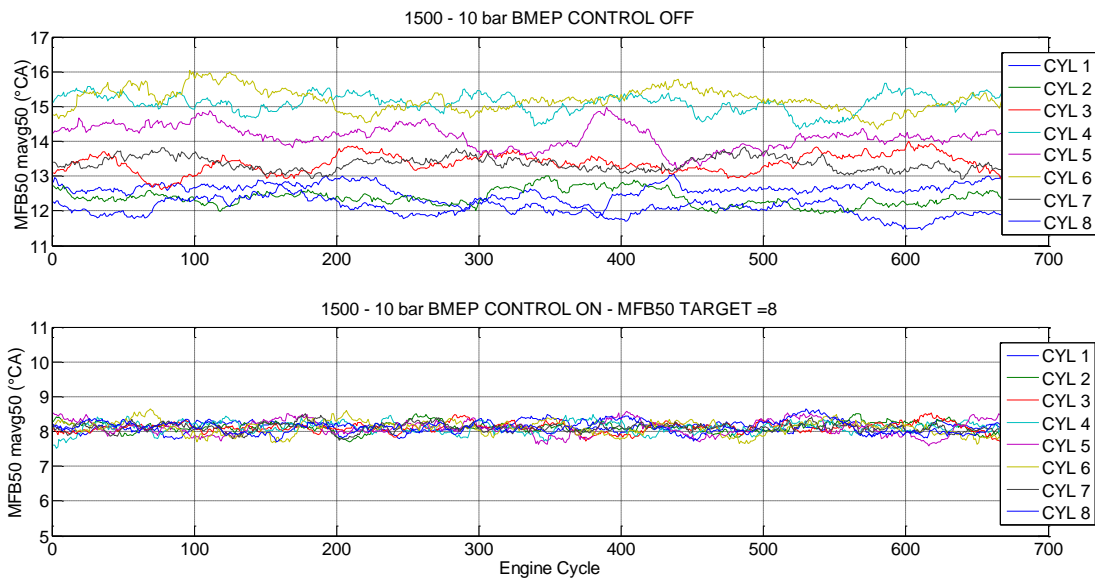


Figure 5.15 – Combustion phase, represented by MFB50 moving average over 50 cycles, with open loop (upper diagram) and closed loop combustion control (lower diagram), MFB50 target set to 8°CA.

Combustion phase non-uniformity can be compensated through the use of a closed loop individual spark advance controller, enabling individual ignition timing corrections, as visible in the lower diagram of Figure 5.14. When the control action is enabled, the combustion is phased to the reference MFB50 value (set to 8°CA in the current test) with good precision on all cylinders.

Controller gains are $K_P=0.15$ and $K_I=0.05$, while the moving average on the MFB50 is evaluated over the last 15 engine cycles. The controller action is proven to be stable in steady state conditions.

Focusing on the operating point of 1500 rpm and 10 bar of BMEP, the steady state measurement is repeated over 750 engine cycles with the open loop calibration and with the closed loop control, respectively with 13°CA, 8°CA and 6°CA MFB50 reference value. The test with 13°CA MFB50 target is chosen since it represents the average combustion phasing with the open loop calibration.

The results, in terms of combustion phase and work produced, are summarized in Figure 5.16 for cylinder 6 and in Figure 5.17 and 5.18 for all eight cylinders. The MFB50 Standard Deviation and IMEP Coefficient of Variation are representative of the cycle-to-cycle variations respectively in the combustion phase and in the overall combustion process efficiency.

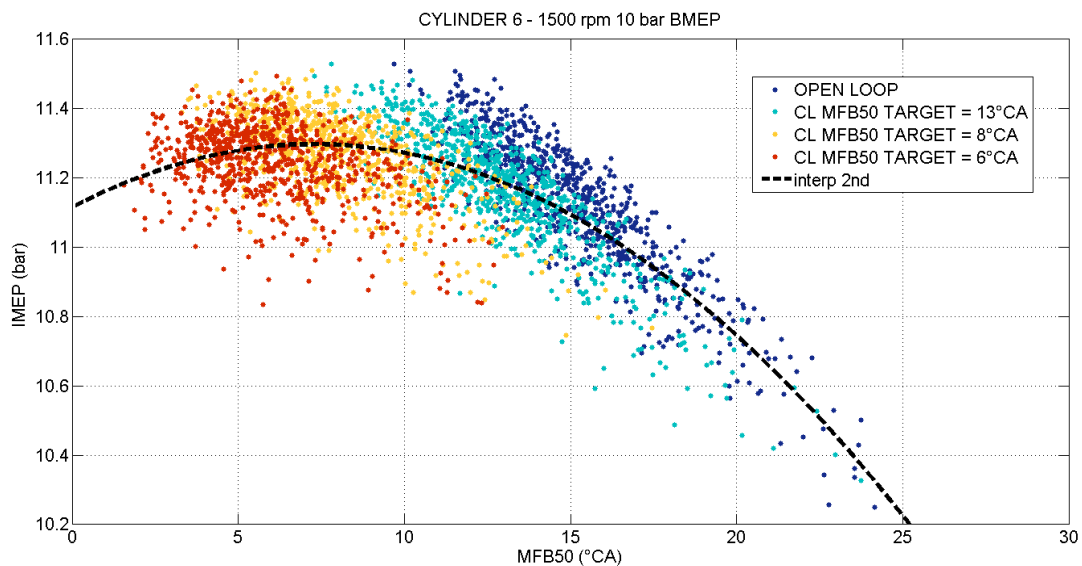


Figure 5.16 – MFB50 (°CA) and IMEP (bar) during steady state measurements for Cylinder 6, 1500 rpm and 10 bar of BMEP with open loop calibration. The closed loop controller moves the mean combustion phase to the desired MFB50, resulting in different IMEP output values.

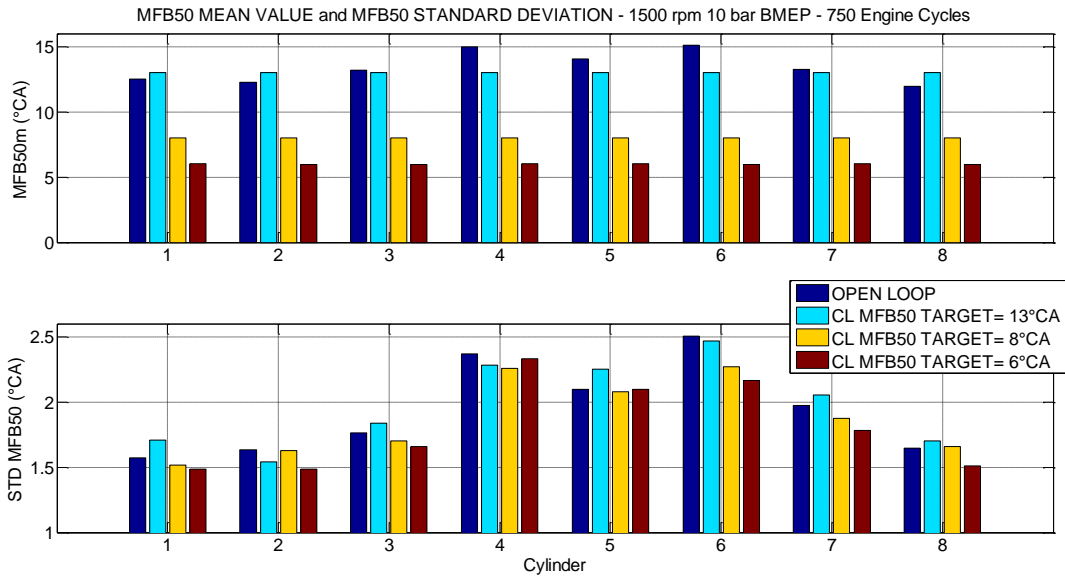


Figure 5.17 – MFB50 mean value (°CA) and MFB50 Standard Deviation (°CA) for all engine cylinders, with control disabled and enabled. Steady state test at 1500 rpm and 10 bar of BMEP, 750 consecutive engine cycles.

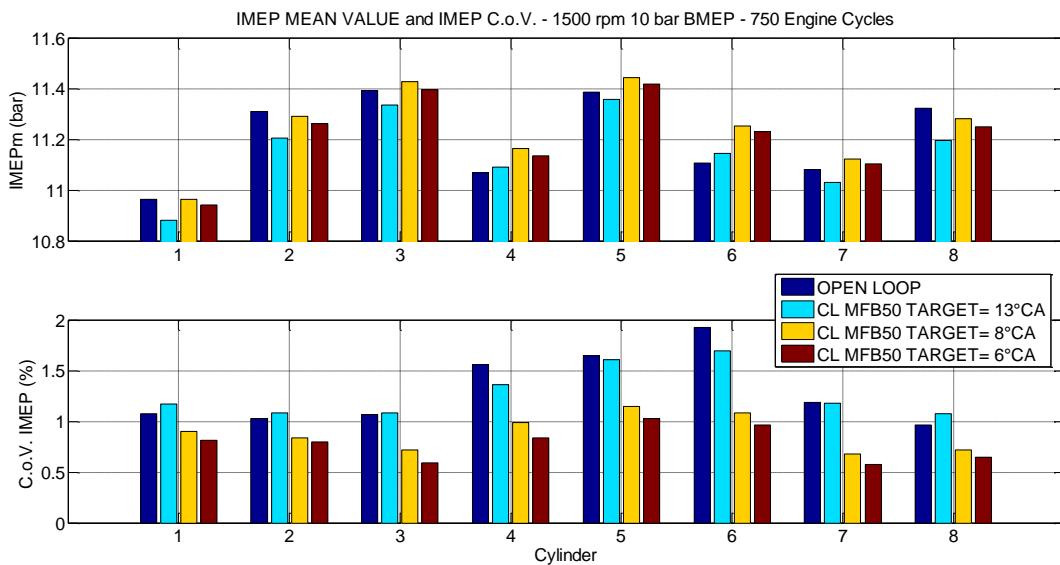


Figure 5.18 - IMEP mean value (bar) and IMEP Coefficient of Variation (%) for all engine cylinders, with control disabled and enabled. Steady state test at 1500 rpm and 10 bar of BMEP, 750 consecutive engine cycles.

The closed loop combustion phase controller is able to adjust the mean MFB50 of the different cylinders to the desired target. When the target is set to 13°CA MFB50, corresponding to the mean combustion phase with the open loop calibration, there is no worsening in the Standard Deviation of the combustion phase and in the Coefficient of Variation in IMEP, confirming the good stability of the proposed control strategy in steady state conditions.

The lower variability of the combustion process when the MFB50 is set to 8°CA and 6°CA cannot be attributed to the control action: when the combustion phase is close to the maximum brake torque timing, the combustion process is more repeatable and stable than for retarded combustions.

The differences in IMEP cannot be compensated through the proposed strategy. Figure 5.19 shows the effect on the mean IMEP and MFB50 on all engine cylinders when the closed loop control action is enabled.

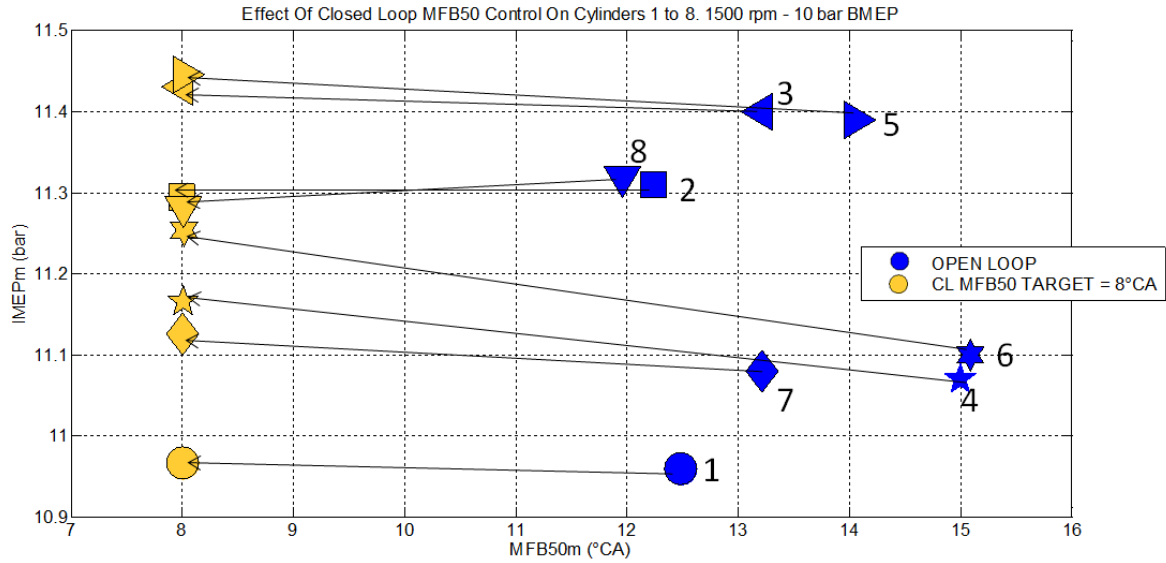


Figure 5.19 – Effects of closed loop control on cylinders 1 to 8. The closed loop control align the mean MFB50 of all cylinders to the desired value, while the differences in IMEP cannot be compensated. 1500 rpm, 10 bar of BMEP, MFB50 target = 8°CA.

The general improvement in IMEP must be attributed to a different and most efficient MFB50 target. This behavior is confirmed by the Brake Specific Fuel Consumption reduction, reported in Figure 5.24 for all measured operating conditions.

The cylinder-to-cylinder variations for all the measurements in different engine operating conditions can be summarized through the definition of two imbalance indexes, one regarding the differences in the combustion phase between cylinders (Eq. 5.1) and one regarding the differences in IMEP (Eq. 5.2).

$$MFB50_{imbalance}(\%) = 100 \cdot \frac{MFB50_{i,max} - MFB50_{i,min}}{MFB50_{mean}} \quad (5.1)$$

$$IMEP_{imbalance}(\%) = 100 \cdot \frac{IMEP_{i,max} - IMEP_{i,min}}{IMEP_{mean}} \quad (5.2)$$

Where $MFB50_{i,max}$ and $IMEP_{i,max}$ are, respectively, the maximum MFB50 and IMEP between cylinders. Mean value over all measured cycles are considered.

The comparison in cylinder-to-cylinder variations between open loop calibration and closed loop control, with MFB50 reference value set to 8°CA, are summarized in Figure 5.20 and 5.21 for all measured engine speed and load operating conditions.

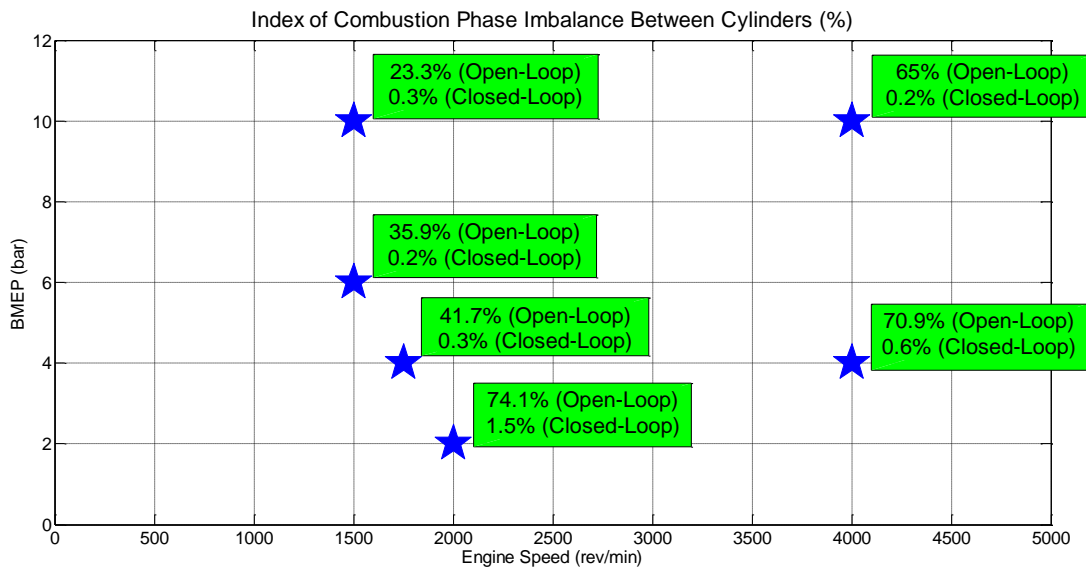


Figure 5.20 – MFB50 imbalance index between cylinders with open loop calibration and with closed loop combustion control, MFB50 target = 8°CA.

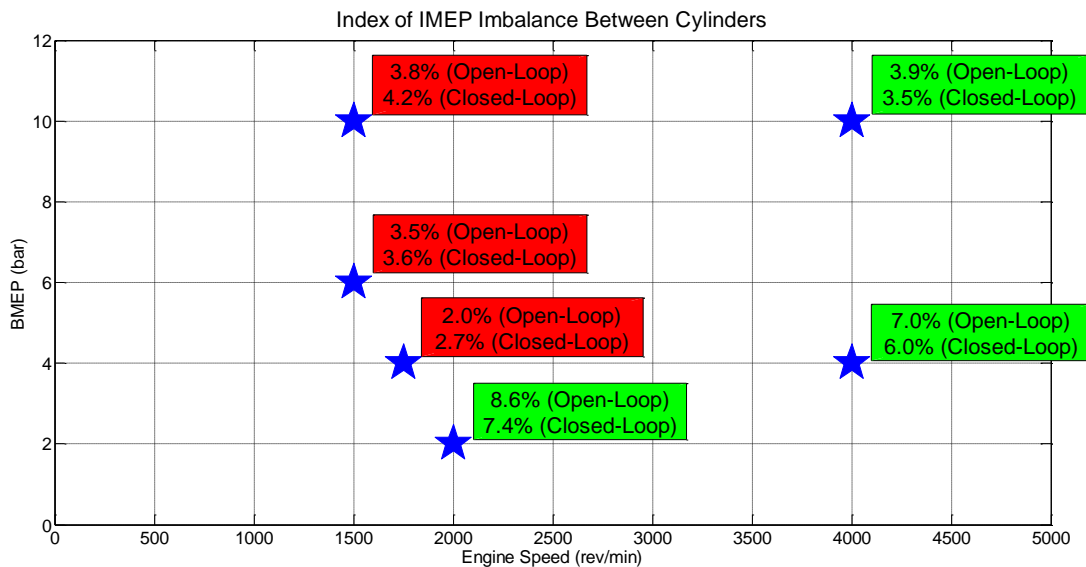


Figure 5.21 - IMEP imbalance index between cylinders with open loop calibration and with closed loop combustion control, MFB50 target = 8°CA.

While the effects on leveling the combustion phase between cylinders is drastic and clear, compared to the open loop calibration, the effects of the closed loop system on the IMEP distribution between cylinders are not relevant.

As for the cylinder-to-cylinder variations, the results in terms of cycle-to-cycle variations can be summarized in Figure 5.22 and 5.23 through the mean MFB50 Standard Deviation ($^{\circ}\text{CA}$) and the mean IMEP Coefficient of Variation (%), evaluated on all engine cylinders.

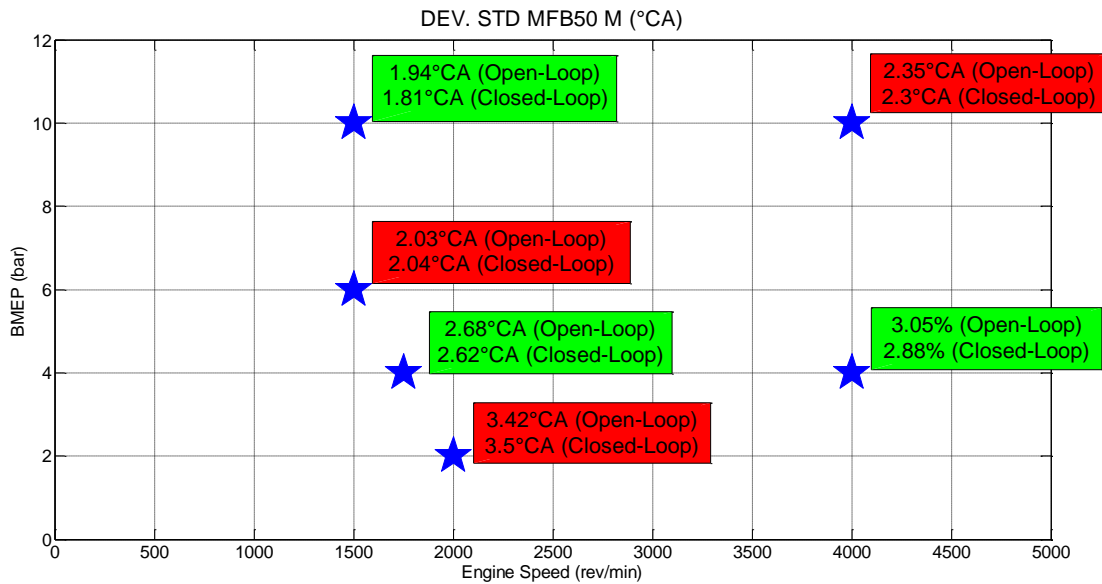


Figure 5.22 – Mean MFB50 Standard Deviation evaluated on all engine cylinders, with open-loop and closed-loop ignition timing control (MFB50 target = 8°CA).

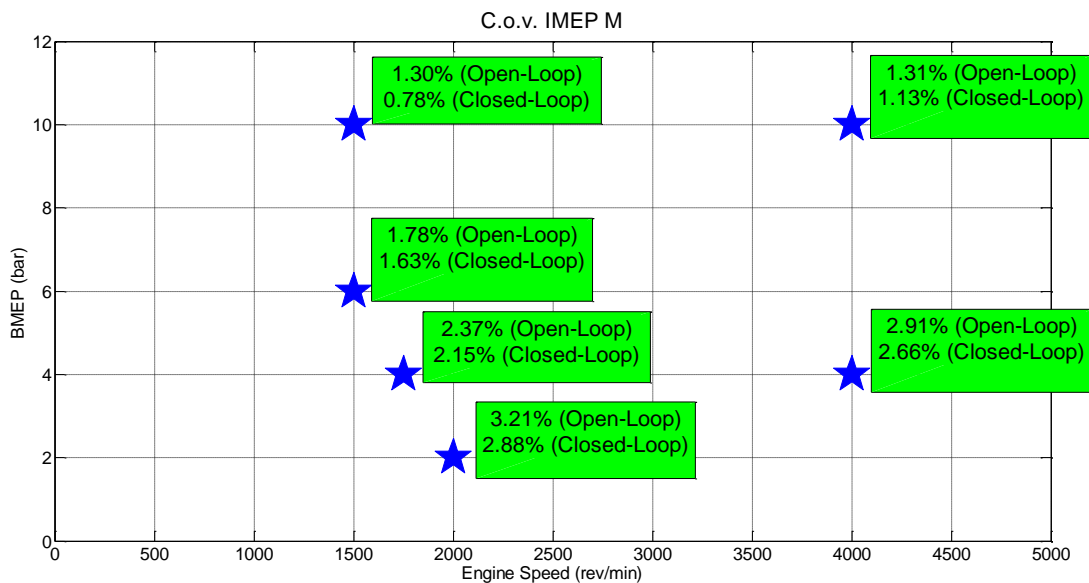


Figure 5.23 – Mean Coefficient of Variation of IMEP evaluated on all engine cylinders, with open-loop and closed-loop ignition timing control (MFB50 target = 8°CA).

The test bench instrumentation allows the evaluation of the Brake Specific Fuel Consumption (g/kWh). The measured variations using the Closed-Loop MFB50 control are summarized in Figure 5.24: the mean MFB50 between cylinders is reported, both in Open-Loop and in Closed-Loop conditions with different reference values for the controller.

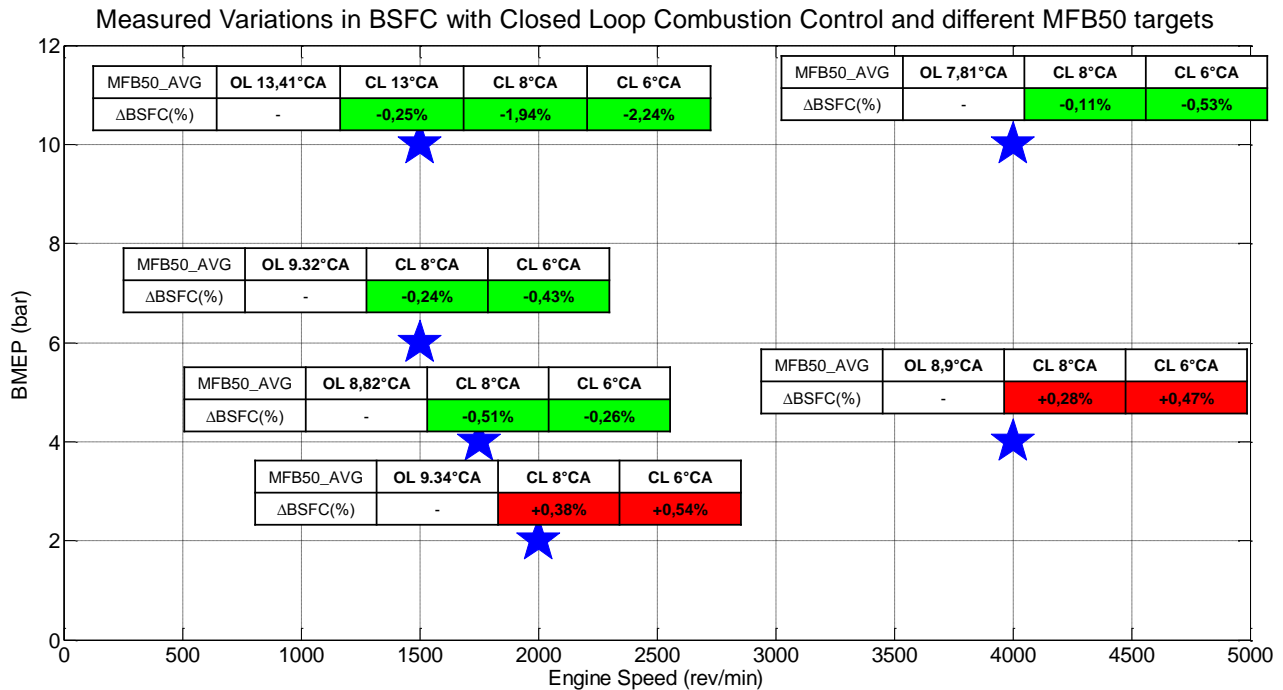


Figure 5.24 – Variation in Brake Specific Fuel Consumption for steady state tests with the standard spark advance calibration and with Closed-Loop control for different MFB50 targets. The average MFB50 between cylinders is reported for different configurations.

It must be noticed that the operating point at 1500 rpm and 10 bar of BMEP is calibrated at 13°MFB50, consequently the consistent improvement must be attributed to a different and most efficient MFB50 target.

5.3.5 Third Set: Transient Tests

Transient test conditions are reproduced by varying load and engine speed, while measuring the combustion phase. Purpose of these tests is to check the capability of the closed-loop control to maintain a stable behavior on spark advance even during transient operations. The reference conditions are represented by the open-loop map based engine calibration.

To reproduce in a repeatable way transient operations, the engine load is varied from 3% Accelerator Pedal Position (1 bar of BMEP) to 10% (5 bar of BMEP) in a 3 s time interval, while engine speed is increased from a starting value of 1000 rpm to 3000 rpm in 10s. The test is repeated with the standard open loop calibration and with the closed loop combustion control. In Figure 5.25, the accelerator pedal position opening law and the engine speed are shown, together with the

applied ignition timing for both conditions. Cylinder-wise ignition timings are applied when the control is enabled.

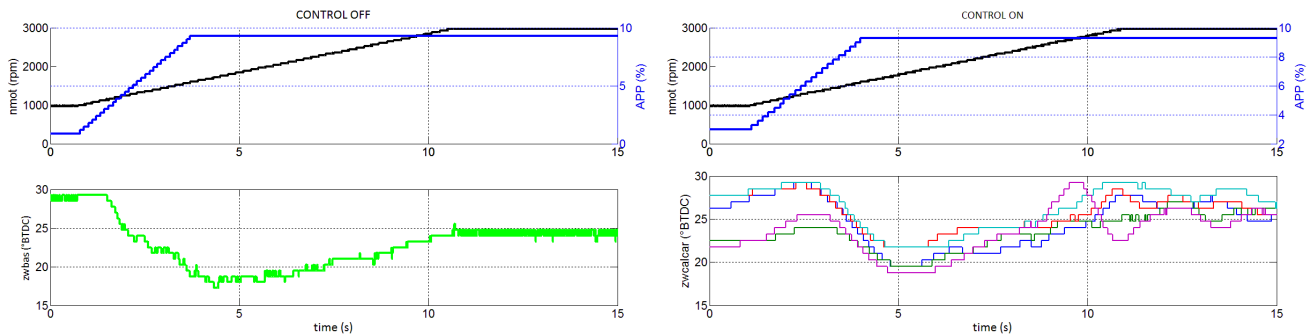


Figure 5.25 – Spark advance actuation during transient operating conditions, with the control disabled (left) and with the control enabled (right).

The controller action on the spark advance is highlighted in Figure 5.26, referring to Cylinder 1. The corresponding measured combustion phase, represented by the MFB50, is reported for both conditions. The engine speed is used to correctly synchronize the different measurements.

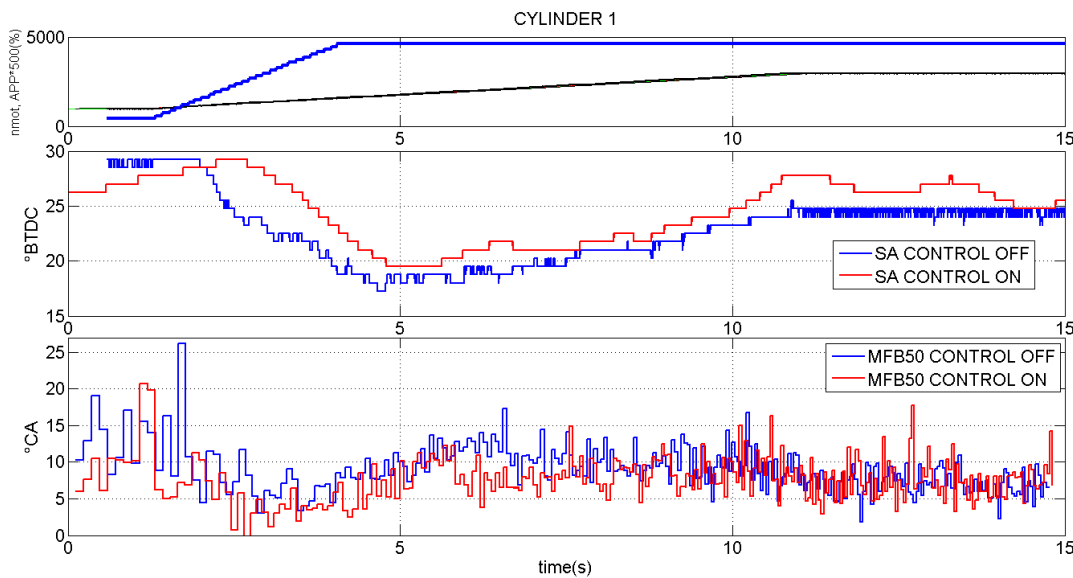


Figure 5.26 – Engine Speed and Load, Ignition Timing and MFB50 measured on Cylinder 1 with open loop control (blue) and closed loop control (red).

The controller makes no use of maps stored in the Engine Control Unit, nevertheless the closed loop ignition timing is comparable to the value applied under map based conditions. Neither of the controllers is able to prevent the over advanced combustion process consequent to the fast load transient (seconds 1.5 to 4.5 in the lower diagram of Figure 5.26).

The effect on the cylinders-average combustion phase is reported in Figure 5.27. Two effects must be noticed:

- The fast load transient (1.5 s - 4.5 s) causes over advanced combustion both with the control disabled and enabled;
- The mean combustion process with the closed loop action is closer to the target value of $MFB_{50} = 8^{\circ}CA$. Under open-loop conditions, the combustion is correctly phased only when stationary load and speed are reached (around 11 s).

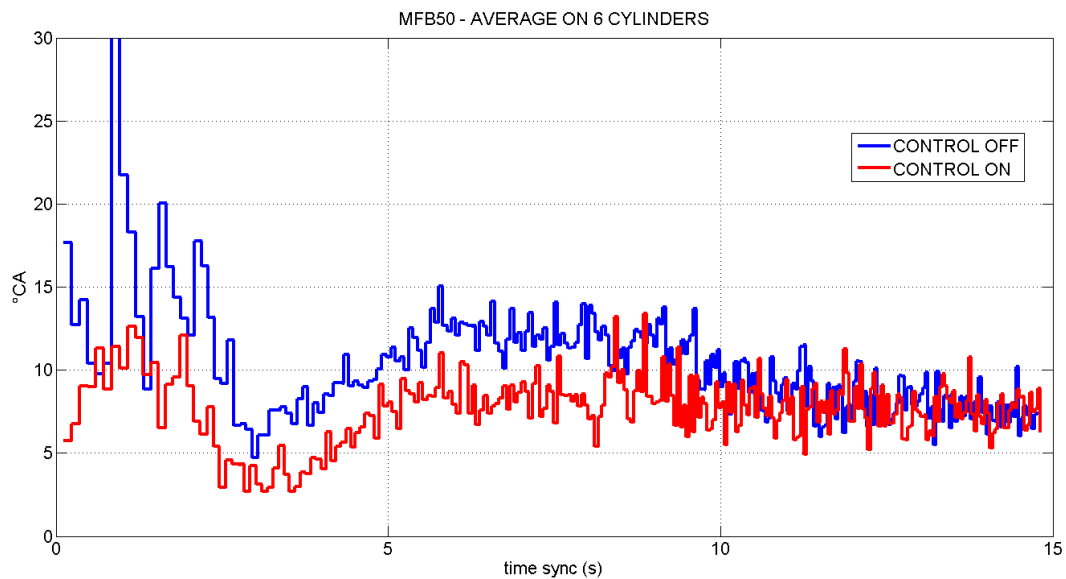


Figure 5.27 – Mean MFB50 over 6 Cylinders during transient operations, with combustion control disabled and enabled.

5.3.6 Fourth Set: Vehicle Implementation

The developed combustion controller has finally been installed and tested on a Ferrari F142M vehicle. The engine is equipped with 8 in-cylinder pressure sensors and with the on-board indicating system for the combustion analysis. Compared to the test bench, where the engine is connected directly to the electric brake, the engine in the car cannot be controlled directly in terms of load and speed. The only way of applying a resisting torque at the crankshaft is through the wheels (running the vehicle) or using the inertia of the engine itself while revving in neutral gear position.

Another element that needs to be considered when exporting the combustion controller to the vehicle is the torque structure. In case of catalyst heating, idle control, gearshift or for drivability reasons (anti-jerk), the system acts directly on the spark advance actuation, ignoring the corrections sent by the combustion phase controller.

Thus, the action on the spark advance of the developed combustion controller is effective only in case of no torque intervention via ignition angle ($B_nozwe=TRUE$). In the remaining time, the output is ignored. The control algorithm is modified: the integral action is held in reset condition, so that no integration occurs while the torque intervention is enabled.

The controller action during the initial section of the NEDC driving cycle (ECE-15) is presented in Figure 5.28.

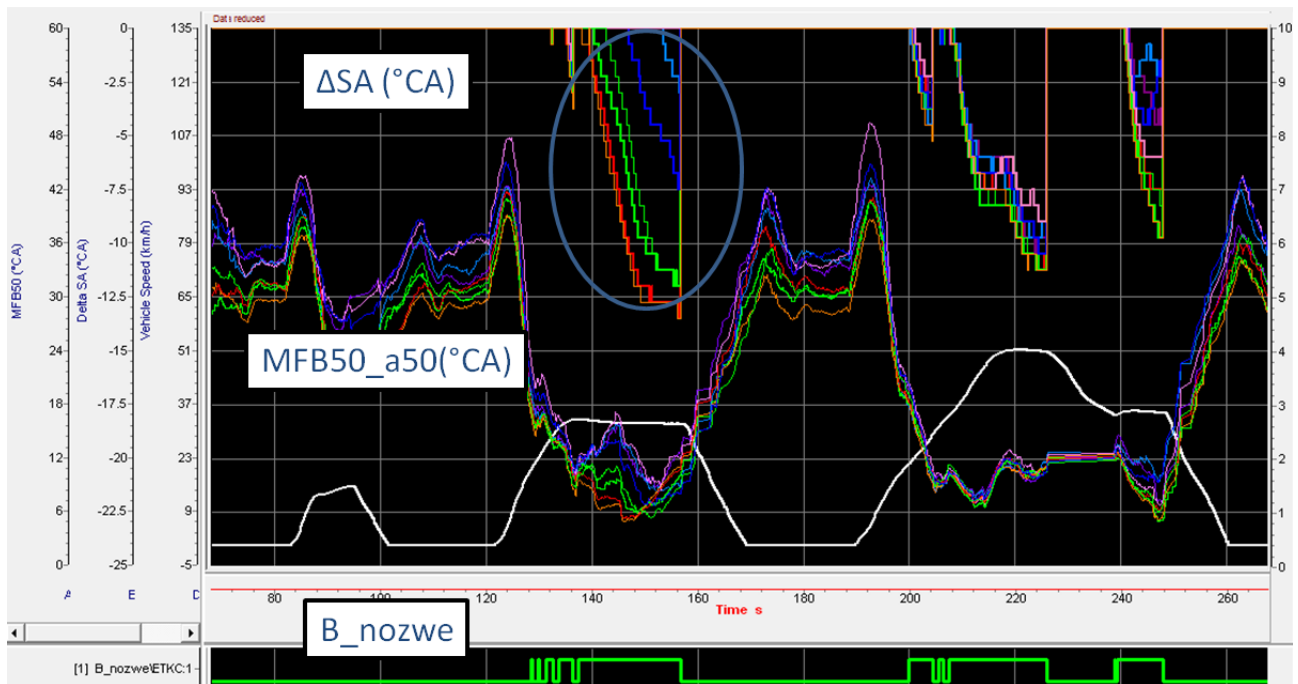


Figure 5.28 – Combustion Controller corrections on ignition timing (ΔSA) during ECE-15 driving cycle performed at the vehicle test bench. MFB50 ($^{\circ}CA$) moving average over 50 engine cycle, Vehicle speed (km/h) and condition of no torque intervention (B_nozwe).

When the condition of no torque intervention is satisfied, the controller requires a spark advance correction on every cylinder (ΔSA) to follow the target MFB50, set for this test at $12^{\circ}CA$ for safety reasons. To make the control action possible, since only spark advance reductions are permitted, the map based spark advance value is manually increased by $7.5^{\circ}CA$. The controller needs then to correct the over-advanced ignition timing, with regard to the desired combustion phase, every time its action is permitted. The PI settings for this test are $KP = 0.2$ and $KI = 0.03$, moving average on the MFB50 computed over the last 15 engine cycles.

Focusing on the third ramp of the ECE-15, where the controller action is enabled (Figure 5.29), the controller takes around 6 seconds to reach a stable spark advance correction for the MFB50 target. The ignition timing adjustments are applied to the map-based value for the specific operating

conditions of the engine, manually corrected to be over-advanced. The same section, repeated without the control action, is reported in Figure 5.30.



Figure 5.29- ECE-15 section with condition for closed loop controller intervention. The requested ignition timing corrections (ΔSA) and the MFB50 moving average over 50 engine cycles are reported.

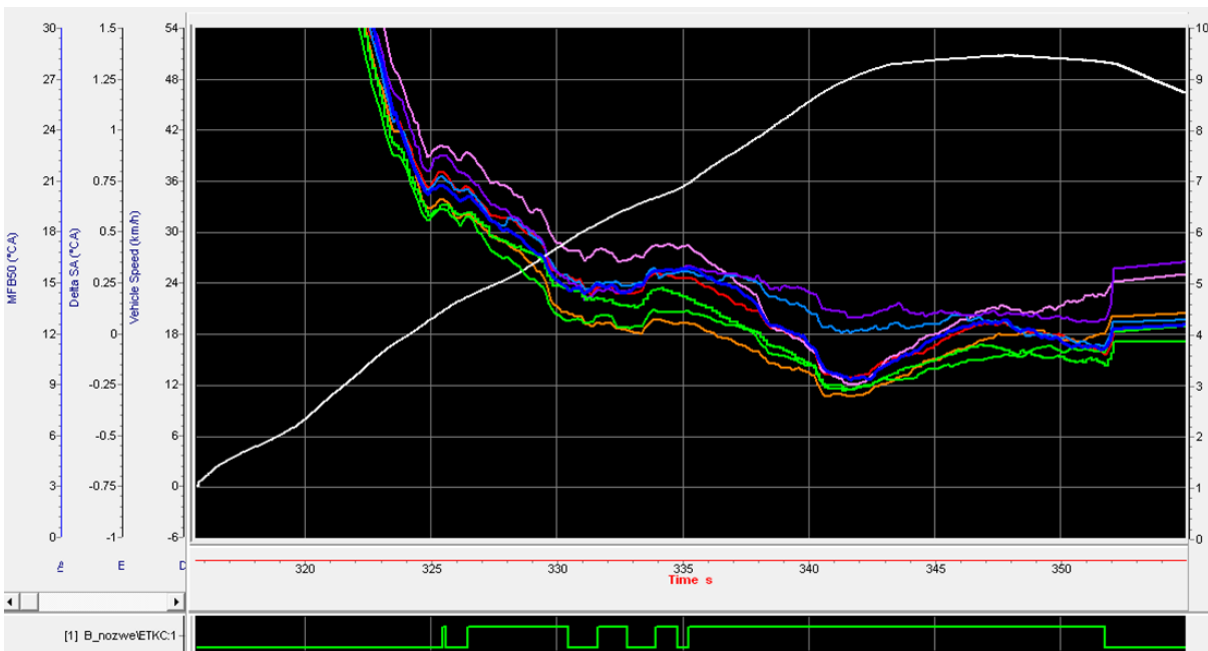


Figure 5.30 - ECE-15 section without closed loop control. MFB50 moving average over 50 engine cycles reported.

When the control action is applied, the MFB50 shows a less stable behavior: every time a reduced ignition timing is requested from the torque structure, the integral action resets. When it is enabled again, a transient phase is requested to reduce the error in the combustion phase caused by the over

advanced map based spark advance. Nevertheless, a reduced dispersion between the cylinders is visible on the MFB50, due to individual ignition timing corrections.

5.4 Real Time Combustion Controller with Ion Signal Feedback

The angle corresponding to the ion thermal peak is evaluated every combustion event by the Ion Control Unit (see Paragraph 3.2). The strong correlation with the pressure signal and the MFB50 allows the use of ThPeakAngle for combustion control purposes. Compared to the MFB50, the ThPeakAngle calculation relies on equipment already existing on every Ferrari engine.

In this first prototype phase, in order to make the information about the location of the thermal peak available to the Rapid Control Prototyping system, the Ion Control Unit writes every *5ms* a message on the vehicle CAN line, containing the ThPeakAngle values for each cylinder and the ID of the last cylinder fired.

The vehicle CAN line is normally used for communication between vehicle CAN nodes, such as brake control unit, steering, gearbox, on-board computer, airbag, traction control, differential, Engine Control Unit and Ion Control Unit. Since messages exchanged between these last two units need to travel with high priority and constant delays, another “private” CAN line exists, and it is the one used for spark advance control in case of knock (see Section 5.3).

Two main issues influenced the real-time implementation of the controller based on the ThPeakAngle evaluated by the Ion Control Unit, together with the wrong real-time evaluation of the ion thermal peak position (issue presented in Paragraph 3.2.3 and currently under development):

- The messages containing the ThPeakAngle values are sent on the vehicle CAN line, while the spark advance correction that needs to be intercepted in order to control the combustion are sent on the private CAN line between Ion Control Unit and Engine Control Unit.
- Only two CAN ports are present on the Rapid Control Prototyping platform and are both used to read and overwrite the spark advance correction on the private CAN line, while the other existing messages are read and copied as if no interruption was present.

The proposed layout to overcome this issue is represented in Figure 5.31. The idea is to isolate the Ion Control Unit vehicle CAN exit port and connect it to the private CAN, so that only messages with ThPeakAngle and cylinder ID are added to the private CAN line traffic, while all the information can be read by the prototyping platform through one single input port. It has been tested that the Ion Control Unit works even if disconnected from the vehicle CAN line.

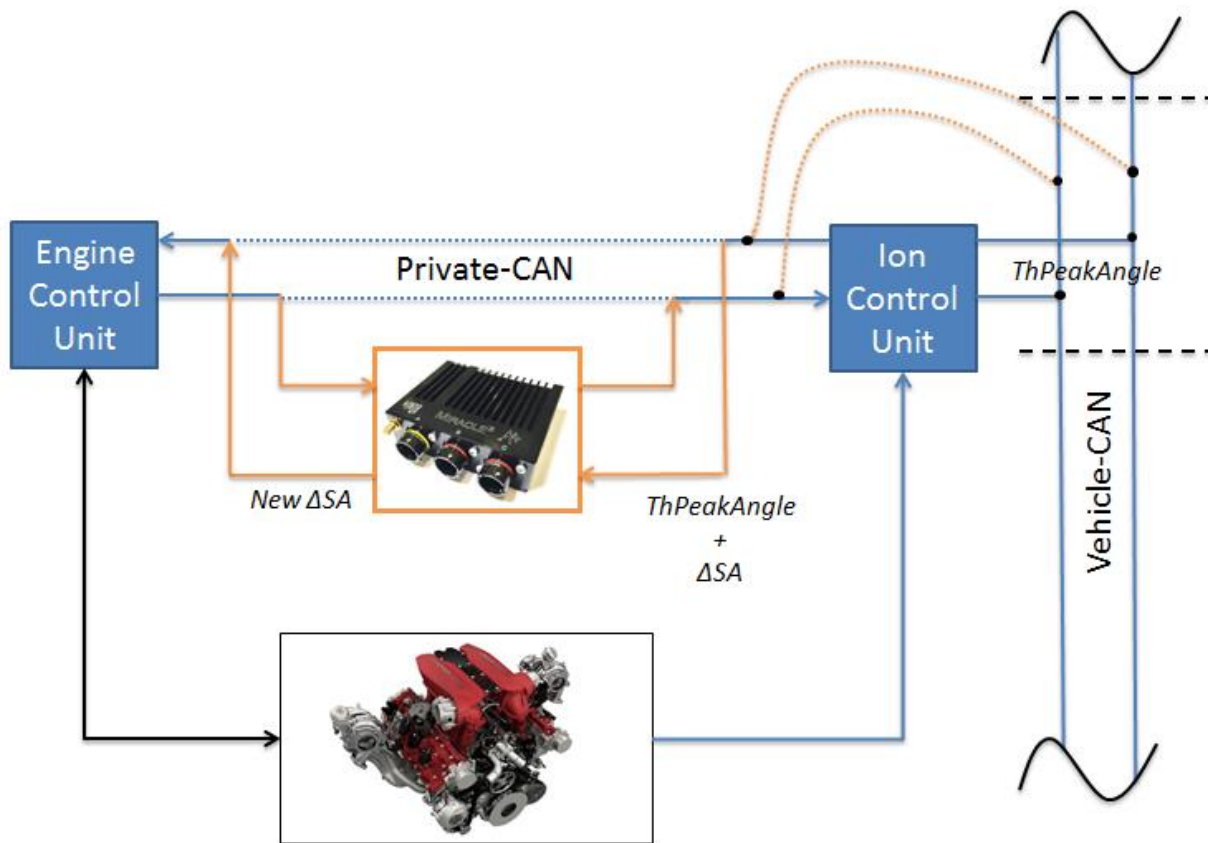


Figure 5.31 - Proposed layout for reading $ThPeakAngle$ and spark advance corrections (ΔSA) from the same CAN line and write the new ΔSA to the ECU.

However, the testing of such layout highlighted the impossibility of connecting together the two CAN lines, since the baud rates of the lines are different (1 MBd/s for the private, 500 kBd/s for the vehicle CAN line). The modification of the Ion Control Unit software is currently being developed by the manufacturer and consists in writing the messages containing the $ThPeakAngle$ values directly on the private CAN line, rather than on the vehicle CAN line.

6 Conclusions

Aim of this work was to evaluate the feasibility of further applications for the combustion quality related information derived from the ion current signal.

Extensive experimental activity has allowed verifying the high correlation level existing between combustion phase indicators derived from the pressure signal and thermal peak location of the ion current signal under non-knocking operating conditions. The Ion Control Unit, already adopted on every Ferrari engine, has been modified for the evaluation of the thermal peak location for every combustion event and for every cylinder.

The proposed application is an innovative feedback control strategy of the spark advance actuation. This led to the development and testing of a closed-loop spark advance controller, through a simulation environment, at the test bench on a Ferrari turbocharged engine and on the vehicle roller bench. The controller algorithm is executed on an external programmable controller, inserted on the CAN line between the Ion Control Unit and the Engine Control Unit.

The control strategy allows a precise control of the combustion phase in steady state conditions, cylinder by cylinder, without using maps stored in the Engine Control Unit and for any operative and boundary conditions. The performance in transient condition can be improved with a more sophisticated controller design. The controller has been tested using the pressure signal feedback and it is already compatible for the ion current feedback control strategy.

The correct alignment of the combustion phase of all cylinders shows a marginal improvement in the engine efficiency, in case the open loop combustion is close to the optimal conditions.

Nevertheless, further applications of the controller could be in monitoring the combustion phases on a long-time interval and adaptively learn the differences between cylinders and try to balance them, or just for diagnostic purposes. And, in the case of a future implementation of pressure sensors inside the cylinder, such system could be the basis for new engine control strategies, not only based on the combustion phase, but directly on the delivered output torque.

7 Bibliography

- [1] Regulation 333/2014 – ‘*Passenger Car Regulation*’-‘Regulation (EU) No 333/2014 of the European Parliament and of the Council of 11 March 2014 amending Regulation (EC) No 443/2009 to define the modalities for reaching the 2020 target to reduce CO₂ emissions from new passenger cars’, Official Journal, L103, 05/04/2014.
- [2] International Council on Clean Transport (ICCT), CO₂ emissions from new passenger cars in the EU: Car manufacturers’ performance in 2015, June 2016
- [3] International Council on Clean Transport (ICCT), The WLTP: How a new test procedure for cars will affect fuel consumption values in the EU, October 2014
- [4] International Council on Clean Transport (ICCT), A technical summary of Euro 6/VI vehicle emission standards, June 2016
- [5] Kadijk, G., Mensch, P., Spreen, J.S., “Detailed investigations and real-world emission performance of Euro 6 diesel passenger cars,” TNO, May 18, 2015
- [6] Yang, L., Franco, V., Mock, P., Kolke, R., Zhang, S., Wu, Y., & German, J. (2015). Experimental assessment of NO_x emissions from 73 Euro 6 diesel passenger cars. *Environmental Science & Technology*. DOI: 10.1021/acs.est.5b04242
- [7] Bericht der Untersuchungskommission “Volkswagen”, Bundesministerium für Verkehr und digitale Infrastruktur, April 2016
- [8] Gian Marco Bianchi, “FLUIDODINAMICA DEI MOTORI A COMBUSTIONE INTERNA M”, Università di Bologna, A.A. 2015/2016
- [9] F. Zhao, M.C. Lai, D.L. Harrington, “Automotive spark-ignited direct-injection gasoline engines”, *Progress in Energy and Combustion Science* 25 (1999) 437–562
- [10] Aaron Isenstadt and John German (ICCT); Mihai Dorobantu (Eaton); David Boggs (Ricardo); Tom Watson (JCI), “Downsized, boosted gasoline engines”, October 2016
- [11] Ulf Stenzel (AVL Engineering and Technology), “48V Mild Hybrid Systems Market Needs and Technical Solutions”, AVL UK Expo, 2014
- [12] 488 GTB-INTERNATIONAL MEDIA TEST DRIVE, <http://www.motorshow.me/GalleryDocs/Doc5931.pdf>
- [13] Heywood, J.B., *Internal Combustion engine Fundamentals*, McGraw-Hill, 1988.
- [14] Nicolò Cavina, “PROPULSORI TERMICI E IBRIDI PER AUTOVEICOLI M C.I.”, Università di Bologna, A.A. 2015/2016
- [15] Andrea Bertola, Jürg Stadler, Thomas Walter, Peter Wolfer, “Pressure Indication During Knocking Conditions”, Kistler Instrumente AG, Winterthur, Switzerland

- [16] Eriksson, Lars. "Methods for Ionization Current Interpretation to be Used in Ignition Control". Diploma Thesis, no. LiTH-ISY-EX-1507. Department of Electrical Engineering. Linköping University, Sweden, 1995.
- [17] L. Guzzella and C. H. Onder, "Introduction to Modeling and Control of Internal Combustion Engine Systems", Springer, 2010.
- [18] Eriksson, Lars and Lars Nielsen. "Ignition Control by Ionization Current Interpretation". SAE 960045, 1996.
- [19] "Delphi Ionization Current Sensing Ignition Subsystem", Delphi, August 2005
- [20] Saitzkoff, A., Reinmann, R., Mauss, F., Glavmo, M., In-Cylinder Pressure Measurements Using the Spark Plug as an Ionization Sensor, SAE Technical Paper 970857.
- [21] Zhu, G. G., Daniels, C. F., Winkelman, J., MBT Timing Detection and its Closed-Loop Control using In-Cylinder Ionization Signal, SAE Technical Paper 2004-01-2976.
- [22] Hellring, M., Munther, T., Rongvaldsson, T., Wickstrom, N., Carlsson, C., Larsson, M., Nyomt, J., Spark Advance Control using the Ion Current and Neural Soft Sensors, SAE Technical Paper 1999-01-1162.
- [23] Haskara, I., Zhu, G., and Winkelman, J., "IC Engine Retard Ignition Timing Limit Detection and Control using In-Cylinder Ionization Signal," SAE Technical Paper 2004-01-2977, 2004.
- [24] Cavina, N., Moro, D., Poggio, L., Zecchetti, D. et al., "Individual Cylinder Combustion Control Based on Real-Time Processing of Ion Current Signals," SAE Technical Paper 2007-01-1510, 2007

Ringraziamenti

Un sentito e doveroso ringraziamento va al professor Cavina e all'ingegner Calogero per aver reso possibile quest'esperienza, accompagnato da una profonda ammirazione per l'impegno e l'entusiasmo con cui svolgono il proprio lavoro. Particolare riconoscenza va ad Andrea, per le lunghe giornate passate a Maranello e per il fondamentale contributo al lavoro di tesi, a Ruggero e Marco, per i preziosi insegnamenti, e a tutti i membri del gruppo Sperimentazione Motopropulsore di Ferrari S.p.A, dal mitico Fabio al grande Albertini.

Desidero ringraziare tutti i ragazzi e ragazze (poche) di Ingegneria per la compagnia e i bei momenti vissuti assieme nel corso di questi cinque anni, anche al di fuori delle "mura" di Viale Risorgimento.

Un grazie anche a Sara, per la felicità che accompagna ogni giorno trascorso assieme e alla mia famiglia, per il costante supporto e per l'investimento ad alto rischio effettuato nella mia formazione.

Un ultimo pensiero, unito ad un grande e purtroppo irrealizzabile abbraccio, va ad Ale. Alla sua memoria dedico la presente tesi, convinto che sarebbe diventato, ormai già da Luglio conoscendolo, un ottimo Ingegnere e che sempre sarebbe rimasto un fedele amico.